

A Towed Ground Effect Vehicle for Sea Floor Mapping and Fish Survey

Jean-Philippe Rozé

June 2004

Submitted for the degree of
Master of Engineering



Submitted to : GMIT and HETAC

Research carried out at : The School of Engineering, GMIT

Research Director : Dr Patrick Delassus

DECLARATION

I hereby declare that the work presented in this thesis is my own and that it has not been used to obtain a degree in this institute or elsewhere.

A handwritten signature in blue ink that reads "Jean Philippe Rozé". The signature is written in a cursive style and is underlined with a single horizontal stroke.

Jean-Philippe Rozé

A Towed Ground Effect Vehicle for Sea Floor Mapping and Fish Survey

Ireland's coastal and marine environments hold significant sand and gravel resources. A 1989 Geological Survey of Ireland (GSI) Report noted that sand and gravel is a valuable but depleting resource. The extraction of sands and gravels from near shore waters can have implications for the management of coasts, tourism and the fishing industry. Available underwater vehicles are controlled in three dimensions using directional wing and variable buoyancy. This study shows that a ballast solution is not suitable to control a close-ground towed vehicle able to avoid obstacles. It also shows that a directional wing solution, using the angle of attack to create a lift is more realistic than the ballast system. However, this design would need to be driven by a close loop control system which induce a high manufacturing, maintaining and running cost for the only driving function of the vehicle. None of the existing submarine products are using ground effect to fly over the sea bed. The objective is to develop a towed underwater vehicle, able to fly at constant distance from the sea bed, cheap to produce, maintain and run. This device would optimise the efficiency and cost of continental shelf survey. The aim of this study is to establish the feasibility of such a vehicle, and propose a conceptual design of a wing able to fly at a constant distance from the sea bed. This work present a Computational Fluid Dynamics (CFD) analysis performed on different wing designs, the towing tank and wing models build to conduct experimental tests, and a conceptual design of the vehicle. In conclusion from the CFD analysis and the experimental tests, the concept of ground effect, which has never really been studied for underwater applications, is realistic solution to optimise the efficiency and cost of continental shelf survey.

FUNDING

The research described in this these was funded by Enterprise Ireland

ACKNOWLEDGEMENTS

There are many people who I would like to thank for having contributed in some way to the development of this thesis. Firstly thanks to Dr. Patrick Delassus for all the help, advice and supports and for giving me the opportunity to come back to Ireland.

Thanks to everybody who helped in my practical work:

In G.M.I.T, John Noone and all in the workshop for there help during the towing tank building, Dr John LOHAN for his advices about testing facilities and methods .

To my home mates specially Berta, Johan, Ivo and Daphne, to everybody working in the lab and specially Carine, Laurence and Kristin thanks for providing company and support, and raising a smile on bad days.

Again, thanks to my parents for being who you are. I would not have gone so far without your support and encouragement.

TABLES OF CONTENTS

INTRODUCTION.....	1
CHAPTER 1 : LITERATURE REVIEW	3
I. EXISTING PRODUCTS:.....	3
I.1 AQUASHUTTLE MARK III	3
I.2 NU-SHUTTLE	4
I.3 SEASOAR MARK II	5
I.4 KLEIN SUB-BOTTOM PROFILER.....	6
I.5 FLYING FISH	6
I.6 SEA KITE	7
I.7 SYNTHESIS OF THE EXISTING PRODUCTS:	9
II. CONTINENTAL SHELF.....	10
II.1 OCEAN MORPHOLOGY	10
II.1.1 <i>Deep sea:</i>	10
II.1.2 <i>Continental margin</i>	11
II.1.2.1 Continental shelf.....	11
II.1.2.2 Continental slope:	11
II.1.2.3 Continental rise	11
II.2 THE IRISH CONTINENTAL SHELF	11
III. DESIGNS AND CONCEPTS.....	12
III.1 SUBMARINE DESIGN:	12
III.1.1 <i>Buoyancy</i>	12
III.1.2 <i>Live scale dive technology</i>	13
III.1.2.1 Static diving	13
III.1.2.2 Dynamic Diving.....	14
III.1.3 <i>Underwater vehicle stability</i>	15
III.2 FOILS DESIGN:	17
III.2.1 <i>Foils geometry</i>	17
III.2.1.1 Wing definition	17
III.2.1.2 Wing section definition:.....	19
III.2.1.3 NACA section.....	20
III.2.2 <i>Hydrodynamics forces</i>	21
III.2.2.1 Definition	21
III.2.2.2 Dimensional theory:.....	21
III.2.2.3 Hydrofoil characteristics - lift coefficient versus incidence	22
III.2.2.4 Effect of Reynolds number on the C_L	23
III.2.2.5 Lift and Drag force on Airfoils	23
III.2.3 <i>Wing in ground effect vehicles</i>	27
III.2.3.1 Wing in Ground Effect vehicles	27
III.2.3.2 Computational fluid dynamics on ground effect aerodynamics	27
IV. FLUID DYNAMIC ANALYSIS	30

IV.1	FLUID PROPERTY	30
IV.1.1	<i>Density</i>	30
IV.1.2	<i>Viscosity:</i>	32
IV.1.3	<i>Pressure</i>	32
IV.1.4	<i>Compressibility</i>	32
IV.2	FLUID DYNAMIC	32
IV.2.1	<i>Conservation of momentum:</i>	32
IV.2.2	<i>The Navier-Stokes Equations</i>	34
IV.2.3	<i>Incompressible Flow</i>	35
CHAPTER 2 :DESIGN SOLUTIONS.....		36
I. INTRODUCTION.....		36
II. BALLAST CONCEPT		37
II.1	APPLICATION OF THE MOTION EQUATIONS TO THE VESSEL.....	37
II.1.1	<i>Assumptions</i>	37
II.1.2	<i>Linearisation of the drag force</i>	39
	The least squares method:.....	40
II.2	QUANTITY OF WATER REQUIRED	41
II.3	BALLAST CONCEPT CONCLUSION.....	42
III. DIRECTIONNAL WINGS		43
III.1	ASSUMPTION:.....	43
III.2	FOIL ANGULATIONS COMPUTATION:.....	43
III.3	DIRECTIONAL WINGS CONCLUSION	45
IV. GROUND EFFECT WING		46
IV.1	THE GROUND EFFECT	46
IV.2	SIMULATION:	48
IV.2.1	<i>First simulation</i>	48
IV.2.1.1	Foil sections	48
IV.2.1.2	Simulation Input data.....	49
IV.2.2	<i>Second simulation</i>	51
IV.2.3	<i>Third simulations</i>	54
IV.2.4	<i>Fourth simulations</i>	56
IV.3	CONCLUSION:.....	57
CHAPTER 3 : TESTING.....		58
I. INTRODUCTION.....		58
II. TEST FACILITY.....		59
II.1	GENERAL DESCRIPTION OF EXISTING FACILITIES	59
II.1.1	<i>Example of water tunnel</i>	59
II.1.2	<i>Example of water towing tank</i>	61
II.2	SIMILARITY TO THE REAL CONDITION	62
II.3	INFLUENCE OF THE SCALE	63
II.3.1	<i>Conservation of the Reynold's number:</i>	63

II.3.2	<i>CFD simulation to observe influence of the scale factor influence</i>	64
II.3.2.1	Influence of the global scale ratio:.....	64
II.3.2.2	Influence of the velocity:	65
II.4	DESIGN	66
II.4.1	<i>Tank design</i>	66
II.4.1.1	USHAPE SECTION	67
II.4.1.2	WINDOWS	67
II.4.1.3	LINER.....	67
II.4.2	<i>Towing system design</i>	67
II.4.2.1	RAIL	67
II.4.2.2	TROLLEY	68
II.4.2.3	FOIL / TROLLEY LINKAGE	68
II.4.2.4	PROTECTIVE COATING	68
II.5	MOTOR AND REDUCTION SYSTEM SELECTION	69
II.5.1	<i>Velocity requirement:</i>	69
II.5.2	<i>Required torque at the towing pulley</i>	69
II.5.2.1	Generals equations:.....	69
II.5.2.2	Estimation of the drag force due to the foil tested and the link between the trolley and the foil:.....	70
II.5.2.3	Estimation of the trolley / rail friction force	71
II.5.2.4	Estimation of the trolley inertial force:.....	71
II.5.2.5	Estimation of the cable force	71
II.5.2.6	Force, torque, angular velocity need at the towing pulley	72
II.5.2.6.1	Torque :	72
II.5.2.6.2	Radius velocity (w) :	72
II.5.3	<i>Motor choice</i>	72
	A motor was available in the Institute workshop. Its characteristics are :.....	72
II.5.4	<i>Transmission system design:</i>	73
II.5.5	<i>Motor speed control system</i>	74
II.5.6	<i>Global view of the towing tank</i>	74
II.5.7	<i>Record visualisation system</i>	76
II.5.8	<i>Total cost</i>	77
III.	PROTOTYPES	78
III.1	DESIGN CONSTRAINTS:.....	78
III.2	MATERIAL:	78
III.3	HYDROFOILS:.....	79
III.3.1	<i>Hydrodynamic profiles:</i>	79
III.4	NEUTRAL BUOYANCY SPECIFICATIONS :.....	80
III.4.1	<i>Buoyancy:</i>	80
III.4.1.1	Determination of the foils weight	80
III.5	MANUFACTURING PROCESS:	81
III.5.1	<i>Shaping technique:</i>	81
III.5.1.1	Rigid polyurethane foam:	81
III.5.1.2	Core shaping:	81
III.5.1.3	Stratification:.....	81

IV. TESTS.....	82
IV.1 TESTS CONDITIONS:	82
IV.2 TEST RESULTS	83
CONCLUSION	85
REFERENCES.....	87

- APPENDIX A**
- APPENDIX B**
- APPENDIX C**
- APPENDIX D**
- APPENDIX E**
- APPENDIX F**
- APPENDIX G**
- APPENDIX H**
- APPENDIX I**

INTRODUCTION

BACK GROUND FOR THE STUDY

Ireland's coastal and marine environments hold significant sand and gravel resources. A 1989 Geological Survey of Ireland (GSI) Report noted that sand and gravel is a valuable but depleting resource. The depletion of, and opposition to the use of, land-based sources is leading to an increased pressure to exploit the offshore resource. The extraction of sands and gravels from near shore waters can have implications for the management of coasts, for tourism and the fishing industry.

Actual ocean surveys are done using several methods. One of them is done by divers, who estimate visually the amount and quality of the resources, but this method is limited by the underwater human work capability, and so it is not appropriate for large area of prospecting. Towed submarine equipped with sonar are also used, this solution is able to process a large area due to a towing velocity ranging from 5 to 10 knots, but even if major evolutions have been made lately on sonar data processing, some difficulty are still persisting to obtain an accurate identification of the land-based resources.

Video camera and sonar combination methods are currently under development for sea bed survey, this technology is very promising, but video recording need to be done from a stable and close to the ground vehicle. Autonomous, manned submarine able to support those kind of equipment is one of the proposed solution, but there velocity is limited to a few knots and also very expensive to produce, maintain and to run.

OBJECTIVES OF THE PROJECT

The objective is to develop a towed underwater vehicle, able to fly at constant distance from the sea bed, cheap to produce, maintain and run. Data analysis would be conducted from both video and sonar. This vehicle will be cheaper and smaller than manned submarines, as well as cheaper and more accurate than existing towed vehicles . An accurate survey of a large area

could, therefore, be performed in a minimal time. This device would optimise the efficiency and cost of continental shelf survey.

The aim of this study is to establish the feasibility of such a vehicle, and propose a conceptual design of a wing able to fly at a constant distance from the sea bed.

This work will present a Computational Fluid Dynamics (CFD) analysis performed on different wing designs, the towing tank and wing models build to conduct experimental tests, and a conceptual design of the vehicle.

ORGANISATION OF THE WORK

This work is organised into three chapters:

Chapter 1 supplies a literature review necessary to follow this work, with:

- A review of existing product used in ocean survey,
- An introduction to the specifications of continental shelf,
- A review of submarine and foils design,
- A theoretical background on fluid dynamics.

Chapter 2 presents several design concepts and select the most suitable for the vehicle. The following points are developed:

- Study of a ballast solution
- Study of a directional wings solution
- Study of a ground effect solution

Chapter 3 presents test conducted on several models and conclude by proposing a conceptual design for the vehicle. The following points are developed:

- Design and manufacture of the test facilities
- Design and manufacture of the tested models
- Model testing and results

CHAPTER 1 : LITERATURE REVIEW

I. EXISTING PRODUCTS:

Ground flyer vehicles are devices designed to float at a constant from the sea bed. None of the existing devices is suitable for the purpose of ground flyer vehicles. However, they give an idea of technologies currently used on towing underwater vehicle, commonly called "fish".[1,2,3,4,5,6,7]

I.1 AQUASHUTTLE MARK III

The Aquashuttle MK III is a stable, highly robust, versatile undulating towed vehicle for deploying a wide range of oceanographic monitoring equipment. Designed and developed by Chelsea Instruments and the Plymouth Marine Laboratory, UK.



Figure 1 Aquashuttle MK III

The vehicle has a strong glass reinforced plastic body with a robust integral stainless steel framework, which can accommodate a wide range of sensor payloads. Its 'flight' profile is maintained by a servo-controlled elevator, the servo being powered by the vehicles own impeller driven alternator.

Real-time control and data display enable the operator to observe the two-dimensional oceanographic conditions and adjust the flight parameters accordingly. Capable of tow speeds from 5 to 25 knots, Aquashuttle will undulate from the surface to 100m.

Applications:

- Oceanographic data gathering from ships of opportunity
- Ecosystem health monitoring
- Real-time two dimensional data gathering in support of oceanographic modelling
- Pollution monitoring and dye tracing studies

- Sea truthing for satellite remote sensing
- Continuous plankton monitoring and sampling
- Estuary coastal zone and open ocean surveys
- Local area site assessment.

1.2 NU-SHUTTLE

The Nu-Shuttle [1] is a stable, robust, versatile undulating towed vehicle for the deployment of a wide range of oceanographic monitoring equipment. Developed by Chelsea Instruments and the Plymouth Marine Laboratory, UK, Nu-Shuttle has been designed to meet the requirements for a low cost, large payload vehicle, which retains the hydrodynamic performance of the Aquashuttle.



Figure 2 **Nu-Shuttle**

Nu-Shuttle is 500mm wide and offers 100 litres of instrumentation space. The vehicle is capable of carrying a suite of instrumentation for the measurement of parameters such as conductivity, temperature, depth, chlorophyll, hydrocarbon and Gelbstoff fluorescence, turbidity, transmittance, bioluminescence, nutrient, redox and dissolved oxygen. It also has the capacity to carry a mechanical Plankton Sampler or an Optical Plankton Counter.

Nu-Shuttle has a stainless steel frame onto which Polyethylene panels are fixed. With this simplicity of construction comes the advantage of ease of access to the total payload area by removal of individual panels.

Nu-Shuttle can be towed from research vessels and ships of opportunity at speeds of 5 to 15 knots, to operational depths of 150m. It can be launched and recovered while the vessel is underway, by a non-scientific crew with minimal training.

Applications:

- Oceanographic data gathering from ships of opportunity
- Ecosystem health monitoring
- Real-time two dimensional data gathering in support of oceanographic modelling
- Pollution monitoring and dye tracing studies
- Sea truthing for satellite remote sensing

- Continuous plankton monitoring and sampling
- Estuary coastal zone and open ocean surveys
- Local area site assessment

1.3 SEASOAR MARK II

SeaSoar [1] is a versatile towed undulating vehicle used to deploy a wide range of oceanographic monitoring equipment. Developed by Chelsea Instruments from an original design by the Institute of Oceanographic Sciences (now the Southampton Oceanography Centre, UK).

SeaSoar is capable of undulating from the surface to 500 metres at tow speeds of up to



Figure 3 SeaSoar Mark II

12 knots (with faired cable) following a controlled and adjustable undulating path through the ocean. Maximum depth achieved is dependent upon system configuration. The PC based SeaSoar Deck Control Unit onboard the ship enables the operator to have real-time computer control over the vehicle's flight profile together with the storage and display of the flight parameters.

Sampled data, obtained from sensors mounted in SeaSoar, are transmitted to the towing vessel for processing, display and storage via a multi-core tow cable. The high data rate and versatility of sensor and sampling packages make SeaSoar an effective and productive platform for large-scale data collection.

The payload area is located within a stainless steel, deep-sided frame that provides strength and volume for instrumentation installation. Quick release stainless steel panels, top and bottom, can be removed without tools and give maximum possible accessibility to the payload.

Applications:

- Open ocean mesoscale oceanographic surveys
- Has been used extensively in most oceans of the world including the Arctic Marginal Ices zone by the UK Defence Research Agency

1.4 KLEIN SUB-BOTTOM PROFILER

The Klein Sub-Bottom Profiler [2] [3] is a 1m long stainless steel and fibre glass device, , weighting 79 kg in air and 65 kg in water. With a maximum operating depth of 600m from the surface, it is capable of recording information at a 60m radius at tow speeds of up to 7 knots.

Modular in design, the Sub-Bottom Profiler can be integrated with the Klein Side Scan Sonar

Towfish. Processed data are displayed as a continuous record on a hard copy recorder or video display.

Application :

- High-resolution profiling of seafloor sediments

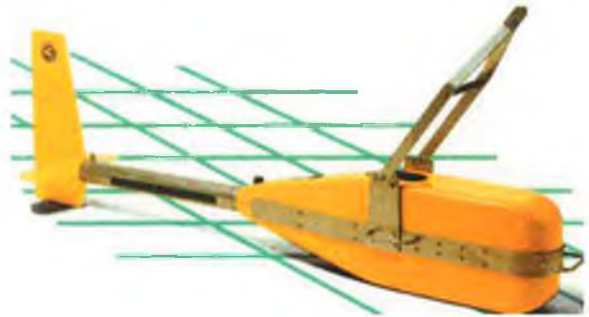


Figure 4

Klein Sub-Bottom Profiler

1.5 FLYING FISH

The Flying Fish, from the Ocean Engineering Group at RIAM [4] [5], is a 3.8m long device, weighting 1300 kg in air and -20 kg in water. It is capable of operating at a maximum depth of 200m from the surface and a tow speed of up to 12 knots.

A main wing and horizontal tail wings controls the heave, pitch and roll of FLYING FISH, which permit its stable attitudes and assure accurate measurements.

Application :

- Chemical and physical measurements to obtain specially continuous and real time data of current velocities, salinity, water temperature, dissolved O₂, CO₂, pH, Chlorophyll in an ocean mixed layer.



Figure 5

Flying Fish

1.6 SEA KITE

Most relevant to this work is the Sea Kite, from Tokai University [6][7]. This UTV (underwater towed vehicle) is composed of a fuselage and several wings having the functions of depth control, altitude control and laterally moving control with stable attitude. CCV (Control Configured vehicle) technology in aeronautical field (Kanai, 1985 and Kato, 1985) is adopted to satisfy the attitude control. According to this technology, the optimum configuration of a vehicle for a particular mission is designed considering motion control and its stability, and a vehicle is actively controlled decoupling some components of the motion. This system propose a new type of autonomous underwater vehicle (AUV) with CCV control with three decoupled modes:

- Pitch angle and vertical velocity,
- Pitch angular velocity and vertical velocity
- Roll angle and yaw angle

The treatment of the attitude control of UTV proposed is different from that of AUV in three points:

- No linearity of motion due to the existence of cable,
- Effect of cable motion on the stability of UTV
- Decoupled mode in the horizontal plane.

For the third point decoupling between roll angles, yaw angle and lateral velocity is taken.

ITEMS		VALUES	ITEMS		VALUES
Length of Fuselage		2.0 m	Vertical Canard	Chord	0.151 m
Volume of Fuselage		0.182 m ³		Span	0.604 m
Mass of Fuselage		182.88 Kg	Upper Vertical Tail	Chord	0.205 m
Main Horizontal Wing	Chord	0.484 m		Span	0.818 m
	Span	0.987 m	Lower Vertical Tail	Chord	0.138 m
Horizontal Tail	Chord	0.247 m		Span	0.551 m
	Span	0.494 m	Location of Vertical Cannard (lv)		0.8 m
Location of Horizontal Wing (lw)		0.0 m	Location of Vertical Tail (lt)		0.7 m
Location of Horizontal Tail (lt)		0.7 m			

Table 1 Sea Kite characteristics

Horizontal wings

The forward horizontal wing is fixing at the centre of co-ordinate system and that of the rear horizontal wing at $l_f=0.7$ m, they obtain the ratio P_1 of the total area of the horizontal wings to the Longitudinal projected area of fuselage and the ratio of the area of the horizontal tail to the main wing under the vertical target movement of ± 200 m around the depth of 500 m and under the conditions of the wing angles less than 15° and of the pitch angle of the vehicle of 0° .

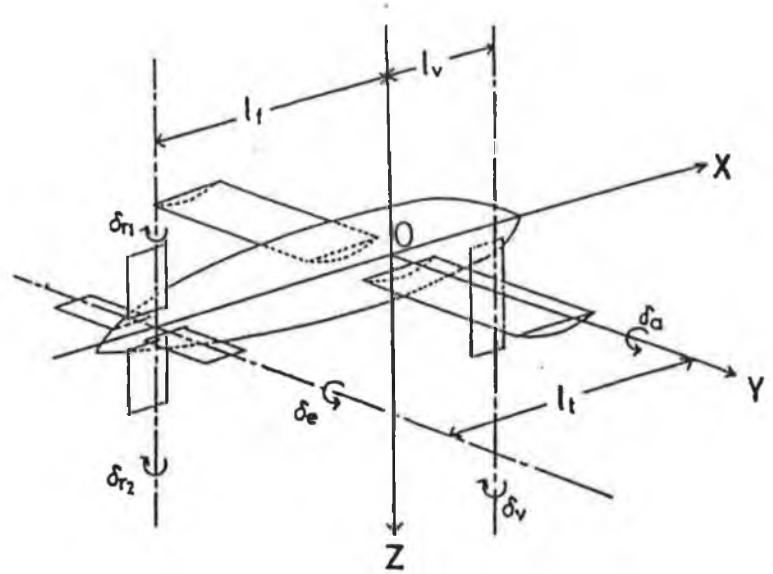


Figure 6 Sea Kite

The equilibrium state is taken when the wing angle of the main wing is at 0° at the designed depth of 500m. Here, the ascending altitude is defined as altitude where the angle of inclination of cable at the hanging point of the vehicle is 90° . It was possible for the vehicle to exert the descent of 200 m over the range of P_1 and P_2 with the angle of the main wing of -15° . They choose P_1 and P_2 as 2.0 and 0.2, respectively. In this case the cable length is 1289.0 m.

Vertical Wings:

Fixing the location of the vertical wings at $l_v=0.9$ and $l_f=0.7$ m, they obtain the ratio Pa_3 of the area of the upper vertical tail to the longitudinal projected area of fuselage, the ratio Pa_4 of the area of the lower vertical tail to the longitudinal projected area of fuselage and the ratio Pa_5 of the area of the vertical canard to the longitudinal projected area of fuselage under the lateral target movement of ± 100 m and under the conditions of the wing angles less than 15° and of the yaw and roll angles of 0° . To prevent asymmetric side force about X-Y plane, they take:

$$Pa_3 = Pa_4 + Pa_5$$

I.7 SYNTHESIS OF THE EXISTING PRODUCTS:

Product	Speed	Deep	Control Method	Material	Dimension
Aquashuttle Mark III	5 to 25 knots	0-100m	Undulating towed vehicle	unknown	unknown
Nu-Shuttle	5 to 15 knots	0-150m	Undulating towed vehicle	Stainless steel frame Polyethylene panels	500mm wide 100 litres
SeaSoar Mark II	12 knots	0-500m	Undulating towed vehicle	Stainless steel panels	unknown
Klein Sub-Bottom Profiler	7 knots	300m	unknown	Stainless Steel and Fiberglas	1.07x0.22x0.41 m 79.4kg(air) 64.4kg(water)
Flying Fish	0-12knots	0-200m	Heave, pitch, roll Ballast & Directional wings	unknown	3.84x2.26x1.4m 1300kg (air) -20kg (water)
Sea Kite	unknown	500m	3D controlled by attitude & positioning sensors, Directional wings	unknown	2x1x1m Around 200kg (air)

II. CONTINENTAL SHELF

II.1 OCEAN MORPHOLOGY

The ocean is composed of different areas with different slopes and depths, from a few metres to thousands of metres depth with an average of 4000m and from nearly nil slopes to vertical cliffs as shown on the following maps. [8]

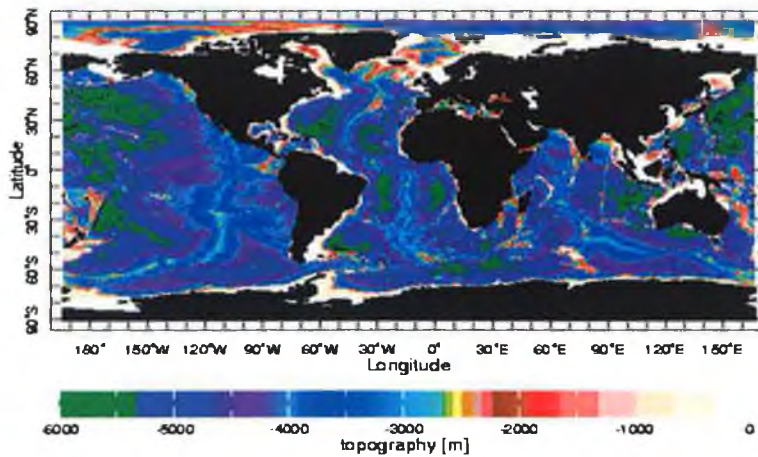


Figure 7 Global ocean topography

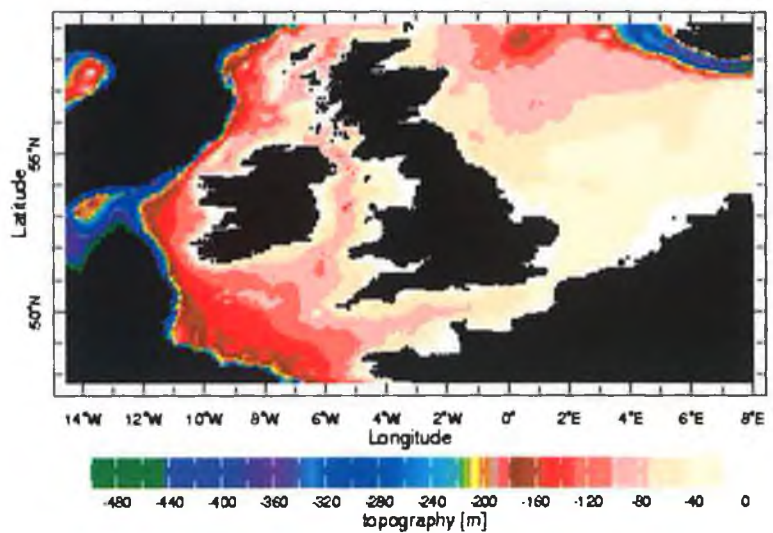


Figure 8 British seas topography

II.1.1 Deep sea:

Deep bottom area: Submerged portion of coast from 200-m depth to deep ocean floor. [9][10]

II.1.2 Continental margin

Continental margin: The zone of transition from a continental mass to the adjacent ocean basin. It generally includes a continental shelf, continental slope, and continental rise. [9][10]

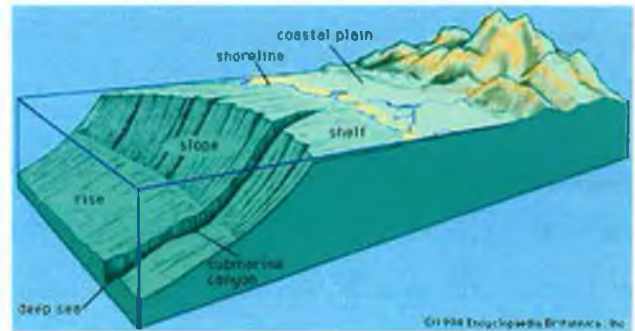


Figure 9 Divisions of the continental margin

II.1.2.1 Continental shelf

The continental shelf is a zone adjacent to a continent or around an island, and extending from the low-water line to the depth at which there is usually a marked increase of slope to greater depth. The shelf is made shallower by deposition of material eroded from the land. The shelf has an average slope less than 0.07° and a maximum of 3° with a maximum depth of 200m

II.1.2.2 Continental slope:

Continental slope is the narrow, steep (3 deg. to 6 deg. gradient) transition zone between the shallow shelf and the deep ocean floor, usually demarcated by the 200 metre isobaths. Sedimentary material on the continental slope is very unstable because of the steep gradient.

II.1.2.3 Continental rise

The wedge of sediments deposited at the base of the continental slope.

II.2 THE IRISH CONTINENTAL SHELF

The width of the Irish continental shelf ranges from 90km to approximately 300km from the shore and represents an area of 850,000km². [11][12]

The Irish Continental Shelf area is relatively unexplored in terms of detailed geology and little is known about recent sedimentary processes such as mass flows, submarine channel morphology and slope stability.

III. DESIGNS AND CONCEPTS

III.1 SUBMARINE DESIGN:

III.1.1 Buoyancy

Buoyancy is the tendency for a fluid to exert a supporting force on a body placed in the fluid. This force is called a buoyant force and is defined by Archimedes' principle as stated below.[13]

Archimedes' principle :

A body in a fluid, whether floating or submerged, is buoyed up by a force equal to the weight of the fluid displaced. The buoyant force acts vertically upward through the centroid of the displaced volume and can be defined mathematically by the following equation:

$$F_b = \gamma_f \times V_d \quad \text{Equation III-1}$$

Where:

- F_b = buoyant force
- γ_f = specific weight of the fluid
- V_d = displaced volume of the fluid

When a body is floating freely, it displaces a sufficient volume of fluid to just balance its own weight. Figure 10 shows several devices which might be used in an undersea exploration project and which illustrate four different types of buoyancy problems:

- The buoy (a) and the ship (e) must be designed to float stably.
- The instrument package (b) would tend to float if not restrained by the anchoring cable.
- The diving bell (c) must be supported by the crane on a ship, while the submarine (d) has the ability to hover at any depth (this is called neutral buoyancy).

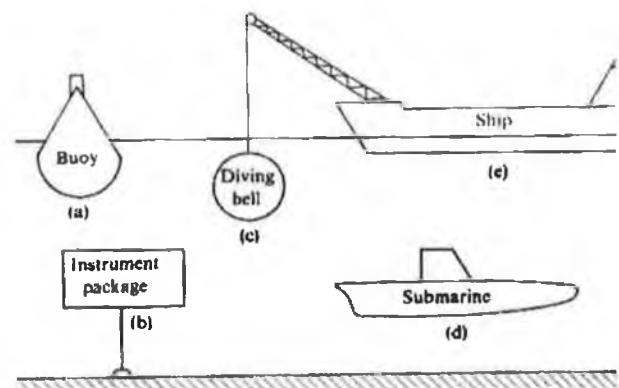


Figure 10 different applications of buoyancy

If the buoyant force is greater than the weight of the boat, this one will float all the time. In this case the buoyancy is termed positive.

If it is the Weight of the vessel, which is greater than the buoyant force the boat will sink and the buoyancy is termed negative.

If the buoyant force is equal to the weight of the boat, this one will stably float underwater. In this case the buoyancy is termed neutral.

III.1.2 Live scale dive technology

There are two ways to submerge a boat: *static* diving and *dynamic* diving. [14]

III.1.2.1 Static diving

The buoyancy of a submarine can be changed by letting water into the Main Ballast Tanks (MBT). The MBT's can be located in three different ways:

- Inside the pressure hull
- Outside the pressure hull as additional tanks
- In between the outer hull and the pressure hull

Figure 11 shows the three possible configurations. Drawback of having the MBT inside the pressure hull is obvious: it takes up space that could otherwise be used for equipment or personnel. This MBT arrangement was used in the WW-I boats and other early submarines. The classical example of a boat with MBT's outside the pressure hull is the German Type VIIC but also American and Dutch submarines in WW-II used this design. Due to the location of the MBT's, they are called saddle tanks. Most modern military submarines use the space in-between the inner pressure hull and the outer hull as MBT.

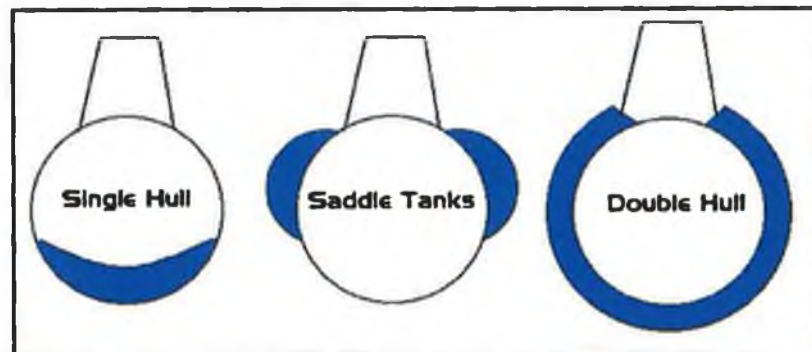


Figure 11: Different locations of the main ballast tank.

To dive the boat, the vent valves on top of the ballast tanks are opened to let air escape the MBT. To surface the boat, the water in the MBT's is forced out by pressurized air. When the boat is deeply submerged, the water is forced out using high-pressure air to overcome the water pressure. When the boat is near the surface, the blowing of the MBT's proceeds with low-pressure air.

At the surface, the main vent valve remains shut to keep the air in the MBT under pressure. The pressure inside the tanks remains equal to that of the low-pressure air system.

Maintaining neutral buoyancy in a submarine is a continuous procedure. For example the diesel engines consume fuel and the personnel eats food so that the total weight of the boat steadily decreases during a mission. This means that while progressing with the mission, the amount of water in the MTT has to be increased to maintain neutral buoyancy. Also the density of the surrounding water plays an important role. A well-known example is the downstream area of a river where fresh and salt water mix leading to a different density than in the open sea. If a submarine enters such a region, the trim has to be adjusted.

When neutral buoyancy is obtained with the MTT's, the depth of the boat can be changed using the speed of the boat and the angle of the dive planes. This is called dynamic diving.

III.1.2.2 Dynamic Diving

The fully dynamic diving boats are the most simple model submarines available. These boats have inherent positive buoyancy which means that they will float back to the surface if control is lost. This is a major advantage for model submarines. To get a positive buoyant boat under the water, the force on the hydroplanes has to overcome the upward force of the floating boat. This requires a combination of sufficient speed or sufficiently large hydroplanes. The closer the boat is rigged towards neutral buoyancy, the smaller the required downward force of the hydroplanes.

Figure 12 shows the angle of the dive planes to keep a positive buoyant submarine under the water. At low velocity, both planes have a downward angle (on the left hand side of Figure 12). The aft hydroplanes are needed to



Figure 12: Angle of the hydroplanes.

prevent the stern of the bow rising above the surface. Just like for the real boats, at sufficiently high velocity the hydroplane can be moved to a neutral position also depth control can be maintained with the fore plane only (on the right hand side of Figure 12).

The force on a hydroplane, which is termed lift force, can be calculated with the following equation:

$$F_L = \frac{1}{2} C_L (\rho v^2) A \quad \text{Equation III-2}$$

Where:

- $F_L(N)$ is the lift force,
- C_L is the lift coefficient which is dependent on the shape of the hydroplanes and also on the angle of attack,
- ρ (kg/m^3) is the fluid density. equal to $1025 kg/m^3$,
- v (m/s) is the velocity of the free stream of fluid relative to the hydroplane. So in this case, that will be the velocity of the boat.
- A (m^2) is the area defined as the product of the span and the length of the hydroplane.

III.1.3 Underwater vehicle stability

The equilibrium condition for submarines, submersibles, balloons, dirigibles and similar vehicles is simply $W = F_B$, where the forces W and F_B must act in the same vertical line. The centre of gravity G and the centre of buoyancy B are both fixed in the vehicle, which takes up a definite attitude in its equilibrium configuration. Thus B must lay either vertically below or vertically above G if W and F_B are the only external forces acting when the vehicle is at rest in its intended attitude. It is the stability of these equilibrium configurations that must now be examined. [15][16][17]

Small disturbances of translation in a horizontal direction do not change the condition of equilibrium. As far as they are concerned the stability is neutral.

To study the effect of small angles of rotation, the vehicle could be conveniently rotated around two horizontal axes at right angles to each other. (Rotation about the vertical axis clearly does not affect the condition of equilibrium.) For example, consider the submerged

submarine represented in Figure 13. It is evident that if B is above G a small inclination of heel or trim produces a righting couple, and so the arrangement in Figure 13 (a) is associated with hydrostatic stability. By contrast the arrangement in Figure 13 (b) shows that if G lies above B there is a tendency for any small inclination to be increased, and so the equilibrium is unstable. The distance GB thus represents a measure of a submarine's hydrostatic stability for heel and trim.

In practice B cannot lie far from the central axis of a submarine, therefore stability G must lie below the centre line.

It is implicitly assumed in the foregoing discussion that the submarine in question has a rigid and incompressible structure..

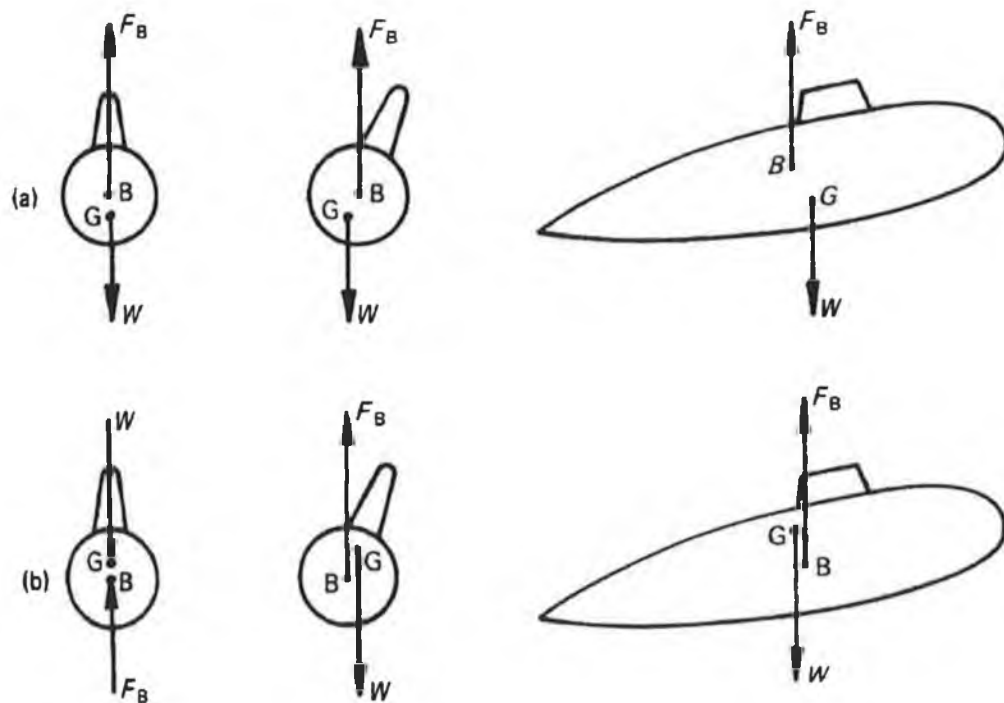


Figure 13 Submarine stability

III.2 FOILS DESIGN:

III.2.1 Foils geometry

[18][19][20][21]

III.2.1.1 Wing definition

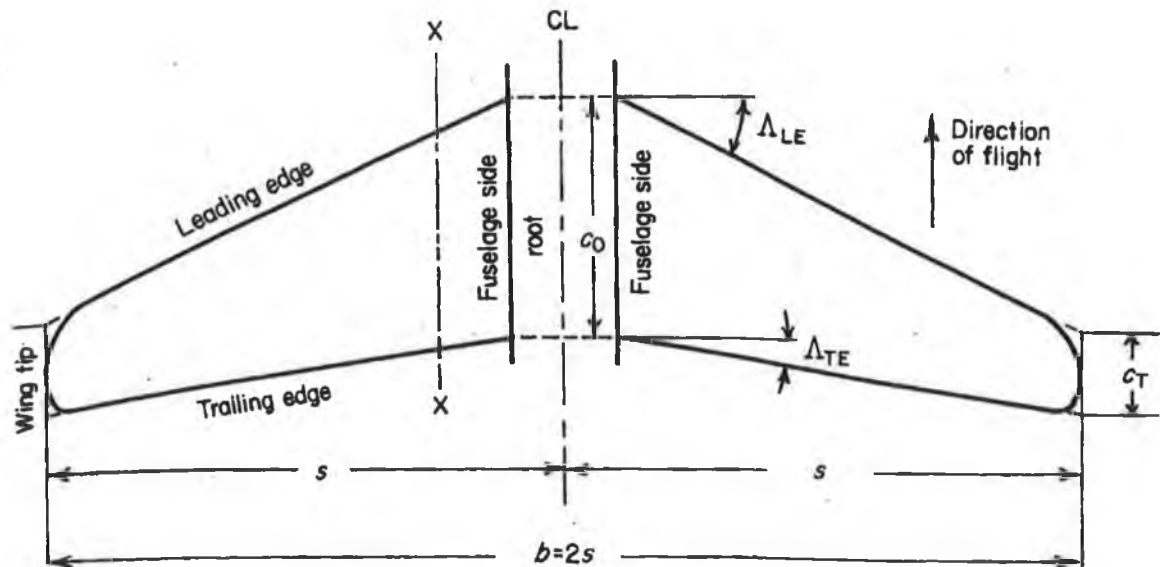


Figure 14 wing representation

Wing span: The wing span is the dimension “ b ”, the distance between the extreme wingtips. The dimension from each tip to the centre-line s is the wing semi-span.

Chords: The chord is the distance between of the leading and trailing edges. The two dimensions C_t and C_o are the tips and root chords respectively. The ratio C_t/C_o is the taper ratio λ , For most wings, $C_t/C_o < 1$.

Mean chords: The standard mean chord or the geometric mean chord is denoted by \bar{c} , defined by S_G/b or S_N/b .

Wing area: The plan area of the wing including the continuation within the fuselage is the gross wing area, S_G . The plan area of the wing excluding the continuation within the fuselage is the net wing area, S_N .

Aspect ratio: The aspect ratio is a measure of the narrowness of the wing platform. It is denoted by A or (AR)

$$A = \text{span}/\text{mean chord} = b/\bar{c} \quad \text{Equation III-3}$$

$$\text{or } A = \text{span}^2/\text{area} = b^2/(b\bar{c}) \quad \text{Equation III-4}$$

If A increase the maximum lift increase as well

Sweepback: The sweepback angle of a wing is the angle between a line drawn along the span at a constant fraction of the chord from the leading edge, and a line perpendicular to the centre-line. It is usually noted Λ or Φ .

Dihedral angle: The angle 2Γ is the dihedral angle of the wings. If the wings are inclined upward, they are said to have *dihedral*, if inclined downwards they have *anhedral*.

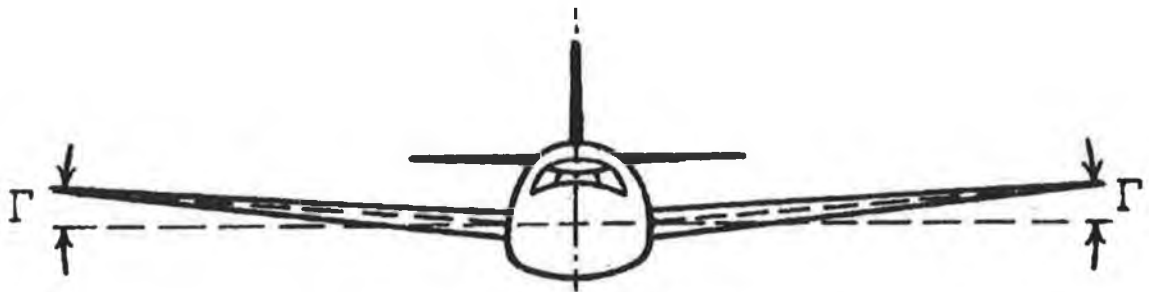


Figure 15 Dihedral angle

III.2.1.2 Wing section definition:



Figure 16 Wing section definition

Chord-Line (1): The straight line connecting the leading and trailing edges of the airfoil is the Chord Line.

Chord (2): The length of the chord-line from leading edge to trailing edge and is the characteristic longitudinal dimension of an airfoil is the Chord.

Camber: the curvature of an airfoil at its surfaces.

Mean Camber Line (3): The line drawn halfway between the upper and lower surfaces is the Mean Camber Line. The chord line connects the ends of the mean camber line. The mean camber of an airfoil may be considered as the curvature of the median line (mean camber line) of the airfoil.

Maximum Camber (4): The shape of the mean camber is important in determining the hydrodynamic characteristics of an airfoil section. Maximum Camber (displacement of the mean camber line from the chord line) and where it is located (expressed as fractions or percentages of the basic chord) help to define the shape of the mean camber line.

The **Maximum Thickness (5)** of an airfoil and where it is located (expressed as a percentage of the chord) help define the airfoil shape, and hence its performance.

The **Leading Edge Radius (6)** of the airfoil is the radius of curvature given the leading edge shape.

The airfoil shown in Figure III-7 is a **Positive Cambered Airfoil** because the mean camber line is located above the chord line.

III.2.1.3 NACA section

The co-ordinates of the upper and lower surface can characterise airfoil geometry. It is often summarised by a few parameters such as: maximum thickness, maximum camber, position of max thickness, position of max camber, and nose radius. One can generate a reasonable airfoil section given these parameters. Eastman Jacobs [18] did this in the early 1930's to create a family of airfoils known as the NACA Sections.

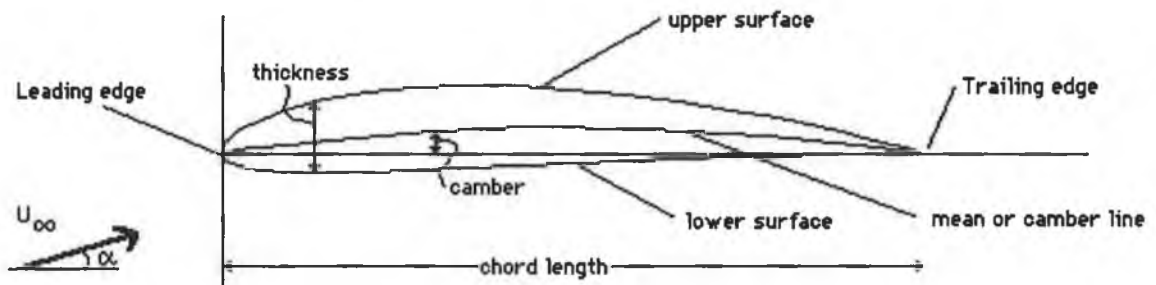


Figure 17 NACA section

The NACA 4 digits and 5 digits airfoils were created by superimposing a simple mean line shape with a thickness distribution that was obtained by fitting a couple of popular airfoils of the time:

$$y = \pm(t/0.2) \cdot (0.2969x^{0.5} - 0.126x - 0.3537x^2 + 0.2843x^3 - 0.1015x^4)$$

The camber line of 4-digit sections was defined as a parabola from the leading edge to the position of maximum camber, then another parabola back to the trailing edge.

NACA 4-Digit Series:

Ex : NACA 4412

4	4	12
Max camber in % chord	Position of max camber in 1/10 of chord	Max thickness in % of chord

Table 2 NACA 4 Digit Series

III.2.2 Hydrodynamics forces

[20][21][22]

III.2.2.1 Definition

For a flight direction of X:

The Lift: L component of force acting in upward in the perpendicular direction of flight (-Z)

The Drag: D component of force acting in the opposite direction of flight (-X)

Crosscurrent force: Y Component of forces mutually perpendicular to the lift and the drag

Pitching moment: M moment acting in the plan containing the lift and the drag

Rolling moment: L_R moment tending to depress one wing tip and raise the other, it is positive when it tends to depress the starboard wing tip

Yawing moment: N is the moment, which tends to swing the nose to one side or the other of the flight direction. It is positive when it swing, the nose to starboard

III.2.2.2 Dimensional theory:

F denotes the hydrodynamic force or one of its components. For fully immersed device, F depends on the following quantities: Fluid density ρ , fluid kinematics' viscosity ν , stream speed V and fluid bulk elasticity K.

The force and moment will also depend on the shape and size of the body and its orientation to the stream. If however, attention is confined to geometrically similar bodies, e.g. spheres or any geometry to different scales, the effects of the shape as such will be eliminated. A single typical dimension, denoted by D, can represent the size of the body.

$$F=f(V,D,\rho,\nu,K)$$

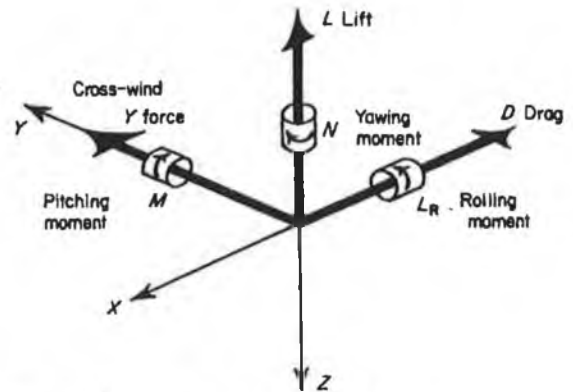


Figure 18 hydrodynamic forces

The quantity $F/ \rho V^2 D^2$ is a non-dimensional quantity often developed and used in hydrodynamics. It is not, however, used in quite this form. In place of ρV^2 it is conventional to use $\frac{1}{2} \rho V^2$, the dynamic pressure of the stream, if incompressible

$$C_F = \frac{F}{\frac{1}{2} \rho V^2 S} \quad \text{Equation III-5}$$

Lift coefficient C_L
$$C_L = \frac{\text{Lift}}{\frac{1}{2} \rho V^2 S} \quad \text{Equation III-6}$$

Drag coefficient C_D
$$C_D = \frac{\text{Drag}}{\frac{1}{2} \rho V^2 S} \quad \text{Equation III-7}$$

Pitching moment coefficient C_M
$$C_M = \frac{F}{\frac{1}{2} \rho V^2 S \bar{c}} \quad \text{Equation III-8}$$

III.2.2.3 Hydrofoil characteristics - lift coefficient versus incidence

Effect of aspect ratio on the $C_L: \alpha$ curve

The induced angle of incidence ϵ is given by

$$\epsilon = \frac{k C_L}{\pi A} \quad \text{Equation III-9}$$

Where A is the aspect ratio.

Considering a number of wings of the same symmetrical section but of different aspect ratios the above expression leads to a family of C_L versus α curves, as in Figure 19

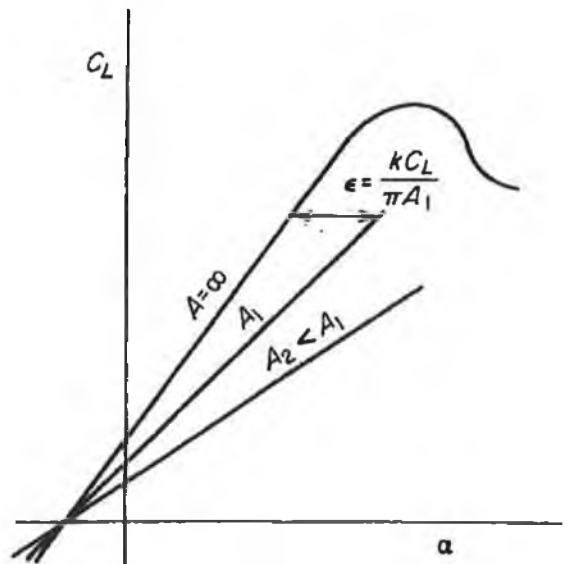


Figure 19 Influence of wing aspect ratio on the lift curve

Since the actual lift coefficient at a given section of the wing is equal to the lift coefficient for a two-dimensional wing at an incidence of α_∞ .

For highly swept wings of very low aspect ratio (less than 3 or so), the lift curve slope becomes very small.

III.2.2.4 Effect of Reynolds number on the C_L

The ratio known as the Reynolds number, Re is:

$$Re = \rho V l / \mu \quad Re \sim \text{inertial forces} / \text{viscous forces} \quad \text{Equation III-10}$$

Where ρ is the density of the fluid, V is the velocity, l is a representative length such as the diameter of a pipe, the length of a ship, the chord of an airfoil, and μ is the kinematics viscosity. The Reynolds number is dimensionless

If $Re \ll 1$ the viscous effects are dominating

If $Re \gg 1$ the inertial effects are dominating

$Re_c \sim 5 \cdot 10^5$ is the critical value of Reynolds number, up to this value, the flow is laminar, after the flow is turbulent

Reduction of Reynolds number moves the transition point of the boundary layer rearwards on the upper surface of the wing. At low values of Re this may permit a laminar boundary layer to extend into the adverse pressure gradient region of the hydrofoil.

III.2.2.5 Lift and Drag force on Airfoils

Lift is defined as force acting on a body in a direction perpendicular to that of the flow of the fluid. The shape of the airfoil comprising the wings of an airplane determines its performance characteristics.

The manner in which an airfoil produces lift when placed in a moving air stream (or when moving in still air) is illustrated in Figure 20. As the air flows over the airfoil, it achieves a high velocity on the top surface with a corresponding decrease in pressure. At the same time the pressure on the lower surface is increased.

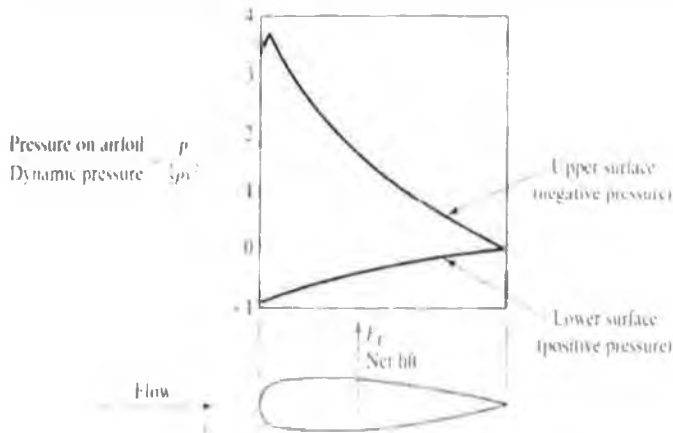


Figure 20 Pressure distribution on an airfoil.

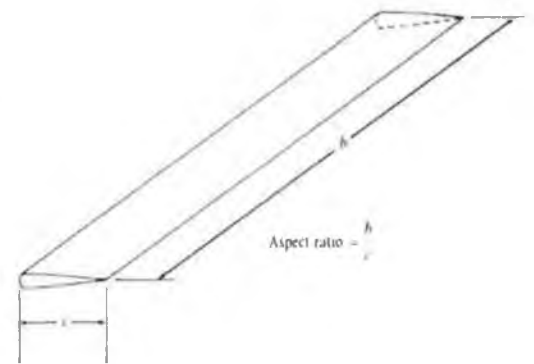


Figure 21: sketch of an airfoil.

The net result is an upward force called lift. The lift force F_L is expressed as a function of a lift coefficient C_L :

$$F_L = \frac{1}{2} C_L (\rho v^2) A \quad \text{Equation III-11}$$

The velocity v is the velocity of the free stream of fluid relative to the airfoil. In order to achieve uniformity in the comparison of one shape with another, the area A is usually defined as the product of the span of the wing and the length of the airfoil section called the *chord*. In Figure 42, the span is b and the chord length is c .

The value of the lift coefficient C_L is dependent on the shape of the airfoil and also on the angle of attack. Figures 22 & 23 shows that the angle of attack is the angle between the chord line of the airfoil and the direction of the fluid velocity.

Other factors affecting lift are the Reynolds number, the surface roughness, the turbulence of the air stream, the ratio of the velocity of the fluid stream to the speed of sound, and the aspect ratio.

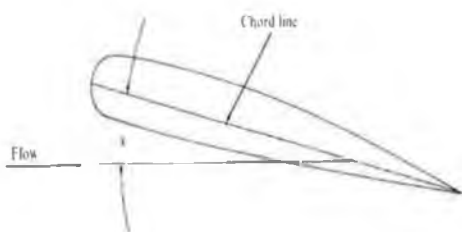


Figure 22 Angle of attack.

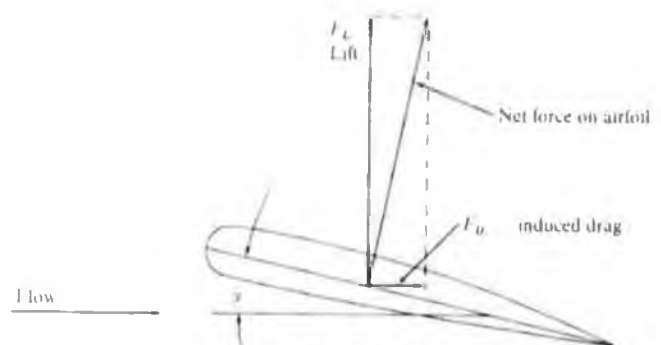


Figure 23 induced drag

Aspect ratio is the name given to the ratio of the span b of the wing to the chord length c . It is important because the characteristics of the flow at the wing tips are different from those toward the centre of the span.

The total drag on an airfoil has three components:

- Friction drag,
- Pressure drag,
- And the third component is called induced drag, which is a function of the lift produced by the airfoil.

At a particular angle of attack, the net resultant force on the airfoil acts essentially perpendicular to the chord line of the section, as shown in Figure III- 14. Resolving this force into vertical and horizontal components produces the true lift force F_L and the induced drag F_{Di} . Expressing the induced drag as a function of a drag coefficient gives:

$$F_{Di} = \frac{1}{2} C_{Di} (\rho v^2) A \quad \text{Equation III-12}$$

It can be shown that C_{Di} is related as follow to C_L :

$$C_{Di} = \frac{C_L^2}{\pi(b/c)} \quad \text{Equation III-13}$$

The total drag is then:

$$F_D = F_{Df} + F_{Dp} + F_{Di} \quad \text{Equation III-14}$$

Normally, it is the total drag that is of interest in design. The total drag can be calculated from the drag coefficient C_D for the airfoil, using the following relation:

$$F_D = \frac{1}{2} C_D (\rho v^2) A \quad \text{Equation III-15}$$

As before, the area A is the product of the span b and the chord length c .

Two methods are used to present the performance characteristics of airfoil profiles.

In Figure 24, the values of C_L , C_D , and the ratio of lift to drag F_L/F_D are all plotted versus the angle of attack as the abscissa. Note that the scale factors are different for each variable. The

airfoil to which the data apply has the designation NACA 2409 according to a system established by the National Advisory Committee for Aeronautics[22].

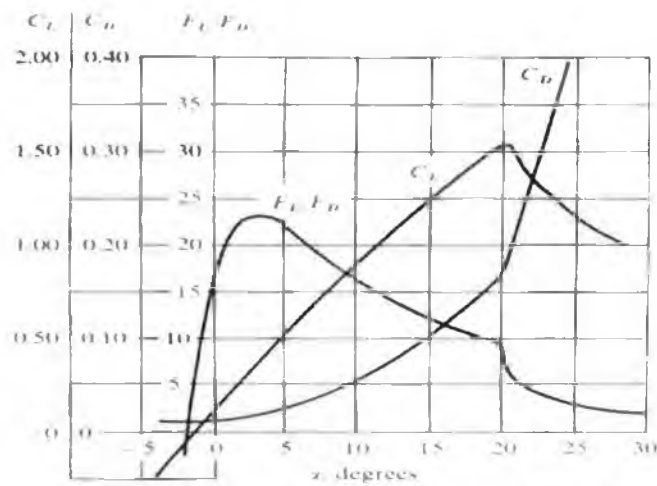


Figure 24 Airfoil performance curves.

The second method of presenting data for airfoils is shown in Figure 25. This is called the polar diagram and is constructed by plotting C_L versus C_D with the angle of attack indicated as points on the curve.

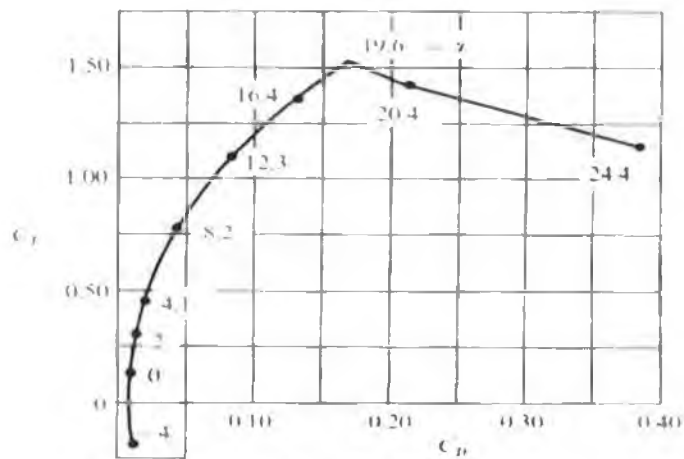


Figure 25 Airfoil polar diagram

In both Figures 24. and 25., it can be seen that the lift coefficient increases with increasing angle of attack up to a point where it abruptly begins to decrease. This point of maximum lift is called the *stall* point; at this angle of attack the boundary layer of the air stream separates from the upper side of the airfoil. A large turbulent wake is created, greatly increasing drag and decreasing lift.

III.2.3 Wing in ground effect vehicles

III.2.3.1 Wing in Ground Effect vehicles

Wing in Ground Effect vehicles were pioneered by the Soviet Union during the Cold War as high-speed craft for maritime operations. The so called Caspian Sea Monster aroused a great deal of interest when it was unveiled to the world looking to be much the same size as a C-130 Hercules, yet travelling at nearly twice the speed with a far greater payload. [23]

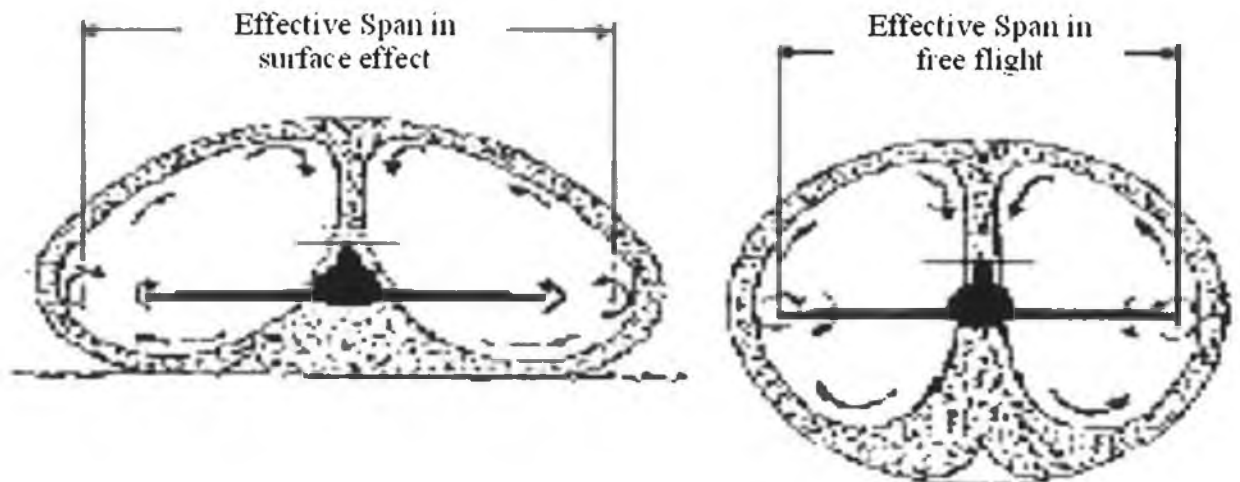


Figure 26 Ground Effect vehicles

To fly in any fluid, lift is generated by means of a pressure differential between the upper and lower surfaces of a streamlined shaped body. Whether in free flight or ground effect the plan form places a footprint pressure on the supporting air called wing loading.

In the case of Ground Effect craft, their lifting surfaces generate a low pressure by virtue of curvature, while underneath is a cushion of super compressed air. This is effectively rammed in as if a filling in a sandwich between the wing and the ground.

Climbing out of the ground effect allows expansion of the filling resulting in loss of lift. The only way to regain this is to increase the wingspan but this changes the WGE craft into an aeroplane. The lift to drag ratio of Wing ships is significantly higher than conventional aircraft, which in effect means less power to achieve a comparable speed or greater speed for the same power.

III.2.3.2 Computational fluid dynamics on ground effect aerodynamics

The accurate prediction of ground effect aerodynamics is an important aspect of wing-in-ground effect vehicle (WIG) design [24]. Computational fluid dynamics (CFD) solutions are

useful alternatives to expensive (especially in the case of ground effect) wind tunnel testing. However, the incorporation of the rigid surface effects often leads to confusion due to such a model being in a vehicle fixed reference frame (air moving, vehicle fixed) rather than the real-life situation of a ground fixed reference frame (air fixed, vehicle moving). [24]

Previous investigations have considered the simple two-dimensional (no sideslip) case, assuming a flat, rigid surface. To accurately model the real-life situation, other important considerations that may need addressing in a ground effect simulation include the effect of a non-rigid surface and the effect of a non-uniform (e.g. wavy) surface. However, the specification of the correct velocity condition on the ground are as important in more complex simulations.

For a Navier Stokes solution, the accurate and appropriate specification of boundary conditions is an important part of the solution process. A ground effect simulation differs from a standard aerofoil or wing simulation by requiring a lower boundary to represent the ground. Various forms of boundary condition have been specified for the ground and some in common use result in incorrect solutions.

For example, in 1996, Hsiun and Chen [24] presented results in which the authors noted a significant decrease in lift at small ground clearances. The authors attributed this to the presence of the boundary layer on the ground surface. However, the boundary conditions used assumed a stationary vehicle and a stationary ground plane, and therefore the presence of the boundary layer on the ground plane may be an inaccurate representation.

Other methods for specifying the ground boundary condition have included

- The use of the symmetry boundary condition (or alternatively, modelling two identical bodies with a plane of symmetry representing the ground);
- the use of the 'slip' boundary condition, which implies zero shear stress at the boundary;
- the specification of the ground to have the same velocity as the free stream.

In all of the above and that which follows, the vehicle is taken to be in a fixed reference frame.

Of the four possible boundary conditions available, the first, defined here as 'image' refers to the use of the image method, first suggested by Wieselsberger [24] in 1922. Setting the lower boundary to be a symmetry condition is also the use of the 'Image' condition Figure 27a.

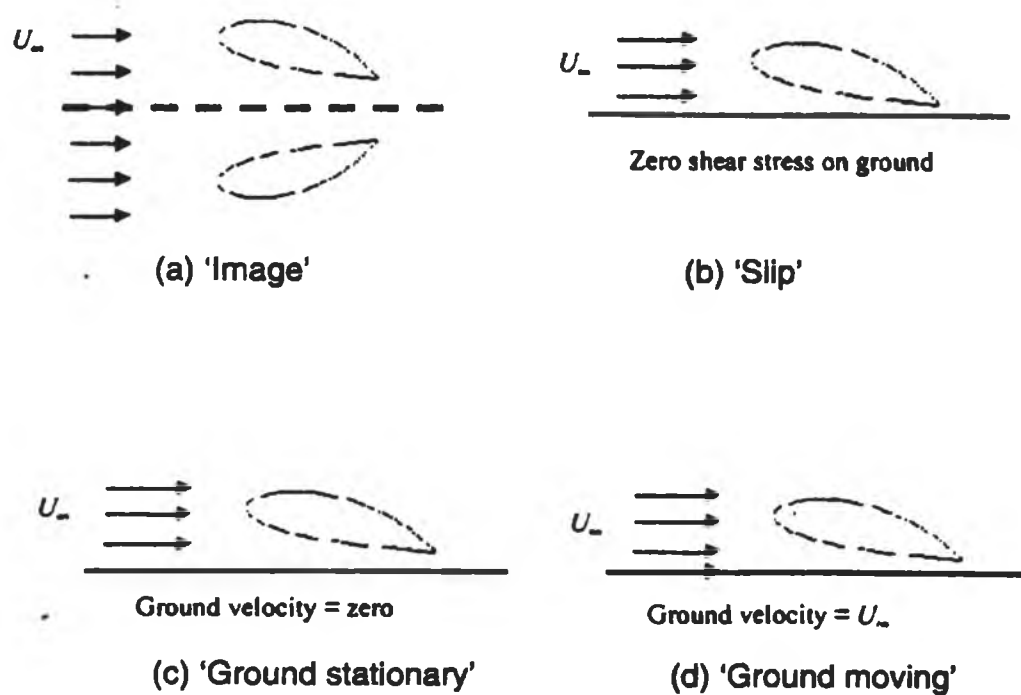


Figure 27 Ground effect representation

The second condition, defined here as 'slip', refers to a condition in which there is zero shear stress at the boundary. It can be seen that this type of condition could allow the ground to be moving at different velocities depending on its position relative to the vehicle, in order to enforce the zero shear stress condition Figure 27b.

The difference between these two conditions is that for a symmetry boundary all gradients are set to zero, and for a slip wall only the normal component of velocity is set to zero. In certain cases, this can cause a difference in the final solution between conditions of Figure 27a. and Figure 27b.

The third condition, defined as 'ground stationary', refers to the type of condition set by Hsiun and Chen [24] Figure 27c. However, by considering the flow situation, it can be seen that this condition may not be appropriate. In a ground-fixed reference frame, the air is stationary, the ground is stationary, and the body flies over the ground and through the air at velocity, U_∞ . By moving to a vehicle-fixed reference frame (such as in the CFD model) it can be seen that the

vehicle is stationary, and both the free stream air and ground should be moving relative to the body at velocity, U .

Setting the ground to be moving at velocity, U , is the fourth condition, defined as 'ground moving'. The ground is given the same velocity as that of the free stream, a condition representing accurately that of the real-Life situation Figure 27d.

It is important to note that the term 'slip' can cause some confusion as it has varying meanings among aerodynamicists and CFD users. A case in point is a note by Steinbach [24], referring to the paper by Hsiun and Chen[24]. The author explains that incorrect boundary conditions have been used; however his suggestion is to set the ground velocity as that of the free stream, which Steinbach [24] calls the 'slip' condition.

The success of the WIG concept depends on the accurate prediction of the aerodynamics of the vehicles. It is therefore of principal importance to use appropriate boundary conditions for any CFD analyses. Although four boundary conditions are in common use in ground effect simulations.

There is only one correct boundary condition that accurately and realistically simulates the real life conditions of ground effect. This condition is the 'ground moving' condition, in which the boundary conditions on the ground should be set equal to the free stream conditions.

IV. FLUID DYNAMIC ANALYSIS

IV.1 FLUID PROPERTY

[25][26][27][28][29]

IV.1.1 Density

Density varies with pressure, temperature and salinity, with pressure the major impact.

Pressure Effect: Density increases about 2.2% per 5000m (500bar), then for 10 to 20bar the density increases 0.044 to 0.088% increases

Salinity/Temperature Effect: Considering the pressure constant, Figure IV-1 shows the Salinity versus the Temperature at different density ($1000+\sigma$). The curves can be used to estimate the density for given Temperature and Salinity

Example of estimating the sea water density using the Temperature-salinity- σ grid (figure 29)

If $T=5\text{ C}$, Salinity 35‰ , then from the grid, $\sigma = 27.7$

Therefore the Density $\rho = 1000+\sigma = 1027.7\text{ kg/m}^3$

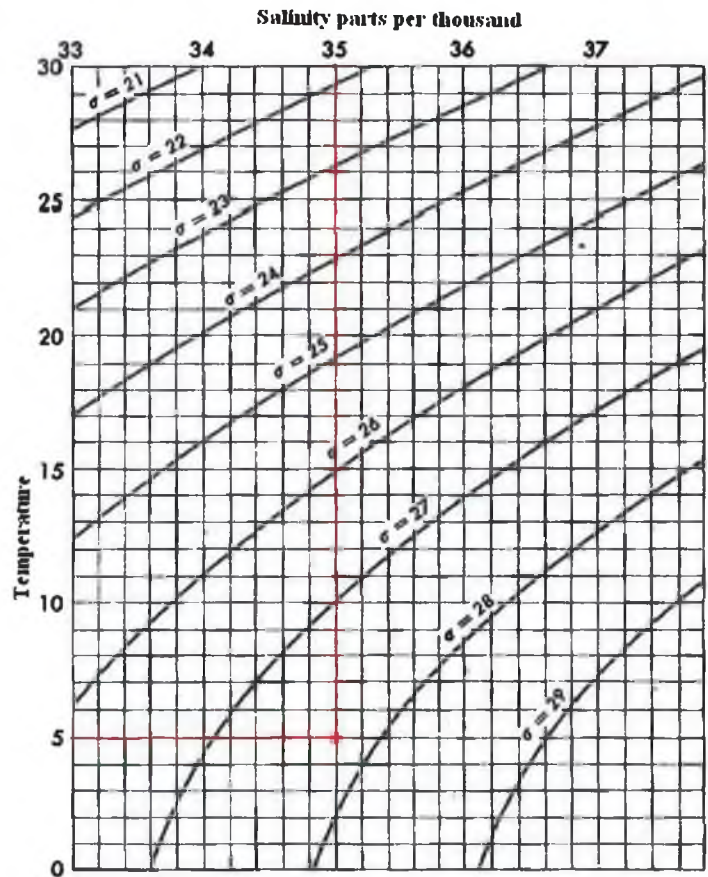


Figure 28
Temperature-salinity- σ grid

It also possible to have an overview of the temperature, density and salinity function of the depth and for various latitude: Figure 29

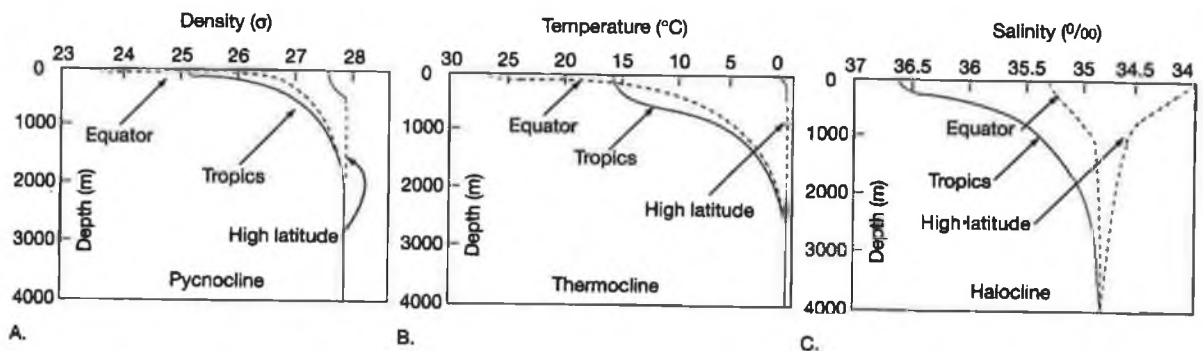


Figure 29 Overview of the temperature, density and salinity vertical distribution for various latitude

IV.1.2 Viscosity:

Viscosity varies with temperature, salinity and pressure.

Viscosity at the sea surface is around $1.07 \cdot 10^{-3}$ kg/ms

However, due to the unique structure of water, viscosity varies anomalously with pressure.

IV.1.3 Pressure

The pressure at a given depth depends on the mass of water lying above that depth.

$$P = g \rho z \quad \text{Equation IV-1}$$

Where :

P is the pressure (Pa)

g is the acceleration due to the gravity (m/s^2)

ρ is the seawater density (kg/m^3)

z is the depth (m)

Example: If $z=150\text{m}$; $g=9.81 \text{ m/s}^2$ and $\rho= 1027.675 \text{ kg/m}^3$

The pressure P is equal to 15.12×10^5 Pa

IV.1.4 Compressibility

Sea water is considered as incompressible, therefore $\text{div}V = 0$.

IV.2 FLUID DYNAMIC

IV.2.1 Conservation of momentum:

This relation is commonly known as Newton's second law [30][31] and expresses a proportionality between applied force and the resulting acceleration of a particle of mass m:

$$F = ma \quad \text{Equation IV-2}$$

If the system is a fluid particle, it is convenient to divide Equation IV-2 by the volume of the particle, so work should be done with density instead of mass. It is also traditional to reverse the terms and place the acceleration on the left-hand side.

Therefore

$$\rho a = \rho \frac{dV}{dt} = F = f_{body} + f_{surface} \quad \text{Equation IV-3}$$

Where, F is the applied force per unit volume on the fluid particle. F has been divided into two types: surface forces and body forces.

The so-called body forces are those that apply to the entire mass of the fluid element. Such forces are usually due to external fields such as gravity or an applied electromagnetic potential. Magneto-hydrodynamic effects are ignored here and only the gravitational body force is considered, which is as follow on unit volume basis

$$f_{body} = \rho g \quad \text{Equation IV-4}$$

Where, g is the vector acceleration of gravity.

The surface forces are those applied by external stresses on the sides of the element. The stress tensor τ_{ij} can be written as:

$$\tau_{ij} = \begin{pmatrix} \tau_{xx} & \tau_{xy} & \tau_{xz} \\ \tau_{yx} & \tau_{yy} & \tau_{yz} \\ \tau_{zx} & \tau_{zy} & \tau_{zz} \end{pmatrix} \quad \text{Equation IV-5}$$

The total force in each direction j (x;y;z) is :

$$\partial f_j = \tau_{xj} \partial y \partial z + \tau_{yj} \partial x \partial z + \tau_{zj} \partial x \partial y \quad \text{Equation IV-6}$$

On a unit volume basis in each direction (x;y;z): since $\tau_{ij} = \tau_{ji}$

$$f_x = \frac{\partial \tau_{xx}}{\partial x} + \frac{\partial \tau_{xy}}{\partial y} + \frac{\partial \tau_{xz}}{\partial z} \quad \text{Equation IV-7}$$

Then the total vector surface force is

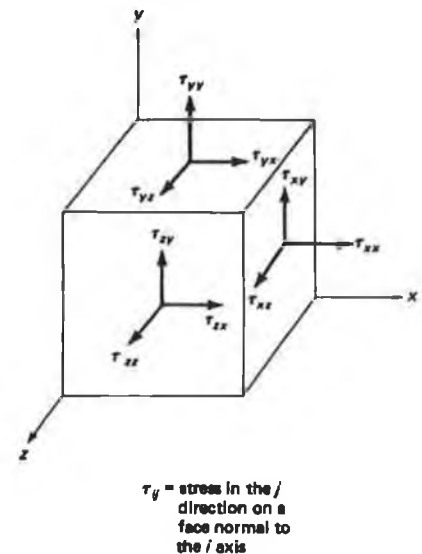


Figure 30 unit element representation

$$f_{surf} = \frac{\partial \tau_{ij}}{\partial x_i} \quad \text{Equation IV-8}$$

Then the Newton's law become:

$$\rho \frac{DV}{Dt} = \rho g + \frac{\partial \tau_{ij}}{\partial x_i} \quad \text{Equation IV-9}$$

The Fluid at Rest

From the definition of a fluid, the viscous stresses must vanish if the fluid is at rest. Thus the shear stresses are zero, and the normal stresses become equal to the hydrostatic pressure:

$$\tau_{xx} = \tau_{yy} = \tau_{zz} = -p$$

$$\text{and } \tau_{ij} = 0 \text{ for } i \neq j$$

When the velocity is zero, the stresses in general flow should be reduce to this special case.

IV.2.2 The Navier-Stokes Equations

The desired momentum equation for a general linear (Newtonian) viscous fluid is now obtained by substituting the stress. The result is the famous equation of motion, which bears the names of Navier and Stokes. [30][31]

$$\rho \frac{dV}{dt} = \rho g - \nabla p + \mu \nabla^2 V + \frac{1}{3} \mu \nabla (\nabla \cdot V) \quad \text{Equation IV-10}$$

↑
↑
↑
↑

Quantity of acceleration per volume unit Volumes forces Pressure forces per volume unit Viscous forces per volume unit

Where:

V is the vector velocity including v_1, v_2, v_3 , which are the Cartesian velocity components.

μ is the dynamic viscosity of the fluid

These are the Navier-Stokes equations, fundamental to the subject of viscous fluid flow.

IV.2.3 Incompressible Flow

If the fluid is assumed to be of constant density, $\text{div } V$ vanishes from the continuity equation and the vexing coefficient λ disappears from Newton's law[30][31]. Equations IV-10 are not greatly simplified, though, if the first viscosity μ , is allowed to vary with temperature and pressure (and hence with position). If, however, it is assumed that μ is constant, many terms vanish, leaving us a much simpler Navier-Stokes equation for constant viscosity:

$$\rho \frac{dV}{dt} = \rho g - \nabla p + \mu \nabla^2 V \quad \text{Equation IV-11}$$

Equation IV-11 is an excellent starting point in the theory of incompressible viscous flow, keeping in mind that constant viscosity is assumed. For non-isothermal flows, it may be a rather poor approximation, particularly for liquids, whose viscosity is often highly temperature-dependent. For gases, whose viscosity is only moderately temperature-dependent, Equation IV-11 is a good approximation and fails only when compressibility becomes important, i.e., when $\text{div } V \neq 0$.

CHAPTER 2 :DESIGN SOLUTIONS

I. INTRODUCTION

Considering the literature review and objectives of the project, the following specifications were proposed for the vehicle:

1. Towing velocity between 4 and 10 Knots (2 to 5 m/s)
2. Overall dimensions of the vehicle is not suppose to exceed 1.5m span, 0.5m chord, 0.5m thickness.
3. Distance between the vehicle and the sea bed h_o of less than 2m

Those values are not definitely fixed but could be used as basic data for future computations and designs.

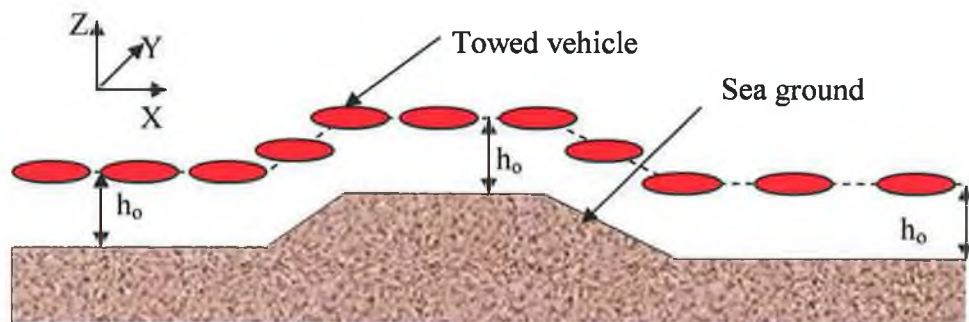


Figure 31 The concept

II. BALLAST CONCEPT

As developed in the previous chapter the ballast is used in many submarine designs. It would be interesting to study the feasibility of this concept on the developed vehicle.

[13][14][15][16][17][32][33][34]

II.1 APPLICATION OF THE MOTION EQUATIONS TO THE VESSEL

II.1.1 Assumptions

Let consider the linear and angular velocities of the vessel in three axis (V_x , V_y , V_z and ω_x , ω_y , ω_z). The sea current generate V_y and the three components of the angular velocities. However these components are negligible compared to V_x , V_z . Furthermore, we assume that the submarine will be designed to assure a perfect stability on the horizontal symmetric plane. Therefore, the three velocities V_y , ω_x , ω_y , and ω_z will be considered equal to zero. Then the motion equations become:

$$m_x \frac{dV_x}{dt} = \sum F_x \quad \text{Equation II-1}$$

$$m_z \frac{dV_z}{dt} = \sum F_z \quad \text{Equation II-2}$$

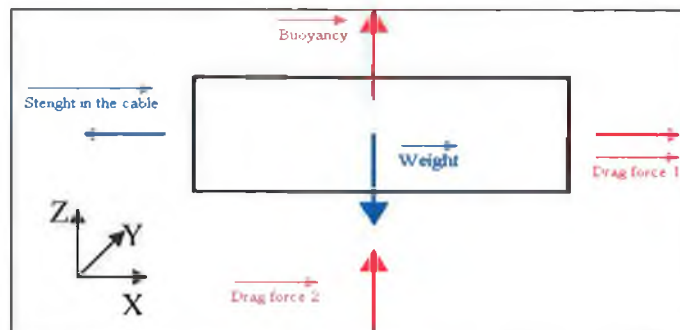
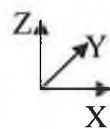


Figure 32 Free body diagram

Five forces act on the vehicle (Figure 32) during the sinking sequence: the weight, both drag forces, the buoyancy and the strength of the cable. The drag forces 1 and 2 are respectively due

to the horizontal and vertical movement of the vessel. Also the drag force 2 will change direction (negative) if the submarine is going up.

The objective of the project being to design a vehicle capable to float at a constant distance from the sea bed, the only equation considered in the following sections will be Equation II-2.

Due to the length and weight of the cable, the towing force (strength in the cable) is horizontal as shown on Figure33 [33]

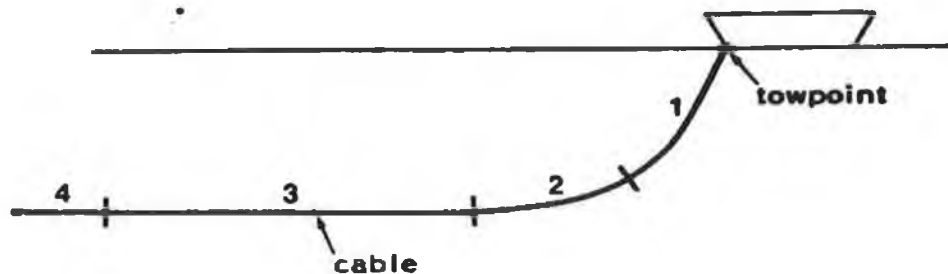


Figure 33: shape of the cable under the water

Therefore the motion equation gives:

$$m_z \cdot \frac{dV_z}{dt} = \text{weight} - \text{dragforce2} - \text{buoyancy} \quad \text{Equation II-3}$$

$$m_z \cdot \frac{dV_z}{dt} = \text{weight} - \text{drag} \pm \text{water current} - \text{buoyancy} \quad \text{Equation II-4}$$

Which can be developed as follow: [33]

$$\begin{aligned} (\text{mass} + \text{addedmass}) \times \frac{d^2z}{dt^2} &= (\text{mass} \times g) - \left(\frac{1}{2} \times \rho_{\text{water}} \times A \times C_d \times \left(\frac{dz}{dt} \right)^2 \right) \pm \left(\frac{1}{2} \times \rho_{\text{water}} \times A \times C_d \times V_c^2 \right) \\ &- (\text{volume vehicle} \times \rho_{\text{water}} \times g) \end{aligned}$$

Equation II-5

Where:

V_c: Water current. Seeing that the vessel will mainly be at about 200 m deep also ± 0.1 m.s⁻¹ is the value of the vertical current.

Velocity to reach 0.10 and 0.15 m.s⁻¹. These values have been chosen to have an efficient control system of the depth.

A: Projected area of a sample vehicle of 1.5m span for 0.5m chord, is 1.5 x 0.5 = 0.750 m²

ρ_{water}: Water density, assumed to be constant.(1025 kg/m³)

Added mass : Very little is known about this coefficient but in some cases it is taken as half of the actual mass so in our case the neutral buoyancy.

C_d : Drag coefficient, equal to 1.1667. Indeed, assuming that the wing is a rectangular plate of 1.5 m span and 0.5 m chord. Knowing that a/b is equal to 3, C_d value is calculated using geometrical progression between 1.16 and 1.17. Figure 34:

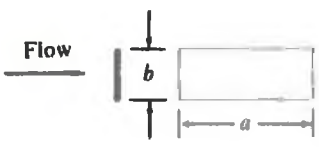
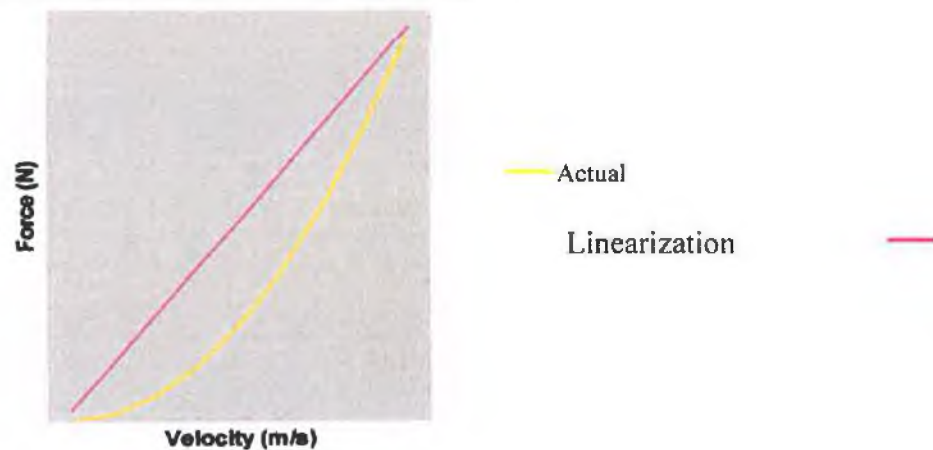
Shape of body	Orientation	C_d	
Rectangular plate		a/b	
		1	1.16
		4	1.17
		8	1.23
		25	1.57
		50	1.76
∞	2.00		

Figure 34: C_d for a rectangular plate

II.1.2 Linearisation of the drag force

Due to the non-linearity of the drag force, the used equation is a second order differential equation with a non-linear coefficient. In order to solve this equation using the Laplace transform[32], the drag must be linearised as shown in Figure 35.

Figure 35:
Linearization of the drag force.



This linearisation allows the following transformation of the equation: Equation II-6

$$(\text{mass} + \text{addedmass}) \times \frac{d^2z}{dt^2} = (\text{mass} \times g) - \left(\frac{1}{2} \times \rho_{\text{water}} \times A \times C_d \times \left(\alpha + \beta \times \frac{dz}{dt} \right) \right) \pm \left(\frac{1}{2} \times \rho_{\text{water}} \times A \times C_d \times V_c^2 \right) - (\text{volume vehicle} \times \rho_{\text{water}} \times g)$$

Where α and β are two coefficients to be determined.

The line minimising the squared distances between the n actual points of given data points and their approximated location is the best-fitting line. Such a line is said to fit the data in the least squares line.

The least squares method:

Then using this method the drag force becomes[32]:

$$F = \alpha + \beta \times V \quad \text{Equation II-7}$$

Where:

$$\alpha = \frac{(\sum F)(\sum V^2) - (\sum V)(\sum VF)}{n \sum V^2 - (\sum V)^2} \quad \text{Equation II-8}$$

$$\beta = \frac{n \sum VF - (\sum V)(\sum F)}{n \sum V^2 - (\sum V)^2} \quad \text{Equation II-9}$$

V and F stand respectively to the velocity and the force.

Using Mathematica 3.0 for the two velocities and V_z (0.10 and 0.15 $\text{m}\cdot\text{s}^{-1}$), α and β can be calculated as shown in appendix A.

Vertical Velocity (m/s)	α (N)	β (kg/s)
0.10	-0.595017	44.6243
0.15	-1.34535	67.2675

Table 3: α and β values

In order to determine if this approximation is acceptable, assuming that the induced error remains within a range of $\pm 20\%$, the values and the percentage error are available in the following Table II-2.

Vertical Velocity (m/s)	Actual Force (N)	Approximated force (N)	Percentage _{max} error
0.10	4.4	3.8	13.6%
0.15	10	8.5	15%

Table 4: Induced error

Both percentage_{max} errors are less than the 20% set . Therefore, the values of α and β can be used to solve the equation.

II.2 QUANTITY OF WATER REQUIRED

To estimate the feasibility of a ballast concept to control the vehicle, the amount of water required must be calculated. The aim of those computations is to apply a sufficient vertical velocity to the vehicle considering the worst conditions and therefore ensure that the vehicle will be able to follow the sea ground as closely and safely as possible.

To evaluate the amount of water the following assumption is made:

- Because the sea currents are unpredictable, the direction of the current will be taken always in the opposite sense of the vehicle motion.

Therefore, the term standing before the drag force due to the current will be negative.

Then taking this fact into account the required quantities of water can be computed as follow using Mathematica 3.0 [32] (Figure 36).

```
<< Calculus`LaplaceTransform`
Clear[addedmass, area, g,  $\alpha$ ,  $\beta$ , cd,  $\rho$ water, volume,
buoyancymass, massballast, h, t, s, lap1, lap2, lap3, lap4, laph, velocity, vc,  $\Delta m$ ]
addedmass = 22.96;
 $\rho$ water = 1025;
area = 1.5*0.5;
volume = 0.0448;
vc = 0.1;
g = 9.81;
cd = 1.1667;
buoyancymass = volume *  $\rho$ water;
massballast = buoyancymass +  $\Delta m$ ;
 $\alpha$  = -0.595017;
 $\beta$  = 44.6263;
lap1 = LaplaceTransform[(addedmass + massballast) * h'[t] ==
massballast * g - buoyancymass * g - 1/2 *  $\rho$ water * area * cd * ( $\alpha$  +  $\beta$  * h'[t]) - 1/2 *  $\rho$ water * area * cd * vc^2, t, s];
lap2 = lap1 /. {LaplaceTransform[h[t], t, s] -> laph, h[0] -> 0, h'[0] -> 0};
lap3 = laph /. First[Solve[lap2 == 0, laph]];
lap4 = lap3 * s;
velocity = InverseLaplaceTransform[lap4, s, t];
t = 100;
FindRoot[velocity - 0.1, { $\Delta m$ , 0}]
```

Figure 36 Mathematica 3.0 , quantities of water ccomputation

Vertical Velocity(m/s)	Δm (kg)
0.10	177.26
0.15	400.784

Table 5: results for the two velocity.

Note:

- The velocity depends on the time but when $t=100$ seconds the final velocity is reached (It is, in fact, after several seconds).
- For every calculation, the z direction will be oriented in the direction of the vertical acceleration. (When the vehicle is sinking, z positive from the sea surface to deep water and when the vehicle is rising, z positive from the deep water to the sea surface).

II.3 BALLAST CONCEPT CONCLUSION

The quantities of water needed to reach both diving velocities (0.1 m.s^{-1} and 0.15 m.s^{-1}) are about 180 and 400 litres. This amount is too big to be pumped in a few seconds and can not be stocked in a vehicle of about 150 litres. Furthermore the addition of external tanks is not appropriate because they would increase the projected area and the volume of displaced water and therefore increase both the drag force and the buoyancy.

This concept will not then be used as a main control system, but it might be used for creating a slightly positive or negative buoyancy needed at some stage of the vehicle evolution.

III. DIRECTIONAL WINGS

From submarine dynamic diving and foil review (Chapter 1: III.1.2.2 and III.2), a solution based on the use of directional wings, could be an alternative to the ballast shown to be unsuitable.

In this section we will study the angle of attack of the foil necessary to create a lift able to raise the vehicle over an obstacle.

III.1 ASSUMPTION:

From the ballast solution investigation, the same assumption will be made for the directional wing. The needed lift force (1740N) is been taken from the previous chapter "BALLAST CONCEPT" (Chapter 2 II) as well as the mass (177.26 kg) of water required to create a vertical velocity of 0.10 m/s.

III.2 FOIL ANGULATIONS COMPUTATION:

From the hydrodynamics forces review (Chapter 1 III.2.2) the net lift F_L is expressed as follows:

$$F_L = C_L(\rho V^2/2)A \quad \text{Equation III-1}$$

Where:

ρ is the density of the water

V the velocity of the vehicle

A the foil area as the product of the span and the chord

C_L lift coefficient depending mainly on the shape and the angle of attack of the foil.

At a particular angle of attack, the net resultant force on the airfoil acts essentially perpendicularly to the chord line of the section, as shown in Figure 37. Resolving this force into vertical and horizontal components produces the true lift force F_L and the induced drag F_{Di} .

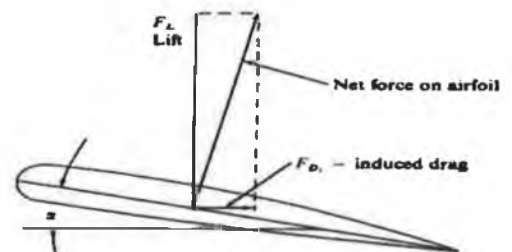


Figure 37 lift representation

Then the lift force becomes:

$$F_L = C_L (\rho V^2 / 2) A \cos(\alpha) \quad \text{Equation III-2}$$

The density of the water assumed to be constant as: $\rho = 1025 \text{ kg/m}^3$

And taking a towing speed of 4 knots (2.0 m/s)

The lift coefficient C_L is calculated for several NACA sections at several angles of attack using the NASA Glenn FoilSim II software (beta 1.4 version):



Figure 38 Glenn FoilSim II software

From the lift coefficients of the NACA 0010, 0015, 0020 and 0025 it is possible to determine the required horizontal section area of the directional wing, to raise a vehicle of a global section area of 0.75 m^2 at a 0.10 m/s vertical velocity

Case 1: NACA0025

The following table gives the necessary horizontal section area to create a lift force of 1740 N which is the low limit force needed to raise the vehicle at 0.1 m/s velocity as explained in the “ballast concept” (chapter 2 II.2).

Those calculations were performed using “Glenn FoilSim II software” with a vehicle velocity of 2 m/s (4knots) and a water density of 1025kg/m³

angle (°)	5	7.5	10	12.5	15	17.5	20
Cl	0.667	0.999	1.33	1.602	1.734	1.655	1.31
Area (m ²)	0.817	0.548	0.414	0.335	0.284	0.247	0.221

Table 6 Necessary section area for a NACA 0025

For example:



Figure 39 Flapper wing

A main foil sample of 1.5x0.5m will need to be angled at less than 7.5 degrees to create the necessary lift. The rotation of the wing could have been done using a flapper as wing

Case 2: NACA0015

angle (°)	5	7.5	10	12.5	15	17.5	20
Cl	0.623	0.933	1.242	1.5	1.62	1.546	1.223
Area (m ²)	0.875	0.587	0.444	0.359	0.304	0.265	0.236

Table 7 Necessary section area for a NACA 0015

The difference between the NACA 0025 and the NACA 0015 is less than 10%

III.3 DIRECTIONAL WINGS CONCLUSION

The calculation of the required angle of attack, gives an estimation of the feasibility of this solution as directional wings. In fact this solution using the angle of attack to create a lift is more realistic than the ballast system

This design would need to be driven by a close loop control system including: sonar to constantly measure the vehicle-seafloor distance, flapper wing or rotation wings activated by motor to create the lift and raise of the vehicle. A PLC controller would be need to manage the system.

However the complexity and cost of this solution made it unsuitable for the vehicle designed.

IV. GROUND EFFECT WING

IV.1 THE GROUND EFFECT

Both ballast and directional wings were shown to be unsuitable. Therefore a new concept of underwater ground effect was developed.

The aim of this study is to design a stable wing pulled over the sea bed at an operational distance.

The profile of the wing has to create a “hydrodynamic effect” capable to maintain a constant distance between the seabed and the wing.

The concept is based on the fact that a positive delta pressure between upper and under surface of the foil create a positive hydrodynamic force “Fh” which will rise the wing.

$$\Delta P = P_{\text{under}} - P_{\text{upper}} \neq 0$$

Assuming that the vehicle could be designed with the following specification:

- A fixed slightly negative buoyancy
 - A hydrodynamic stable shape on “free water” when far from the seabed ($\Delta P=0$, $F_h=0$)
- Figure IV-1
- A shape creating hydrodynamic ground effect when close to the seabed so ($\Delta P>0$, $F_h>0$)

Therefore three dynamics states of the wing could be established Figure 40

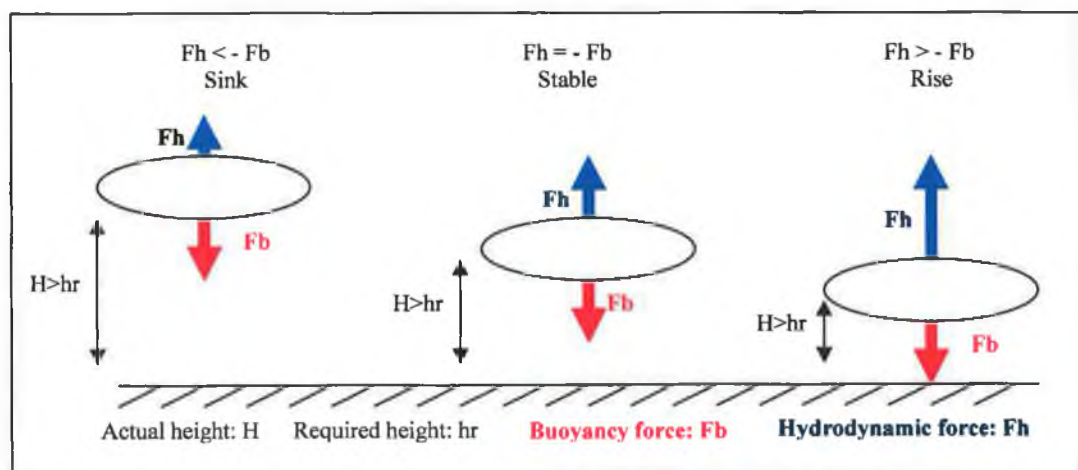


Figure 40 Functional concept

1. If the vehicle is far from the ground, the hydrodynamic stability of the shape in “free water” ($F_h=0$) added to the fixed negative buoyancy of the vehicle ($F_b<0$) gives $F_h+F_b<0$. So the vehicle will move close to the seabed.
2. If the vehicle is at a working distance from the seabed, the ground effect creates a slightly positive ΔP ($F_h>0$) which would cancel the slightly negative buoyancy ($F_b<0$) so $F_h+F_b=0$, therefore the vehicle will stay at a constant distance from the seabed.
3. If the vehicle is too close to the seabed, the ground effect creates a highly positive ΔP ($F_h \gg 0$) which would overtake the slightly negative buoyancy ($F_b<0$) so $F_h+F_b>0$, therefore the vehicle will move away from the seabed.

In the following section different wing profiles will be tested to assess their “underwater ground effect properties”

IV.2 SIMULATION:

To establish the feasibility of such a concept, different foils sections have to be considered to assess their underwater ground effect ability.

Therefore, to choose the most efficient foil section (stable on free water and creating hydrodynamic ground effect when close to the seabed), the following simulations were made using Computational Fluid Dynamics (C.F.D.) software (Ansys-Flotran).

IV.2.1 First simulation

[23][24][35][36][37][38]

IV.2.1.1 Foil sections

The first wing profile to be tested is the classic NACA Section. The NACA section is generally used for airplane wings and marine foils.

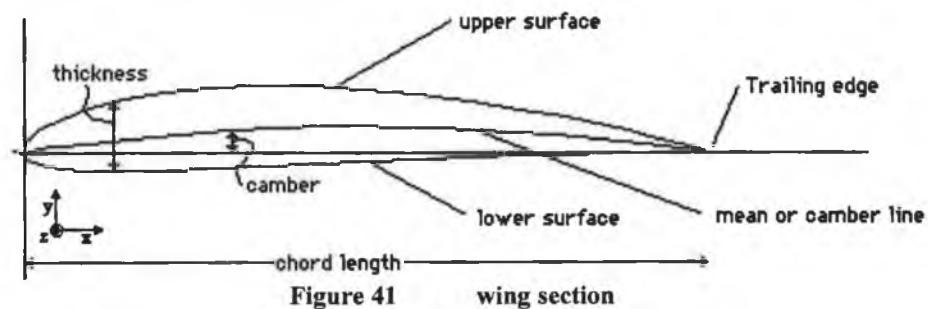


Figure 41 wing section

With x axis positioned on chord dimension, y axis positioned on thickness dimension, and z axis positioned on span dimension

All the following models will have different design but similar dimensions.

Foil 01: NACA 0025 one of the mostly used NACA

Chord: 0.5m

Max Camber: 0 % of chord

Position of the max Camber: 0 x 1/10 of chord

Thickness: 25 % of chord

⇒ Symmetric wing on the horizontal (xz) plan

Foil 02: HALF - NACA 0025

Chord: 0.5m

Max Camber: 0 % of chord

Position of the max Camber: 0 x 1/10 of chord

Thickness: 25 % of chord

⇒ Non symmetric wing on the horizontal (xz) plan

IV.2.1.2 Simulation Input data

The simulation will be undertaken using FLOTRAN from ANSYS.

The following parameters will be applied:

- Fluid property: Fluid density: 1020 kg/m^3
Incompressible
Viscosity: 0.001003 Kg/m-s
- Environmental pressure conditions: 10 bar (about 100m depth)
- Fluid velocity: 2 m/s
- Element used: 2D flow element FLUID141
- Reynolds number: $Re = \rho VL / \mu$
 ρ : Density 1020 Kg/m^3
 V : Velocity 2 m/s
 L : wing chord 0.5 m
 μ : Viscosity 0.001003 Kg/m-s
 $\Rightarrow Re = 1.02 \text{ E}+6$
 \Rightarrow **Turbulent flow (Re > 1 E+5)**
- Boundary conditions

The literature review presented previously in “Chapter 1 III.2.3.2” concerning Computational Fluid Dynamics (C.F.D.) on aerodynamics ground effect showed that the accurate and realistic condition to simulate the real conditions of ground effect is the 'ground moving' condition.

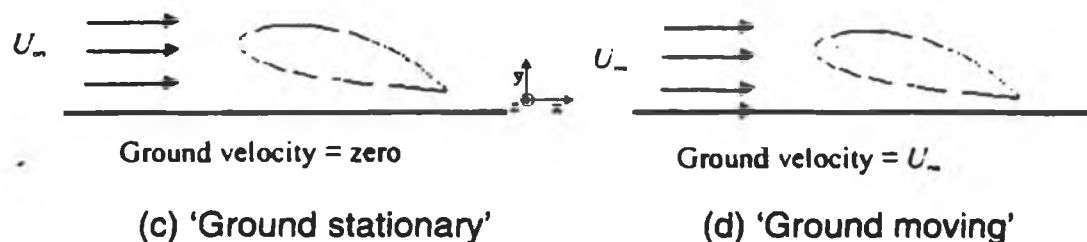


Figure 42 Ground Simulation

Therefore the “ground moving” boundary conditions are:

Fluid velocity on the foils surface : 0 m/s

Fluid velocity on the ground surface : 2 m/s

Print-screens of the simulation process (model geometry, loading, boundary conditions) are available in Appendix B.

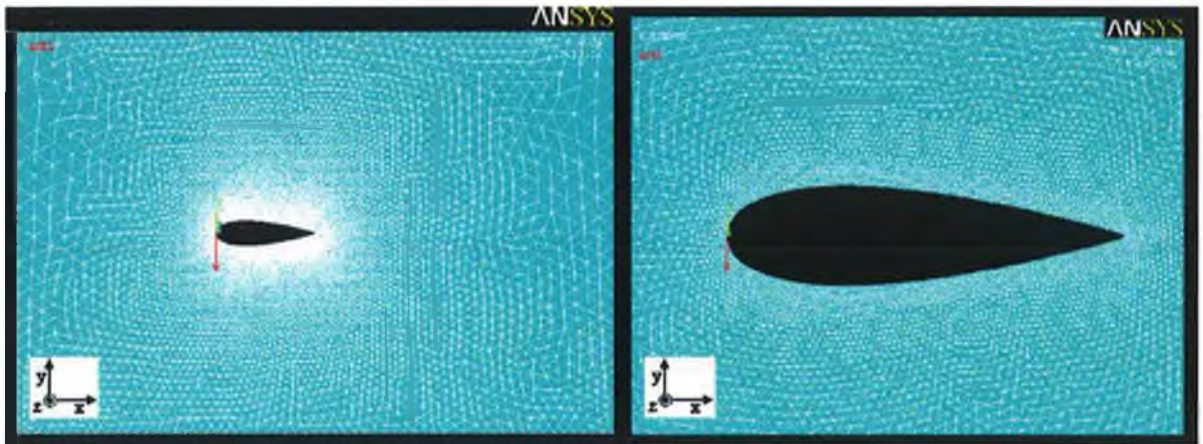


Figure 43 Mesh distribution representation
Enlarged display of the mesh is available in Appendix D.

RESULTS AND COMMENTS of the NACA section 0025

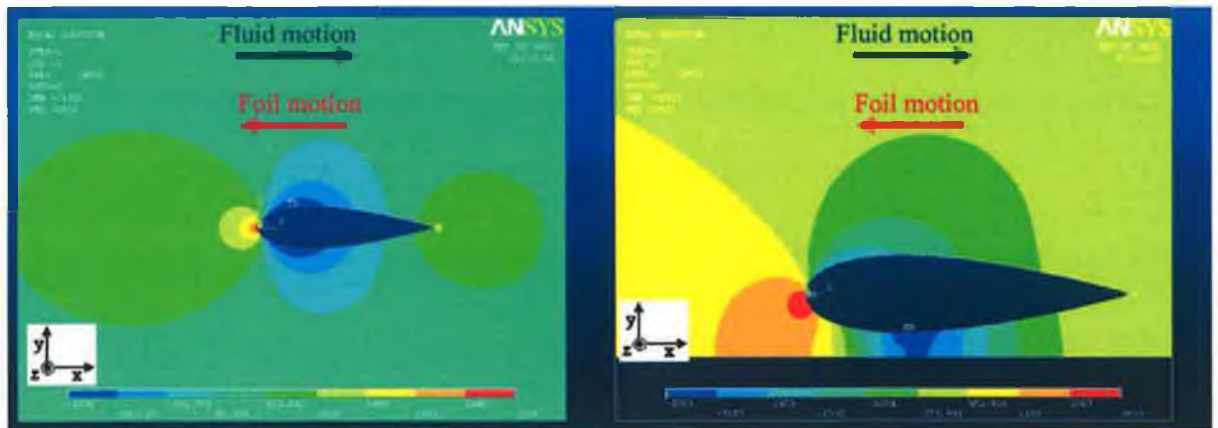


Figure 44 Free ground results

Figure 45 Ground proximity results

More results of C.F.D conducted on pressure and lift are available on appendix E and F, respectively.

Free water configuration:

- This design is stable in free water. Therefore it is possible to expect a sinking motion of the wing due to a negative buoyancy.

Close Ground configuration:

- Closer to the ground, the pressure distribution stays homogenous on the upper surface.
- Pressure is lower on the under surface than on the upper surface of the wing. Therefore the wing is going to be sucked to the bottom.
- Considering only the lower surface of the foil, the low-pressure distribution is located at the decreasing thickness of the section.

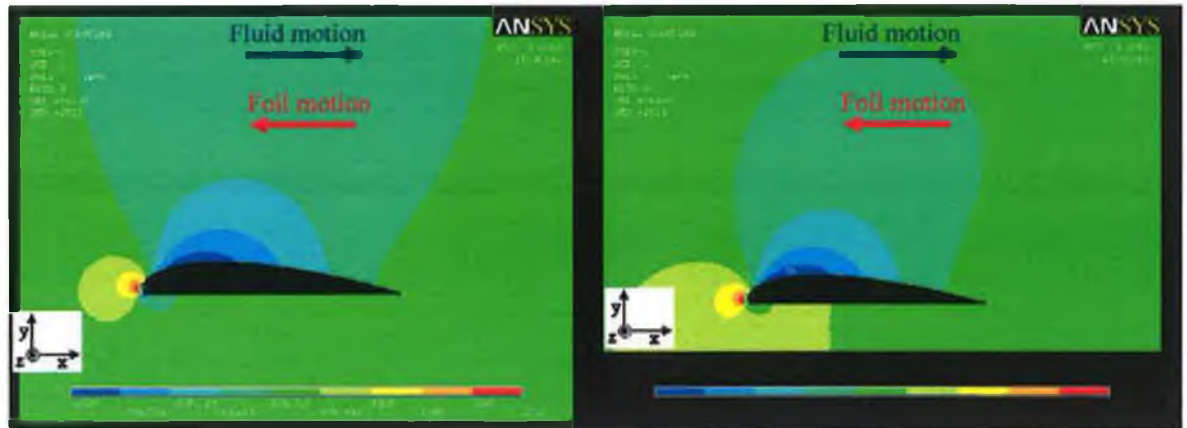
RESULTS AND COMMENTS of the Half NACA section 0025

Figure 46 Free ground results

Figure 47 Ground proximity results

More results of C.F.D conducted on pressure around the foil section are available on appendix E.

Free water configuration:

- This design is not stable in free water. therefore, it not possible to expect a sinking motion of the wing using negative buoyancy

Close Ground configuration:

- There is no major effect on the pressure distribution on the wing surface.

From those simulations it will be assumed that the expected wing should have an xz plan of symmetry to be stable on free water but the shape may be different to a classic NACA section.

IV.2.2 Second simulation

Using the conclusion from the previous simulation, different wings sections will be tested.

Any further simulation will be undertaken using the same parameters as the first simulation.

Two symmetrical profiles are tested to assess their stability in free water evolution (ellipse and diamond section)

Foil 03: Ellipse section:

Chord: 0.5 m

Max Thickness: 0.125 m

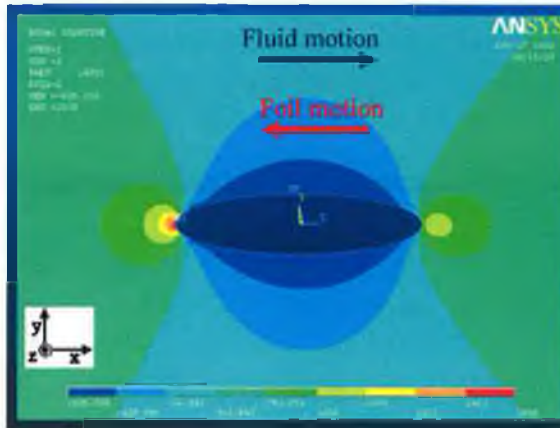
RESULTS AND COMMENTS of the Ellipse section:

Figure 48 Free ground results

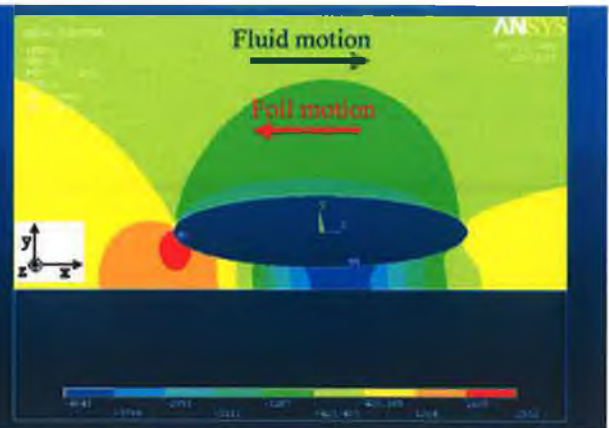


Figure 49 Ground proximity results

More results of C.F.D conducted on pressure around the foil section are available on appendix E.

Free water configuration:

- This design is stable in free water. Therefore it is possible to expect a sinking motion of the wing due to a negative buoyancy.

Close Ground configuration:

- Closer to the ground, the pressure distribution stays homogenous on the upper surface.
- Pressure is lower on the under surface than on the upper surface of the wing. Therefore the wing is going to be sucked to the bottom
- The pressure is higher on the front lower surface, than on the middle and back of the section
- Considering only the lower surface of foil, the low-pressure distribution is located at the decreasing thickness of the section.

The fact that the pressure is not homogenous on the lower surface is more accentuated than with a NACA 0025.

Foil 04: Diamond section:

Chord: 0.5m

Max Thickness: 0.125 m

RESULTS AND COMMENTS of the Diamond section:

Figure 50 Free ground results

Figure 51 Ground proximity results

More results of C.F.D conducted on pressure, lift and turbulence around the foil section are available on appendix E, F and G, respectively.

Free water configuration:

- This design is stable on free water. Therefore it is possible to expect a sinking motion of the wing due to a negative buoyancy.

Close Ground configuration:

- Closer to the ground, the pressure distribution stays homogenous on the upper surface.
- The pressure is very high at the first third of the lower surface.
- Considering only the lower surface of foil, the low-pressure distribution is located at the beginning of the decreasing thickness of the section.

The fact that the pressure is not homogenous on the under surface is more accentuated than with an ellipse. Also, there is more surface under high pressure than under low pressure.

From the previous simulations it is possible to assume that any symmetrical section on the horizontal plane will be stable on free water. Therefore only close ground configuration will be made on following simulations.

Also, in both design, diamond and ellipse shape, the high and low-pressure distribution are respectively located on the increasing and decreasing part of the section.

In conclusion, the under pressure distribution could be developed in two different ways:

1. Increase the instability of the foils (high pressure at front and low pressure at the back). Therefore, the objective would be to apply a sufficient rotation momentum around Z, and obtain the adequate angle of attack able to create a raising lift. However, by increasing the low pressure at the back of the under surface would sink the wing to the bottom. There is no way to predict which of these occurrences will be predominant, consequently, this development will not be taken into consideration.
2. Increase the surface of the foils subjected to high pressure in order to raise the vehicle by hydrodynamic effect. This option was chosen for further development.

IV.2.3 Third simulations

Taking in consideration the previous simulations results and comments, further wings sections were tested to develop the feasibility of hydrodynamic effect able to raise the vehicle.

At first, a foil which combines a diamond front and an ellipse tail were tested, followed by the study of a “reversed NACA”. Those both designs were chosen to have the decreasing thickness of the section as far back as possible. Therefore it expected to have the maximum under surface of the foils subjected to high pressure.

Foil 05: mixed of diamond & ellipse section:

Chord: 0.5m

Max Thickness: 0.125 m

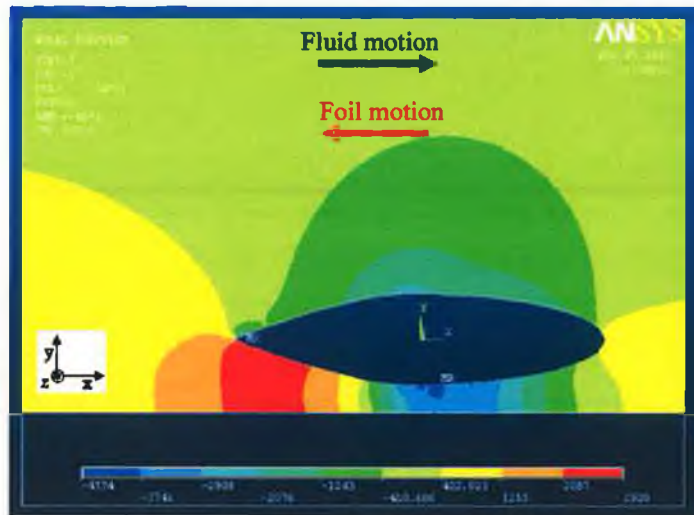
RESULTS AND COMMENTS of the half diamond half ellipse section:

Figure 52 Ground proximity results

More results of C.F.D conducted on pressure around the foil section are available on appendix E.

Close Ground configuration:

- The pressure on the upper surface is higher on the front than a on the back.
- The pressure on the first third of the section is much higher on the under surface than on the upper one. With about 3000 N/m^2 difference between both surfaces at the same abscissa.
- The pressure at the beginning of the second half of the section is lower on the under surface than on the upper one. With about $1000\text{-}1500 \text{ N/m}^2$ difference between both surfaces at the same abscissa.

From this simulation, it can be concluded that this design which combines a diamond front and an ellipse tail is not able to create the hydrodynamic effect necessary to raise the vehicle.

Foil 06: reverse NACA 0025:

Chord: 0.5m

Max Camber: 0 % of chord

Position of the max Camber: 0 1/10 of chord

Thickness: 25 % of chord

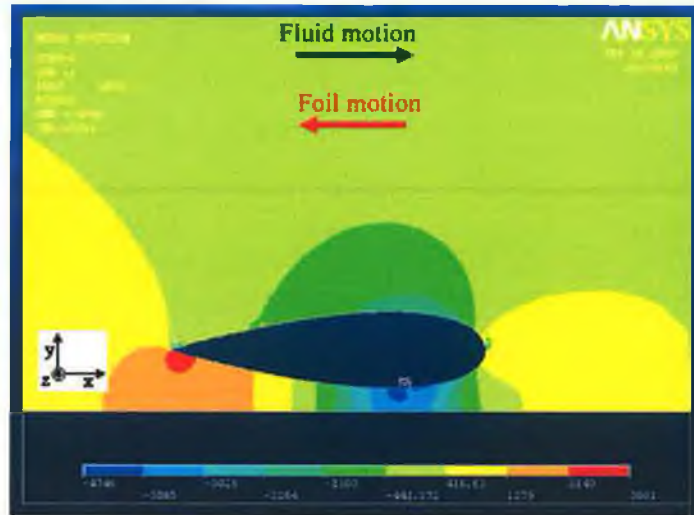
RESULTS AND COMMENTS of the reverse NACA 0025:

Figure 53 Ground proximity results

More results of C.F.D conducted on pressure, lift and turbulence around the foil section are available on appendix E, F and G, respectively.

Close Ground configuration:

- The pressure on the upper surface is higher on the front.
- The pressure, on the full length of the section, is higher on the bottom surface than on the top one. With about 4500 N/m^2 at the front and 1000 to 500 N/m^2 difference between both surfaces at the back.

From this simulation, we conclude that this design using a reversed NACA 0025 upside down generates a delta pressure between the upper and the lower surface of the foil, this should create the necessary force to raise the vehicle.

IV.2.4 Fourth simulations

Using the conclusion from the previous simulation, a final wing section was tested.

The aim of the following design is to create a maximum surface under high pressure to raise the vehicle by hydrodynamic effect.

Foil 08: HALF diamond section:

Chord: 0.25m

Max Thickness: 0.1 m

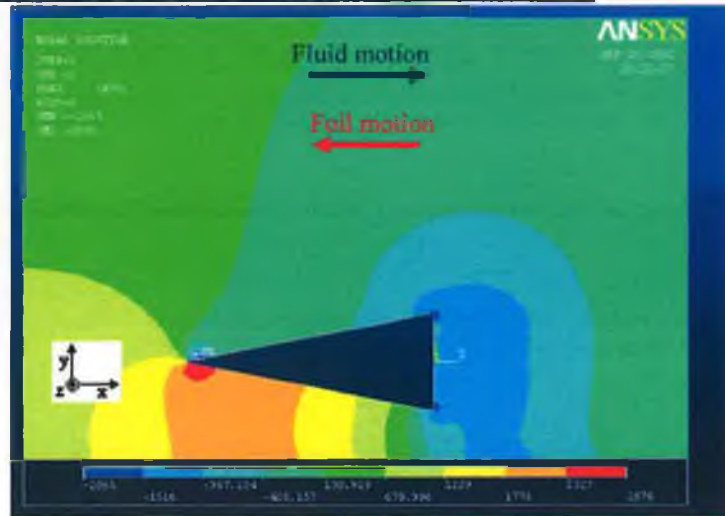
RESULTS AND COMMENTS of the HALF diamond section

Figure 54 Ground proximity results

More results of C.F.D conducted on pressure, lift and turbulence around the foil section are available on appendix E, F and G, respectively.

Close Ground configuration:

- The pressure is, at any abscissa, higher on the under surface than on the upper one.
- However, lots of turbulences are created on the trailing edge

From this simulation, it can be concluded than the wing will rise due to the hydrodynamics “ground effect”. But the created turbulences would create an instability dynamic of the wing.

IV.3 CONCLUSION:

Those simulations of ground effect have shown the behaviours of different wing sections depending on the position. It was shown that the variation of lift is directly dependant on the shape of the wings.

From the results of the different simulations, only two shapes (the reverse-NACA and the diamond shape) were selected for further research.

CHAPTER 3 : TESTING

I. INTRODUCTION

From the simulations, some designs demonstrate a possibility to create ground effect, and the feasibility of rising the vehicle when it is too close to the ground. Now this assumption must be confirmed by testing some of the most promising designs.

Firstly, a test facility and models had to be designed and built to be able to carry out tests.

Secondly, the tests were to be conducted in three steps:

The 1st step was to test the reactivity of the foil sections in “free water” and “ground proximity” using a “straight wing” at neutral buoyancy to explore only the hydrodynamic effect.

The 2nd step was to test some foils geometries including variation of aspect ratio, sweep back angle and dihedral angle parameters to establish the lateral stability of the vehicle.

The 3rd step was to test the most successful models of previous steps with a slightly negative buoyancy to keep the vehicle close to the bottom using towing configuration similar to the reality.

Due to time constraints for the project, only the first step was carried out. The others steps could be done as part of a subsequent project.

II. TEST FACILITY

FACILITY REQUIREMENT:

- The test facility should be able to be manufactured and used in the workshop of the GMIT.
- Velocity of the test facility: a scale factor should be used to evaluate the right testing velocity depending on:
 - The test facility dimensions,
 - The models dimensions
 - The towing velocity of the final device at real life.
- Model dimension: this parameter will be influenced by the facility characteristics and by the manufacturing process carried out using the workshop facilities of the GMIT.
- Test pressure: the water is assumed to be incompressible fluid, so it will be assumed that the pressure of the test condition do not affect the results.

Hydrodynamic test are generally conducted using two types of facilities, the first one is the “water tunnel” facility using fluid in motion and a fixed tested model, the second one is a “towing tank” using a moving model through a tank of water.

II.1 GENERAL DESCRIPTION OF EXISTING FACILITIES

II.1.1 Example of water tunnel

This facility is primarily used for flow visualization and low Reynolds number turbulent flow experiments. It has also been used to examine the structure of a 3-D turbulent boundary layer using laser-Doppler velocimetry (LDV) and hydrogen-bubble flow visualization. [39]

The water is circulated through 457mm diameter PVC piping to a rectangular path roughly 4.6m x 6.7m using an Ingersoll-Rand axial pump driven by a 7.35kw motor. The motor is controlled using a Toshiba TOSVERT-130 H/H1 transistorised inverter. The total water capacity of this facility is approximately 4.5m³. The tunnel is supported 1.2m above the laboratory floor using an aluminium channel frame with plywood supports.

The pump unit specified for the water tunnel has a capacity of approximately $0.07 \text{ m}^3/\text{s}$

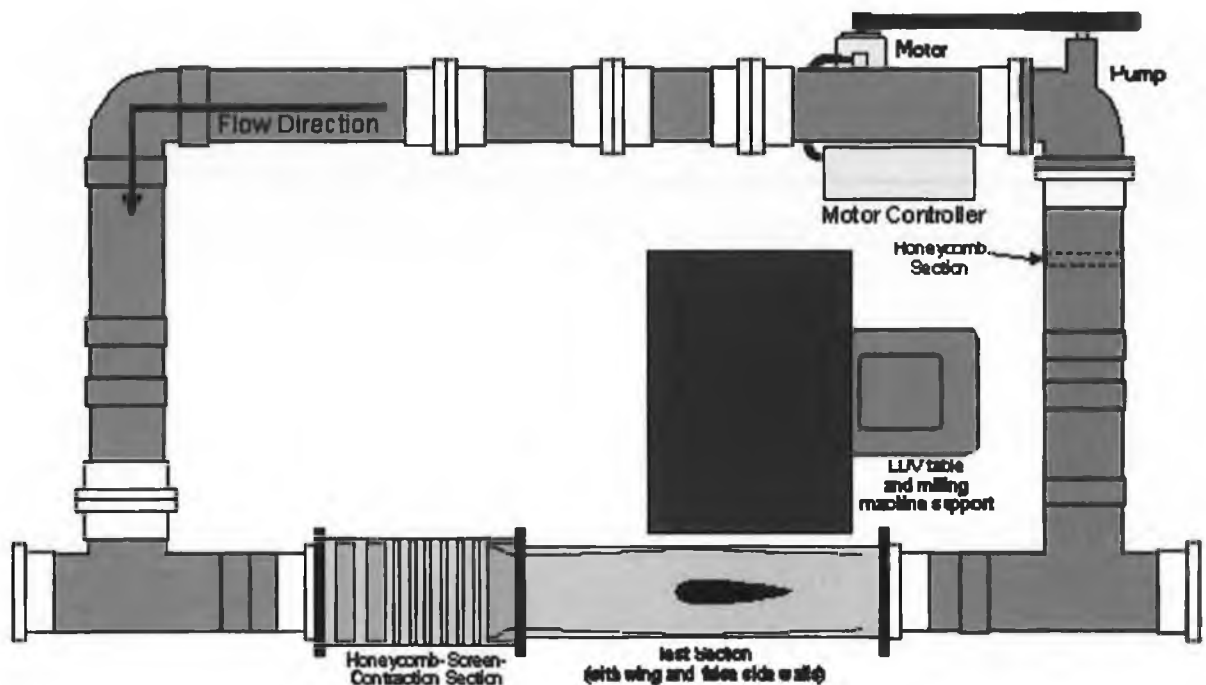


Figure 55 water tunnel [39]

As settling chamber two honeycomb sections and six turbulence screens are used to remove flow swirl. The flow passes through a 1.6:1 ratio contraction as it enters the test section. A third section of honeycomb is positioned upstream of the pump inlet, to further isolate the pump pressure fluctuations from the test section flow. This facility is suitable for flow speeds from 0.2 to 0.45m/s.

Advantages:

The dimension of this water tunnel is manageable.

Disadvantages

The pump unit rate of flow is very high, which require an expensive pump (~5000€)

This type of facilities with a fluid moving around a fixed foil model and ground is in contradiction with the real conditions.

II.1.2 Example of water towing tank

The facility consists of a water tank with glass walls and a towing trolley running on rails mounted above the tank on independent bearings. The water in the tank is at rest. Models attached to the trolley can be towed under water with constant or variable speed. The facility is powered by an electrical 7 kW-DC-motor [41].

Technical Data :



Figure 56 Front view of the water towing-tank

Facility	Test section size: Cross-section 1,1m x 1,1m; length 18m Minimum velocity: 0,01 m/s, maximum velocity: 5 m/s Reynold's Number taken for 1m: $5 \cdot 10^6$
Models	Typical size: span: 0,15 - 0,6 m, length 1-2 m,
Field of Application	Fundamental experiments on boundary layer transition and separation, Investigation of separated flows and vortex flows(e.g. slot flows, tunnel entrances, ground effects)
Measurement	Hydrogen bubble visualization, particle image velocimetry (PIV). Velocity measurement Pressure measurements Data is saved and processed on-line with a graphical computer program



Figure 57 Water Towing Tank in Göttingen

Advantages:

The towing of the trolley is not expensive(only a motor belt cable and pulley)

This type of facilities with a foil model moving in a fixed fluid on top of a fixed ground is in accordance with the real conditions.

Disadvantages

This water tunnel is approximately 18m long, which is compatible with the space available

II.2 SIMILARITY TO THE REAL CONDITION

The literature review on ground effect aerodynamics establishes that the appropriate condition to simulate the conditions of ground effect is the 'ground moving' condition. For the test this condition should also be taken into consideration to choose the right testing facility. [24]

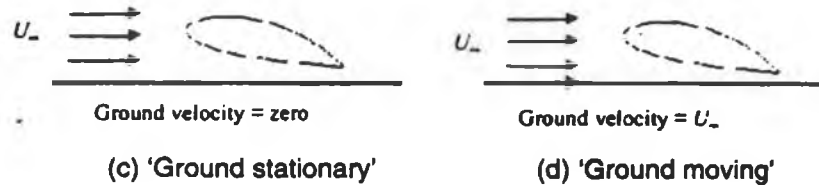


Figure 58 ground effect simulation

In this case, the most suitable facility would be the water towing tank, which will satisfy the condition of “ground moving”(d) relatively to the wing, in opposition to the water tunnel generating a “stationary ground”(c). Even if the viscosity of water is nearly negligible the non-respect of this condition could influence accuracy and realism of the tests due to the proximity of the ground.

The towing tank will give a further opportunity to visualise the wing behaviour in motion above a non-flat ground surface.

Cost estimate of the different testing facilities:

- The water-tunnel appears to be expensive. This cost is mainly due to the high flow rate pump which should cost around 5000 Euros. Also most of the piping work would have to be processed outside of the institute, leading to some extra cost.
- The towing tank would need a basic three-phase motor and inverter for less than 500 Euros. Also the main part of metal work could be process at the GMIT workshop.

	Motor / Pump cost	Metal work	Total material estimated cost
Water tunnel solution	High flow rate pump 5000€	4000€	9000€
Towing tank solution	Motor & Inverter 500 €	4000€	4500€

Table 8 Quotation summary

II.3 INFLUENCE OF THE SCALE

II.3.1 Conservation of the Reynold's number:

in the following discussion, the real life device will be referred as Prototype and the scaled model used for testing will be referred as model.

Previous studies [20][22] have shown the Reynolds number of the model (Re_m) and prototype (Re_p) must be equal:

$$Re_m = Re_p \quad \text{Equation II-1}$$

$$\left(\frac{\rho V d}{\mu} \right)_m = \left(\frac{\rho V d}{\mu} \right)_p \quad \text{Equation II-2}$$

Where: ρ is the fluid density
 V is the vehicle velocity
 d is the vehicle dimension
 μ is the fluid viscosity

Therefore, the model velocity should be

$$V_m = V_p \frac{\rho_p d_p \mu_m}{\rho_m d_m \mu_p} \quad \text{Equation II-3}$$

In this study:

	Chord(mm)	Span(mm)	Thickness(mm)	Model Scale
Prototype dimension	1600	2000	410	1/10
	800	1000	205	1/5
Model dimension	160	200	41	

Table 9 Model scale

From the previous equation, with sf as the scale ratio:

$$\frac{d_p \mu_m}{d_m \mu_p} = sf \quad \text{Equation II-4}$$

Therefore

$$V_m = \frac{V_p}{sf} \quad \text{Equation II-5}$$

If the scale ratio is between 1/5 and 1/10 the model velocity must be between 5 and 10 times the prototype velocity. This result mean than the testing facility should have a minimal velocity in between 10m/s and 20m/s considering the real life velocity of 2m/s (4knots)

This constraint makes the realisation of the test difficult. Furthermore, in the ground effect study, other parameters such as the distance between the wing and the ground have to be taken into consideration.

Consequently, CFD simulation was done to observe the influence of these parameters on the validity of the test.

II.3.2 CFD simulation to observe influence of the scale

In this study, the vehicle is moving close to the ground and not in “free water”. Therefore, the influence of the distance between the wing and the ground is of prime importance. In order to estimate the influence of the global scale ratio (scale between the wing and its environment) and the velocity of the model, some simulations were undertaken.

II.3.2.1 Influence of the global scale ratio:

This simulation was done to evaluate the influence of the global scale factor on the pressure distribution, using a constant fluid velocity.

Reverse naca0025 scale: 1/3
Chord: 166mm
Ground/foil distance: 0.033m

Reverse naca0025 scale: 1/1
Chord: 500mm
Ground/foil distance: 0.1 m

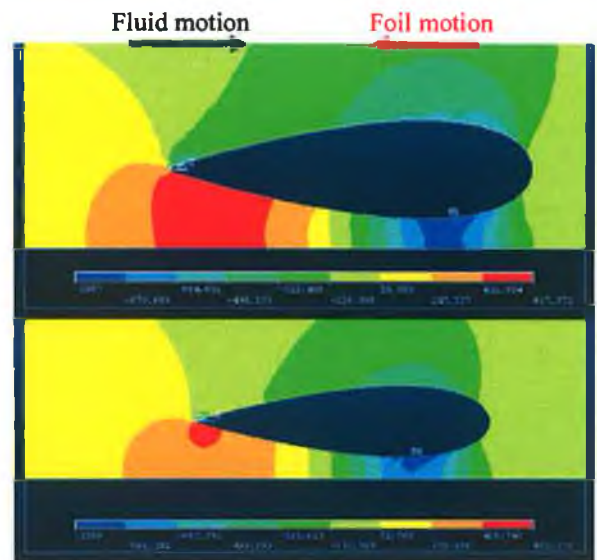


Figure 59 global scaling factor variation

REV-NACA 0025 chord (mm)	Wing-ground distance (mm)	Global Scale factor	delta Pressure (Pa)	Velocity (m/s)
166	33	1/3	1674	1
500	100	1/1	1652	1

Table 10 Global scaling factor influence

We can conclude, from table I-1, that, at constant velocity, the scale of the model has no influence on the delta pressure, as long as the same scale ratio is applied to the distance between the wing and the ground.

In conclusion, if the global geometry has been modelled proportionally to the real dimensions, there is no need to modify the velocity to ensure the validity of the test.

II.3.2.2 Influence of the velocity:

This simulation has been done to estimate the influence of the velocity on the pressure distribution, without scale factor variation.

Reverse naca0025 velocity: 1 m/s

Chord 166mm,

Ground/foil distance: 0.033m

Reverse naca0025 velocity: 1.5 m/s

Chord 166mm,

Ground/foil distance: 0.033m

Reverse naca0025 velocity: 2 m/s

Chord 166mm,

Ground/foil distance: 0.033m

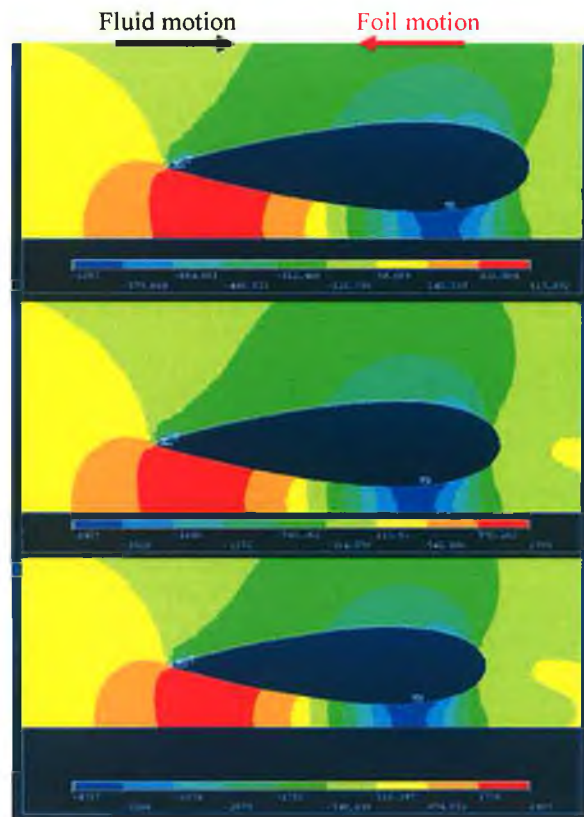


Figure II-60 Velocity variation

Velocity m/s	Minimal Pressure Pa	Maximal Pressure Pa	Delta Pressure Pa
1	-1057	617	1674
1.5	-2457	1399	3856
2	-4357	2497	6854

Table 11 Velocity influence

From those data, we a relation between the velocity and the pressure:

$$\Delta P_{1.5}/\Delta P_1 = 2.31 \approx 1.5^2 \quad (1.5/1=1.5)$$

$$\Delta P_2/\Delta P_{1.5} = 1.76 \approx 1.34^2 \quad (2/1.5=1.34)$$

$$\Delta P_2/\Delta P_1 = 4.09 \approx 2^2 \quad (2/1=2)$$

So from those considerations, and in this situation :

$$\text{If } V_1 = x \cdot V_2 \Rightarrow \Delta P_1 = x^2 \cdot (\Delta P_2)$$

II.4 DESIGN



Figure 61 Global view of the towing tank

II.4.1 Tank design

The design of the tank is based on existing water tank and, for budget reason, was manufactured within the institute workshop

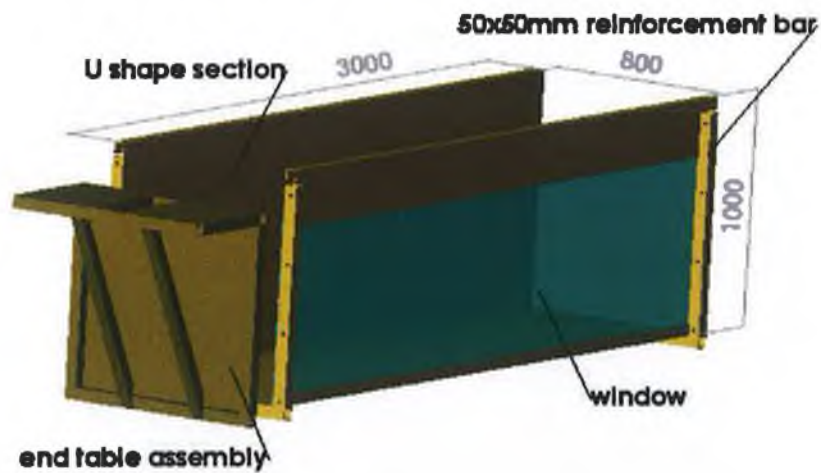


Figure 62 3D View of one tank section

II.4.1.1 USHAPE SECTION

Four “U shape” sections, ordered from an external company, were bent from 5mm thick steel sheets. Each section had been reinforced in the GMIT workshop using steel box section bars 50mmx50mm on the extremity. This construction process will assure general tank rigidity.

II.4.1.2 WINDOWS

Safety glass (8 mm thick) were fixed on the inside of the “U shape” using silicone “evo-stick” glue.

See detailed drawing in APPENDIX H

II.4.1.3 LINER

A liner was used on the inside of the overall tank to avoid water leaking.

II.4.2 Towing system design

II.4.2.1 RAIL

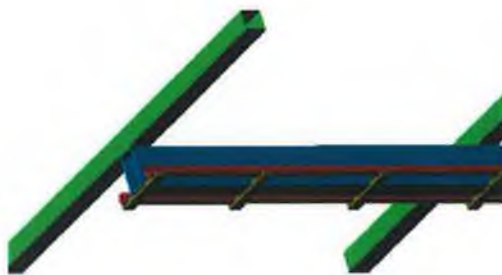


Figure 63 Rail view

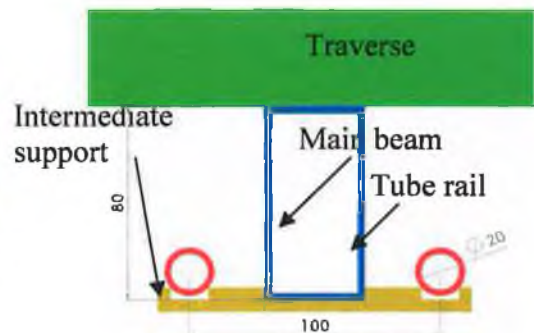


Figure 64 section of the rail assembly

The rail assembly is made of a 12m long main beam using steel box bar 80x40mm. Two 12m tubes (20mm diameter) were welded to an intermediate machined support to assure the parallelism all along the length of the rails. Also traverse box bars (1000x25x50mm) were welded at intervals of one meter on top of the main box beam in order to be able to lay the rail on top of the tank.

See detailed drawing in APPENDIX I

II.4.2.2 TROLLEY



Figure 65 Trolley assembly

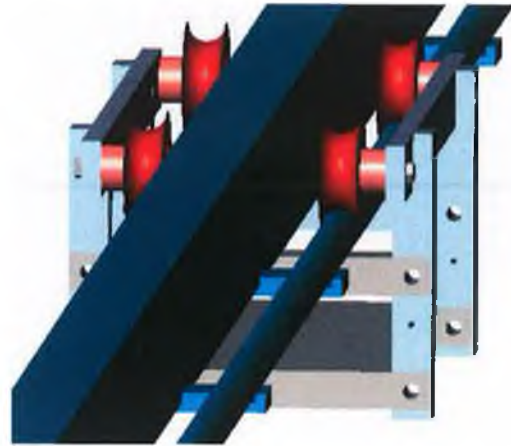


Figure 66 rail and trolley assembly

A long four wheels trolley has been designed to increase longitudinal stability.

See detailed drawing in APPENDIX J

II.4.2.3 FOIL / TROLLEY LINKAGE

The link between the trolley and the wing has been designed to be able to adjust, from test to test, the distance between the wing and the ground.

That link part had been made of cylindrical bar diameter 5mm; total immersed length: 1150 mm

The adjustment of the distance between the wing and the ground, can be made by adding or suppressing washer at the assembly between this part and the trolley

At this stage, the proposed design allow only one degree of freedom to the foil, this chose had be done to simplify test development.



Figure 67 Foil / trolley linkage

II.4.2.4 PROTECTIVE COATING

All steel parts of the structure were painted with a primer, as a protective coating, and a finish coating for corrosion protection.

II.5 MOTOR AND REDUCTION SYSTEM SELECTION

Motor and reduction system have to be able to support the testing request conditions.

II.5.1 Velocity requirement:

$$\omega = V / R_p \quad \text{Equation II-6}$$

Where:

ω is Radius velocity of the towing pulley

V : test velocity 2 m/s

R_p is the pulley radius (0.1m)

therefore :

$$\omega = 20 \text{ rad/s}$$

II.5.2 Required torque at the towing pulley

II.5.2.1 Generals equations:

$$T_p = F_p \cdot R_p \quad \text{Equation II-7}$$

$$F_c = \eta_{c/p} \cdot F_p \quad \text{Equation II-8}$$

Also:

$$\Sigma \text{ FORCES} = \text{INERTIAL FORCES}$$

$$D + Ft - F_c = -Ma \quad \text{Equation II-9}$$

Therefore :

$$F_c = Ma + D + Ft \quad \text{Equation II-10}$$

Where:

T_p : is the torque of the pulley (N.m)

F_p is the force of the pulley at its radius (N)

R_p is the pulley radius (m)

F_c is the cable force create by contact with the pulley and applied to the trolley (N)

$\eta_{c/p}$ is the cable/pulley system efficiency

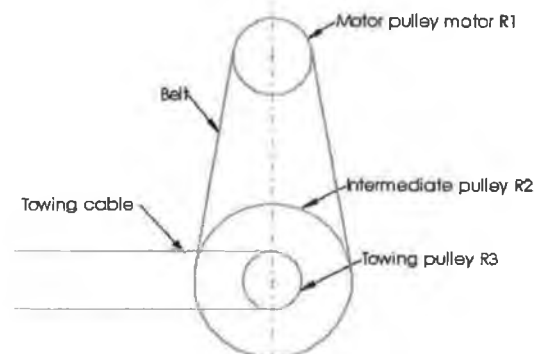


Figure 68 Transmission schema

D : drag force of the immersed body (N)

F_t is the friction force due to the contact between the trolley and the rail(N)

M is the mass of the moving parts (trolley and emerged body) (kg)

a is the acceleration of the moving parts (trolley and emerged body) (m/s^2)

II.5.2.2 Estimation of the drag force due to the foil tested and the link between the trolley and the foil:

The drag force of the immerge body must be calculated using, as typical foil tested, a NACA 0025 (chord: 1600mm span:200mm) and as link between the trolley and the foil a cylindrical bar (diameter 5mm; total immersed length:1150 mm).

The drag force equation is as follow:

$$D = \frac{1}{2} C_d \times \rho \times V^2 \times S \quad \text{Equation II-11}$$

With: D : drag force (N)

C_d : drag coefficient(function of the geometry and the Reynolds number)

Foil Naca 0025 about : 0.05

Cylinder about : 1

ρ : density of the water (1000 kg/m^3 fresh water)

V : test velocity 2 m/s

S : surface of the part creating drag (m^2)

Naca 0025 chord 160 span 200mm = 0.0769 m^2

Cylinder Φ 5mm length 1150mm = 0.0181 m^2

Drag force Naca 0025 foil :

$$D_{\text{foil}} = 0.5 \times 0.05 \times 1000 \times 2^2 \times 0.0769$$

$$D_{\text{foil}} = 7.69 \text{ N}$$

Drag of the immersed link between the foil and the trolley:

$$D_{\Phi 5\text{mm}} = 0.5 \times 1 \times 1000 \times 2^2 \times 0.0181$$

$$D_{\Phi 5\text{mm}} = 36.2 \text{ N}$$

Total drag force :

$$D_{\Phi 50\text{mm}} + D_{\Phi 5\text{mm}} = 7.69 + 36.2 = 43.9 \text{ N}$$

II.5.2.3 Estimation of the trolley / rail friction force

$$F_{\text{friction}} = Q \mu R / R_a \quad \text{Equation II-12}$$

Where:

Q is vertical force equal to Masse multiplied by the gravity ($4.5 \times 9.81 = 44,1 \text{ N}$)

μ is the Friction coefficient nylon/steel (0.55)

R_a is the external radius of the trolley wheel (R_a=40 mm)

R = internal radius of the trolley wheels (R=4 mm)

Therefore:

$$F_{\text{friction}} = 44,1 \times 0.55 \times 4/40 = 2.4 \text{ N}$$

II.5.2.4 Estimation of the trolley inertial force:

$$\text{Trolley inertial force} = m_{\text{tr}} \cdot a \quad \text{Equation II-13}$$

Where:

m_{tr} : is the trolley mass 4kg

a : is the trolley acceleration 2m/s^2

Therefore:

$$\text{Trolley inertial force} = 4.5 \times 2 = 9 \text{ N}$$

II.5.2.5 Estimation of the cable force

From Equation II-5 , and using previous calculations results as :

$$M a = 9 \text{ N}$$

$$D = 43.9 \text{ N}$$

$$F_t = 2.4 \text{ N}$$

Therefore:

$$F_c = 55.3 \text{ N}$$

II.5.2.6 Force, torque, angular velocity need at the towing pulley

Considering $\eta_{c/p}$ as the cable/pulley system efficiency of 0.90

from Equation II-3 $F_c = \eta_{c/p} \cdot F_p$ Equation II-14

$$F_{p01} = F_c / \eta_{c/p} \quad \text{Equation II-15}$$

Therefore :

$$F_{p01} = 61.4 \text{ N}$$

II.5.2.6.1 Torque :

From Equation II-7 and with Pulley radius $R_{p01} = 0.1 \text{ m}$

Therefore :

$$T_{p01} = 6.14 \text{ Nm}$$

II.5.2.6.2 Radius velocity (ω) :

From Equation II-16 and with linear velocity $V = 2 \text{ m/s}$

Therefore :

$$\omega = 20 \text{ rad/s}$$

II.5.3 Motor choice

Power required for this application :

From the following equation:

$$P_{\text{motor}} = T_{\text{motor}} \times \omega_{\text{motor}} \quad \text{Equation II-17}$$

Using the results of previous calculation that

$$\omega = 20 \text{ rad/s}$$

$$T_{p01} = 6.14 \text{ Nm which equal } T_{\text{motor}}$$

Therefore :

$$P_{\text{motor}} = 123 \text{ W or } 0.123 \text{ kW}$$

A motor was available in the Institute workshop. Its characteristics are :

Tri-phases Marelli motor :

Power : 0.55 kw

Nominal Velocity : 2730 rpm

Nominal Torque : 1.9 Nm

Nominal intensity $I_{N 400V Y}$: 1.44 A

Nominal intensity $I_{N 230V \Delta}$: 2.5 A

This motor must be able to answer to the specified requirement.

II.5.4 Transmission system design:

Considering a system with 3 pulleys with:

T_1 the torque, R_1 the radius, ω_1 radius velocity of the pulley on the motor shaft driving a first belt

T_2 the torque, R_2 the radius, ω_2 radius velocity of the pulley driven by the belt

first belt

T_3 the torque, $R_3=0.1\text{m}$ the radius, ω_3

radius velocity of the pulley driving the towing cable, moving the trolley

F_{belt} the belt force and V_{belt} the linear belt velocity applied to the pulley 1 and 2

F_{cable} the cable resistant force and V_{cable} the linear cable velocity applied to the pulley3

From the facility requirement:

$$F_{\text{cable}} = F_{\text{pulley 01}} = 61.4 \text{ N}$$

$$\Rightarrow T_3 = 6.14 \text{ Nm} \quad \text{due to } R_3 = 0.1\text{m}$$

$$V_{\text{cable}} = 2\text{m/s}$$

$$\Rightarrow \omega_3 = 20 \text{ rad/s} \quad \text{due to } R_3 = 0.1\text{m}$$

From the characteristics of the motor:

$$T_1 = 1.9 \text{ Nm}$$

It is also established that :

$\omega_2 = \omega_3$; $T_3 = T_2$ because the pulley 2 and 3 are on the same shaft

$$\Leftrightarrow T_3 = T_2 = 6.14 \text{ Nm}$$

$$\Leftrightarrow \omega_2 = \omega_3 = 20 \text{ rad/s}$$

also : $F_{\text{belt}} = T_1/R_1 = T_2/R_2$

so : $T_1/T_2 = R_1/R_2$

and because: $T_1 = T_2 \Rightarrow T_1/T_3 = R_1/R_2$

which mean that :

$$R_1/R_2 = 1.9/6.14 = 0.309$$

So with if $R_1 = 30 \text{ mm}$ $R_2 = 97 \text{ mm}$

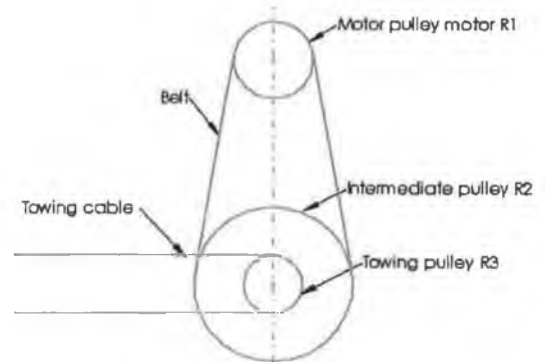


Figure 69 transmission schema

For this table it is decided to use $R_1 = 34 \text{ mm}$ and $R_2 = 100 \text{ mm}$ so $T_{1 \text{ required}} < T_{1 \text{ available}}$

Motor velocity:

$$V_{\text{belt}} = \omega_1 \times R_1 = \omega_2 \times R_2$$

$$\text{So : } \omega_1 = \omega_2 \times R_2 / R_1$$

$$\text{with } \omega_3 = \omega_2 = 20 \text{ rad/s} = 191 \text{ min}^{-1}$$

$$\Rightarrow \omega_1 = 191 / 0.309$$

$$\Rightarrow \omega_1 = 618 \text{ min}^{-1}$$

Summary :

$$R_1 = 30\text{mm}$$

$$R_2 = 100\text{mm}$$

$$R_3 = 100\text{mm}$$

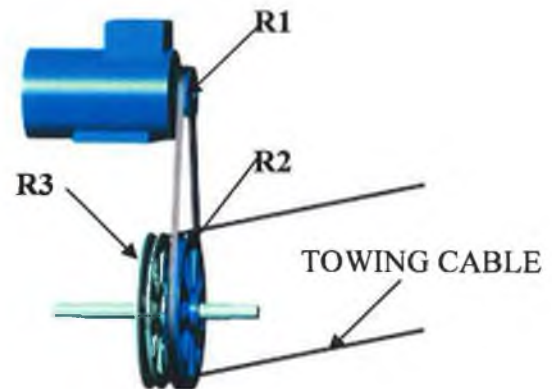


Figure 70 Transmission design

II.5.5 Motor speed control system

To assume the control of the motor on acceleration, steady velocity then deceleration, an inverter must be used.

The Telemecanique ALTIVAR 28 referenced ATV28HU41M2U has been chosen which is able to drive a motor up to 2.2 kW in case of upgrading the towing tank.

Towing tank drawing and the inverter characteristics are available in APPENDIX H

II.5.6 Global view of the towing tank

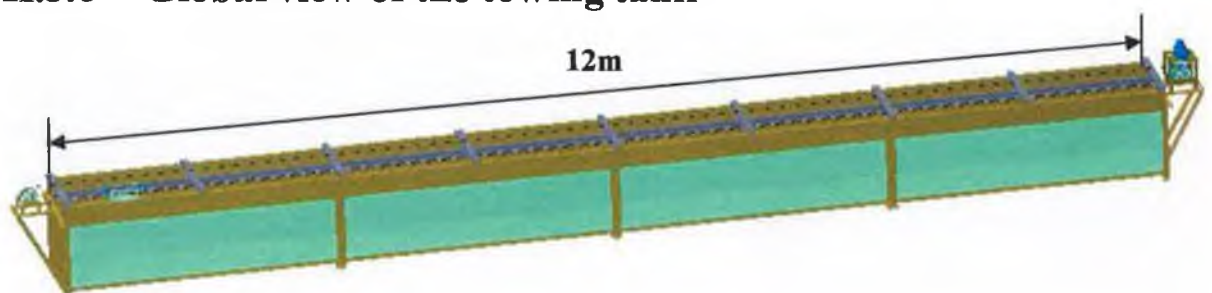


Figure 71 General view of the towing tank

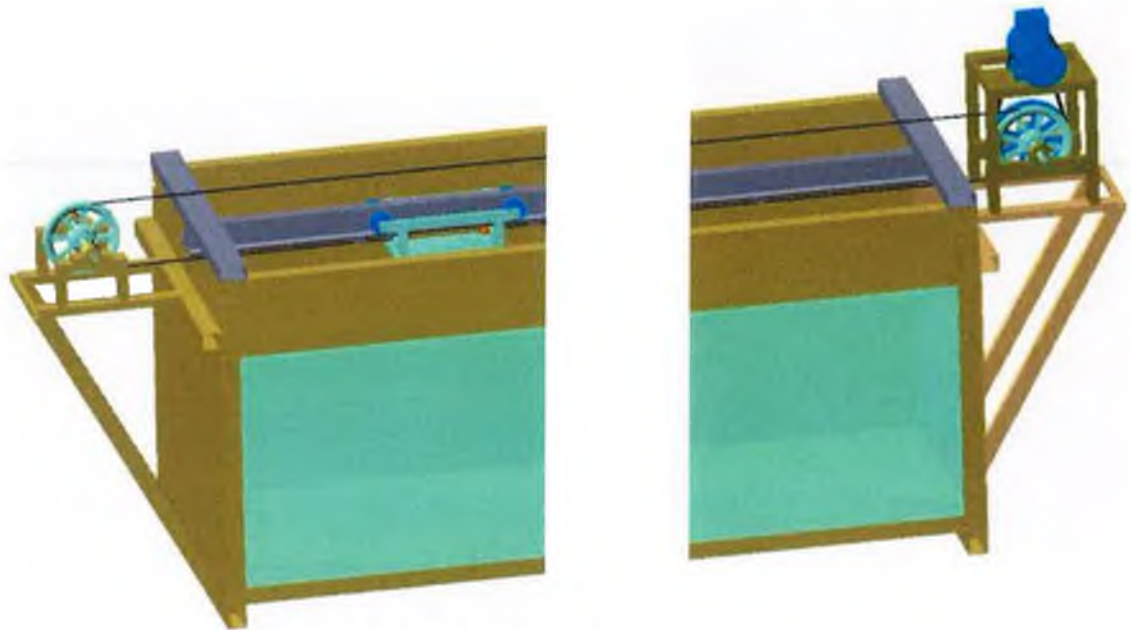


Figure 72 Figure 73 Both ends views of the towing tank

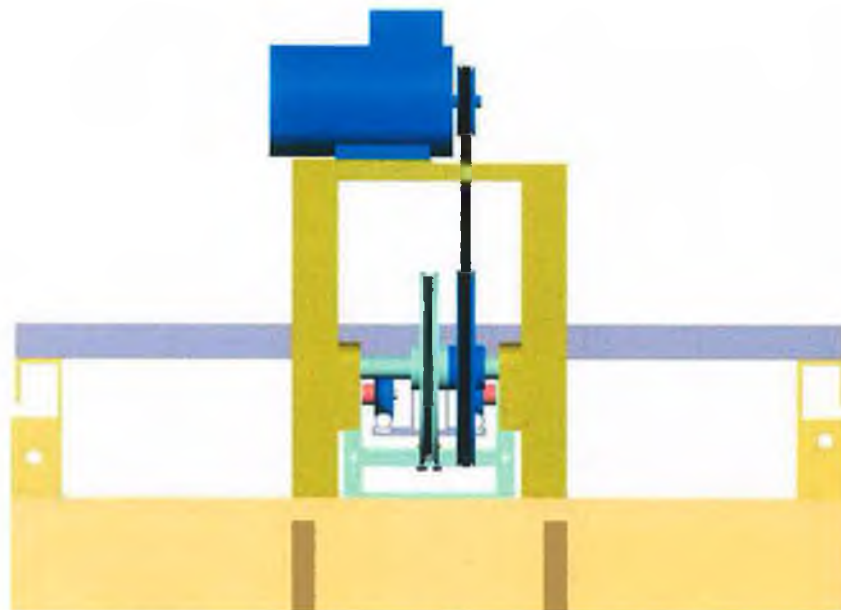


Figure 74 Partial 2D view of the towing tank

Manufactured testing facility



Figure 75 Inside view of the towing tank partially on water, including the rail and the trolley:

II.5.7 Record visualisation system

A digital camcorder Sony DCR TRV 325 as been chosen to record the experiments.

Camera characteristics:

800 000 pixels

optical zoom x 25

horizontal resolution 500 lines



Figure 76 Sony DCR TRV 325

Also the “black room” must be established around the camera to avoid reflection on the windows. Therefore, the recorded light is coming only from the top of the towing-tank



Figure 77 General view of the towing tank, and the outside of the black room which is located under the blue plastic cover:

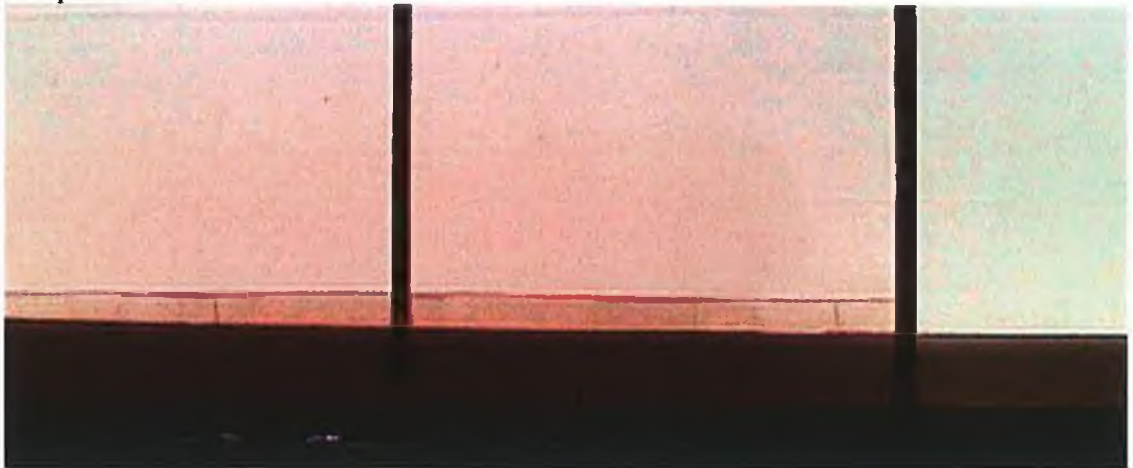


Figure 78 View of the testing area from the inside of the black room:

II.5.8 Total cost

The cost of the towing tank as been estimate at a 7000 euros value.

Item	cost
4x Ushape sections	4000€
Steel work Material	1000€
Trolley and Towing equipment	250€
Motor inverter	300€
Video Camera	1100€
Accessories	350€

Table 12 Detail cost of the test facilities

III. PROTOTYPES

III.1 DESIGN CONSTRAINTS:

Following the Computational Flow Dynamics simulations and the analytical studies, several profiles have been chosen for experimentation.

Models specification:

1. Each model must be designed with neutral buoyancy, to be able to analyse the compartment of the foil due to hydrodynamic effect without buoyancy force influence.
2. The models should be corrosion resistant and have a good behaviour in water.
3. The foils should be economical to manufacture.
4. Every hydrofoils must be designed to have a similar dimension and so able to be compared.

III.2 MATERIAL:

Taking the models specification into account, the composite material made of fibreglass and polyester resin had been chosen to manufacture the submarine wings. [42][43][44][45][46][47]

The resin is mixed with fibreglass in a simple fabrication process which requires no expensive equipment. Also for a 40% glass fibre composite material, the rough estimate of the tensile strength is approximately equal to 150 MPa and the flexural strength equal to 190 MPa. Glass-reinforced polyester is used in building applications such as cladding panels, marine industry, car bodies and surfboards.

III.3 HYDROFOILS:

III.3.1 Hydrodynamic profiles:

On completion of the tests, the most successful foil section will be selected according to the following criteria:

- Ability to create a lift when it flies to close to the ground.

As a first approach, only the section on the XY plane of the foil will be modified. The section on the XZ plane will be a basic rectangle.

Models are shown on Figure 78

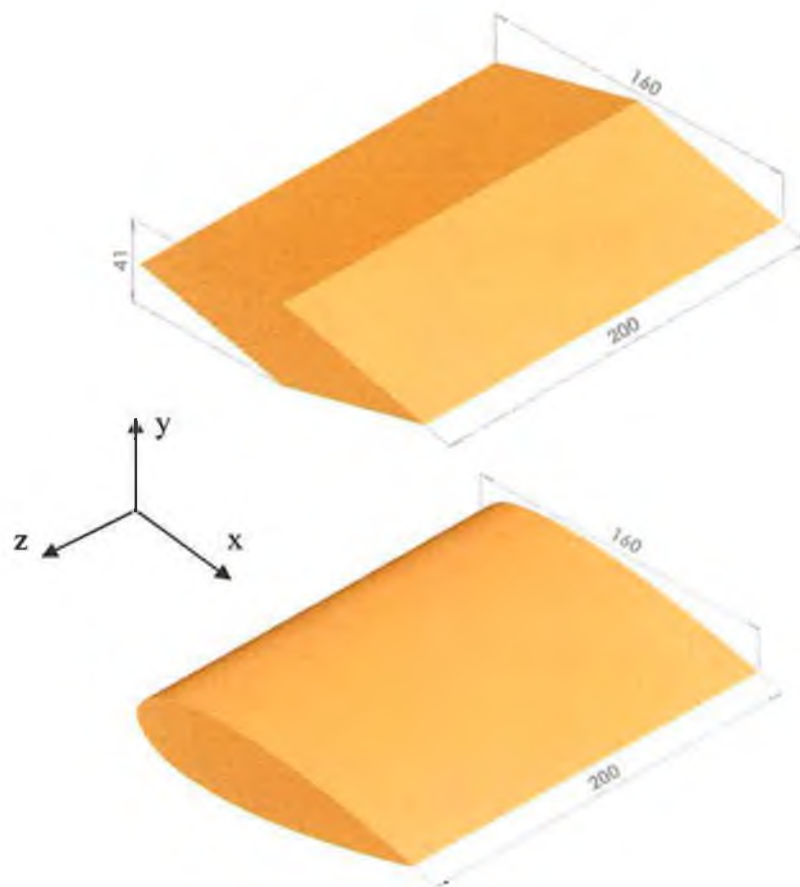


Figure 79 Diamond and NACA section models

Note : X-axis defines the chord of the section, Y-axis defines the thickness of the section and Z-axis defines the span of the wing.

III.4 NEUTRAL BUOYANCY SPECIFICATIONS :

III.4.1 Buoyancy:

As mentioned previously, the models must have a neutral buoyant at the operational depth. Overall buoyancy is not the only factor to be considered: the stability of the vehicle in the water is also important. Indeed, there are two constraints on the centres of mass and buoyancy, which a submersible vessel must obey (Chapter1 III.1.3):

1. The centre of buoyancy and the centre of gravity of the vessel must lie on a common vertical line. Were these to lie on different vertical lines, they would create a torque, which would rotate the vessel.
2. The centre of gravity of the vessel must be below the centre of buoyancy.

III.4.1.1 Determination of the foils weight

The density of the polyester resin is 1863.1 kg/m^3

Using CAD modelling it is possible to estimate easily the displaced volume of water of each wing. Indeed, the volume of the full wing is equal to the displaced volume of water. Considering that the purpose of our project is to design wings with neutral buoyancy, the only constraint is that the wing must have a global density of 1000 kg/m^3 . This density is calculated in terms of material mass divided by the displaced volume of water (also called total volume).

NACA 0025 neutral buoyancy specification:

The volume of the foil can be estimated using 3D CAD computation. This volume is also in this case the volume of the displaced water = $8.777 \times 10^{-4} \text{ m}^3$

- Density of water = 1000 kg/m^3
- Total wing mass needed = $1000 \times 8.777 \times 10^{-4} = 0.877 \text{ kg}$

Lozenge neutral buoyancy specification:

The volume of the foil can be estimated using 3D CAD computation. This volume is also in this case the volume of the displaced water = $6,56 \times 10^{-4} \text{ m}^3$

➤ Density of water = 1000 kg/m^3

➤ Total wing mass needed = $1000 \times 6.56 \times 10^{-4} = 0.656 \text{ kg}$

III.5 MANUFACTURING PROCESS:

III.5.1 Shaping technique:

III.5.1.1 Rigid polyurethane foam:

There is a lot of different polyurethane foam, which can be manufactured, in an extremely wide range of grades, densities (from 6 kg/m^3 to 1220 kg/m^3) and polymer stiffness from very flexible elastomer to rigid hard plastic. For this application, rigid polyurethane foam has been used to avoid melting due to polyester resin. The applications of rigid polyurethane foam are very large such as in construction, in the refrigeration industry, in plumbing and chemical plant, in ships and boats where foam fills a cavity to form a sandwich structure, in surfboards where a block of polyurethane is shaped and then covered with fibre glass and polyester resin to form the outer shell. The last application is called the shaping technique.

III.5.1.2 Core shaping:

The first step is to cut a block of rigid polyurethane foam using a hot wire and a printed section of the wing at 1:1 scale. The final shaping of the core is done using sandpaper of varying grit to smooth the shape. The finished shape should be as smooth as possible with no uneven surfaces. If there are any rough spots on the finished shape, this will affect the behaviour of the wing once in the water.

III.5.1.3 Stratification:

The next stage is called the stratification and involves covering the core with a layer of polyester resin and glass fibres. Once the resin and the catalyst are mixed in the correct ratios (according to the manufacturer's instructions), there is only around 20 minutes to complete this job. When the first layer of resin is applied, fibre mat are laid directly on the resin. Once the fibre is in position, a roller is used to impregnate the fibre with the resin and remove any trapped air. To get the required thickness, several layers of polyester resin and fibre are

applied. At the end, to ensure a perfect finish a last layer of gel-coast should be applied and smoothed using sand paper.

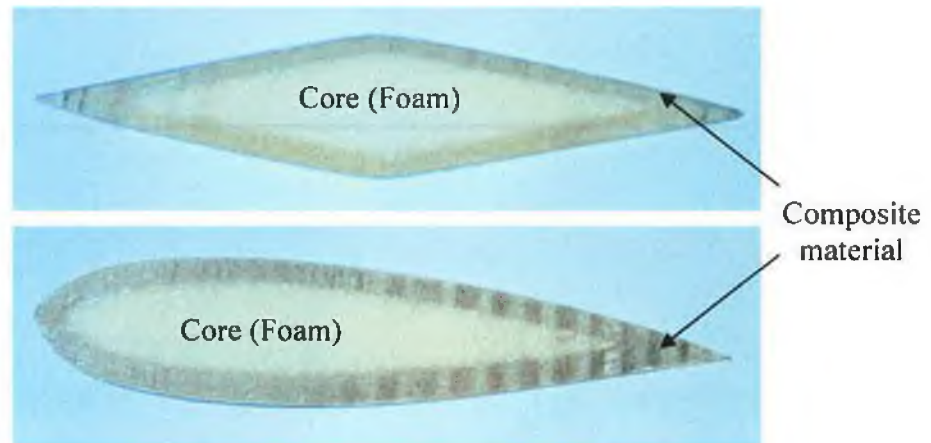


Figure 80 **model wing section**

IV. TESTS

IV.1 TESTS CONDITIONS:

Acceleration: 1 m/s^2

Steady velocities: 2 m/s

Time of steady velocities : 3 s

Deceleration: 1 m/s^2

Depth position:

Stage 01 free flow situation: Distance to the bottom: 233 mm

Distance to the surface: 667 mm

Stage 02 ground effect flow situation: Distance to the bottom: 33 mm

Distance to the surface: 667 mm

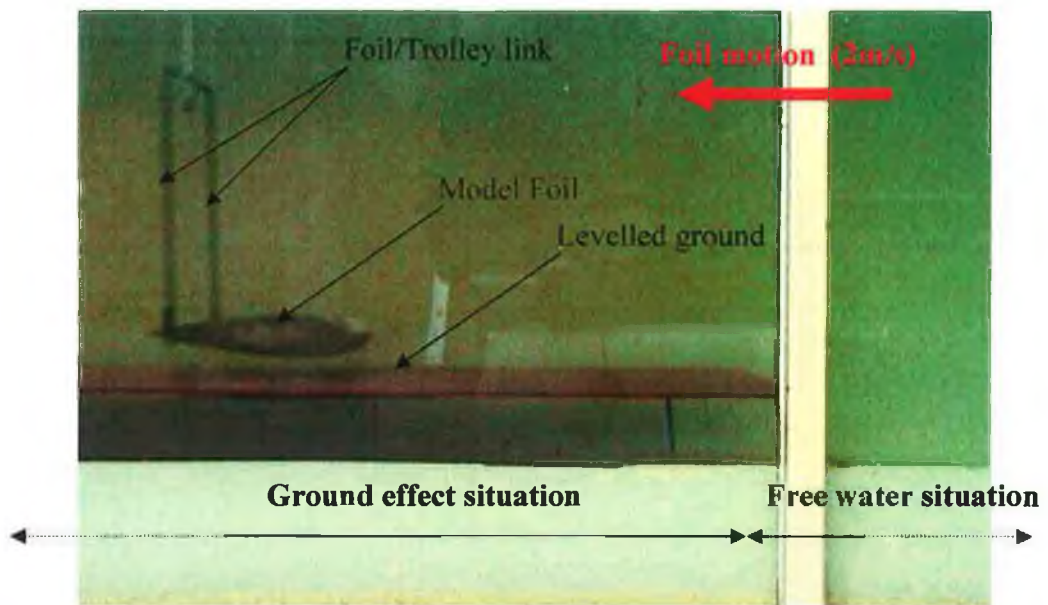


Figure 81 Testing situation display

IV.2 TEST RESULTS

NACA 0025

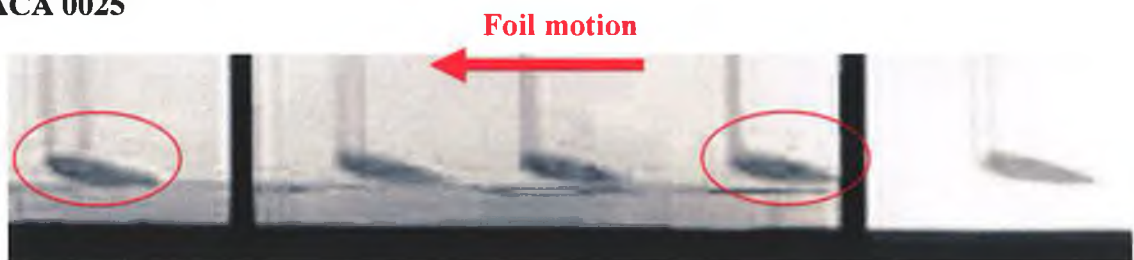
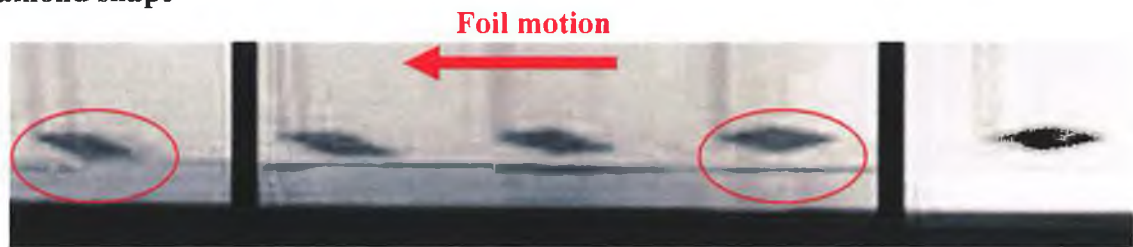


Figure 82 NACA 0025 test display

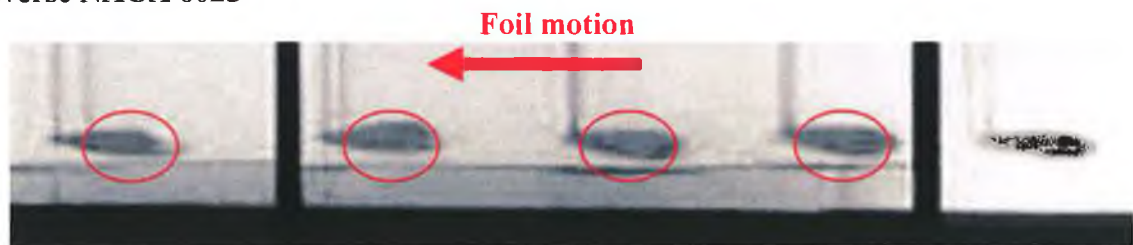
On free water situation, the foil is stable and flying with a sensibly nil angle of attack

On ground effect situation, the foil is moving with an angle of attack sensibly positive, which mean that the tail of the foil had been sucked to the ground. Those results confirm the simulation done previously with Ansys.

Diamond shape**Figure 83 Diamond shape test display**

On free water situation, the foil is stable and flying with a close to nil angle of attack

On ground effect situation, the foil is moving with an angle attack slightly positive, which mean that the tail of the foil had been sucked to the ground. Those results are according to the simulation done previously with Ansys

Reverse NACA 0025**Figure 84 Reversed NACA 0025 test display**

On free water situation, the foil is stable and flying with a close to nil angle of attack

On ground effect situation, the tail of the foil is rising at the beginning, then the movement is not stable any more and the tail goes up and down. This could be due to different effects, tail turbulences or appearance of negative lift due to temporary negative angle of attack at top tail position. Those results confirm the simulation done previously with Ansys however it is obvious that other factors influence the dynamic of the wing in ground effect situation.

From the previous experimental tests it can be concluded that the “reverse NACA” section is the most promising shape of all the shapes studied. During the experimental tests, this wing section was the only one able to stay away from the ground.

CONCLUSION

The objectives is to develop a towed underwater vehicle, able to fly at constant distance from the sea bed, cheap to produce, maintain and run. The aim of this study was to establish the feasibility of such a vehicle, and create a conceptual design of a wing able to fly at a constant distance from the sea bed.

Available underwater vehicles are controlled in three dimensions using directional wing and variable buoyancy.

CONCLUSIONS REACHED

This study showed that a ballast solution is not suitable to control a close-ground towed vehicle able to avoid obstacles. The amount of water needed to expect an efficient control system of the device is much greater than the space available in the towed vehicle.

It was also shown that a directional wing solution, using the angle of attack to create a lift is more realistic than the ballast system. However, this design would need to be driven by a close loop control system including: sonar to constantly measure the vehicle-seafloor distance, flapper wing or rotation wings activated by motor to create the lift and raise the vehicle. A PLC controller would be needed to manage the system. Therefore directional wing solution induce a high manufacturing, maintaining and running cost for the only driving function of the vehicle.

None of the existing submarine products are using ground effect to fly over the sea bed. A CFD analysis and experimental testing were conducted on wing models to study the feasibility of such a vehicle.

From the CFD analysis and the experimental tests, the following observations were made:

- The proximity of ground has an influence on the pressure distribution around the wing.
- The shape of the wing has an important influence on the ability to lift the wing on close ground configuration.

- Sections having an increase of thickness over the longest portion of the chord are more suitable to create a ground effect lift.
- The “reverse NACA” section is the most promising shape of this studies. During the experimental tests, this wing section was the only one able to stay away from the ground. Afterward the movement became unstable, this could be due to different effects such as tail turbulences or appearance of negative lift due to temporary negative angle of attack at top tail position

This study showed that the concept of ground effect, which has never really been studied for underwater applications, is realistic solution to optimise the efficiency and cost of continental shelf survey.

FURTHER DEVELOPMENTS

- It was observed in CFD simulation and testing that the turbulence have an influence on the flying stability of the wing. Therefore further research much be done to optimised the tail shape of the wing to avoid turbulence.
- Also the test condition done with a wing / trolley linkage, allowing only one of free degree of rotation of the wing around the horizontal axis, must be developed to free the model on vertical translation. Therefore, further study must be done to design linkage able to give more freedom to the wing.

REFERENCES

EXISTING PRODUCT

1. E.S.I. Environmental Sensors Inc catalogue: <http://www.esica.com/index.html> (dec/00)
2. Klein Associate Inc., catalogue: <http://www.kleinsonar.com/frames/subframes.html> (dec/00)
3. International Industries, Inc. catalogue: <http://www.intnlind.com/Klein/SBP.html> (dec/00)
4. WATARU KOTERAYAMA, "Space-continuous Measurement on ocean Current and chemical properties with the intelligent towed vehicle "Flying Fish" " Journal of Ocean Engineering, vol. 25, No.1, January 2000
5. W KOTERAYAMA & T. AKAMASTU , 1993, "Development of a towed vehicle for physical and chemical measurement in the upper mixed layer" Proc Ocean'93 vol. 3 pages497-501
6. KATO N., "Underwater towed vehicle manoeuvrable in both vertical and horizontal axis", The International Society of Offshore and Polar Engineers Conference, 1991, Vol. 2, Pages 85-92,
7. KATO N., "Guidance and control of underwater towed vehicle manoeuvrable in both vertical and horizontal axis", The International Society of Offshore and Polar Engineers Conference, 1992, Vol. 2, Pages 505-512,

CONTINENTAL SHELF

8. IRI/LDEO Climate Data Library <http://ingrid.ldgo.columbia.edu/> (dec/00)
9. MYERS JOHN J., 1969, "Handbook of Ocean and Underwater Engineering", ed Mc Graw-Hill Book Company.
10. RICHARD D TERRY, March 1966 "Ocean Engineering" Vol. IV, by North American Aviation Inc
11. HARDISTY J., 1990, "The British Seas", by Routledge, London ISBN 0-415-03586-4

12. UNNITHAN V. & SHANNON P.M., August 2000, "Reconnaissance Survey of the Irish continental Shelf/Shelf Edge" in Marine Resource Series No.12 2000, ed : Marine Institute , ISSN 1393 4643

SUBMARINE DESIGN

13. GRACZYK T., JASTRZEBSKI T. & BREBBIA C.A., "Marine technology and transportation", Computational mechanics publications, 1995.
14. HEIZWOLF J. J., Submarine dive technology, www.heizwolf.com/subs/tech, 2001.
15. J N NEWMAN, "Marine Hydrodynamics", The MIT Press, 1977, ISBN 0-262-14026-8
16. MYERS, HOLM AND MCALLISTER, "Handbook of ocean and underwater Engineering", New York, McGraw-Hill, 1969
17. J N NEWMAN, "Marine Hydrodynamics", The MIT Press, 1977, ISBN 0-262-14026-8

WING THEORY

18. IRA H. ABBOTT & ALBERT E. VON DOENHOFF, "Theory of wing sections", New York Mc. Graw-Hill Book Company, 1949
19. ROBERT T. JONES, "Wing theory", New Jersey, Princetown University Press, 1990, ISBN: 0-691-08536-6
20. JOHN J. BERTIN & MICHAEL L. SMITH; "Aerodynamics for engineers" 2nd edition, Prentice-Hall International Inc.1989, ISBN: 0-13-018227-3
21. E. L. HOUGHTON & P. W. CARPENTER, "Aerodynamics for Engineering Students" 4th edition, Edward Arnold, ISBN: 0-340-54847-9
22. O.G. TIETJENS, "Applied Hydro-and aerodynamics", McGraw-Hill, 1934

GROUND EFFECT

23. LT IAN ATKINS RN, "Wing in Ground Effect Machines" Supervisor: Dr A R Greig, University College London in the 1997 -1998
24. T. J. BARBER, E. LEONARDI AND R. D. ARCHER, "A technical note on the appropriate CFD boundary conditions for the prediction of ground effect aerodynamics" the aeronautical journal, Nov 199

FLUID PROPERTIES

25. "Seawater: its composition, properties and Behaviour" The Open University, Pergamon Press plc, 1989, ISBN 0-08-036368-7
26. HARROLD V. Thurman "Introductory Oceanography 7th edition" Macmillan Publishing Company, New York, 1994, ISBN 0-02-420811-6
27. WILLIAM S. & ARX, Sc.D "An Introduction to Physical Oceanography" Addison-Wesley Publishing Company, Inc 1967
28. SVERDRUP H.U, JOHNSON M. W. & FLEMING R. H., "The Oceans their Physics, Chemistry, and General Biology" Prentice-Hall, Inc., New York, 1970
29. HORNE R.A., "Marine Chemistry, the Structure of Water and the Chemistry of Hydrosphere " Wiley-Interscience

FLUID DYNAMICS

30. MASSEY B.S., "Mechanics of fluids", 6th edition, Chapman & hall, 1989.
31. MOTT R. L., "Applied Fluid Mechanics", 2nd edition, Charles E. Merrill Publishing Company, 1979.

BALLAST COMPUTATION

32. QUEHIN S., "A low cost free drifting position transmitter for the measurement of the Thermocline", Galway-Mayo Institute of Technology, 2000.
33. MILINAZZO F., WILKIE M. and LATCHMAN S.A., "An efficient algorithm for simulating the dynamics of towed cable systems", Ocean Engineering, (1987), Vol.14, n° 6, 513-525.
34. WOLFRAM S., "The Mathematica Book", 3rd edition, Wolfram Media, Cambridge University Press, 1996.

SIMULATIONS

35. NOWAK & SOLIES, "wind tunnel test of a high lift generation and Stall/spin Recovery system", journal of aircraft, vol. 37 No 3 may-june 2000 pages 383-389
36. LISSAMAN "low Reynolds number Airfoils" fluid Mechanic Annual review, 1983 Vol 15 pages 223-239

37. SAHIN, HYMON "Numerical calculation of submerged bodies a free surface" Ocean engineering, May 1993, vol 20, page 339-347
38. O.C.ZEINKIEWICZ & RL TAYLOR,"the finite element Method" vol3 fluid dynamics, fifth edition, by Butterworth-Heinemann 2000

TEST FACILITIES

39. Department of aerospace and ocean engineering water tunnel, <http://www.aoe.vt.edu/> (dec2001)
40. The NASA Glenn Research Centre, <http://www.grc.nasa.gov/> (dec2001)
41. Göttingen Institute, http://www.sm.go.dlr.de/sm-sm_info/TRTinfo/wsg.html (dec2001)

WING MODELS

42. DOYLE J. R., "U-Kite Development", Galway-Mayo Institute of Technology 2000
43. Chong C.V.Y, "Properties of materials", Macdonal & Evans Handbooks, 1978
44. Hall C., "Polymer materials – An introduction for technologists and scientists", The Macmillan Press LTD, 1982
45. Woods G., "The ICI Polyurethanes Book", John Wiley and Sons, 1987
46. <http://www.psrc.usm.edu/macrog/mech.htm> - "Mechanical properties of polymers" (April 2002)
47. <http://www.tifac.org.in/news/poly.htm> - "Properties of polyester resins" (April 2002)

THE LEAST SQUARES METHOD α AND β CALCULATION

```
Clear[ $\rho$ , area, cd, curve, v, finalvelocity, table, line]
 $\rho$  = 1025;
area = 1.5  $\times$  0.50;
cd = 1.1667;
curve =  $\frac{1}{2}$   $\times$   $\rho$   $\times$  area  $\times$  cd  $\times$  v2;
finalvelocity = 0.15;
table = Table[{v, curve}, {v, 0, finalvelocity, 0.03}];
line = Fit[table, {1, v}, v]
Plot[{curve, line}, {v, 0, finalvelocity}];
```

-1.34535 + 67.2675 v

-0.595017 + 44.6263 v

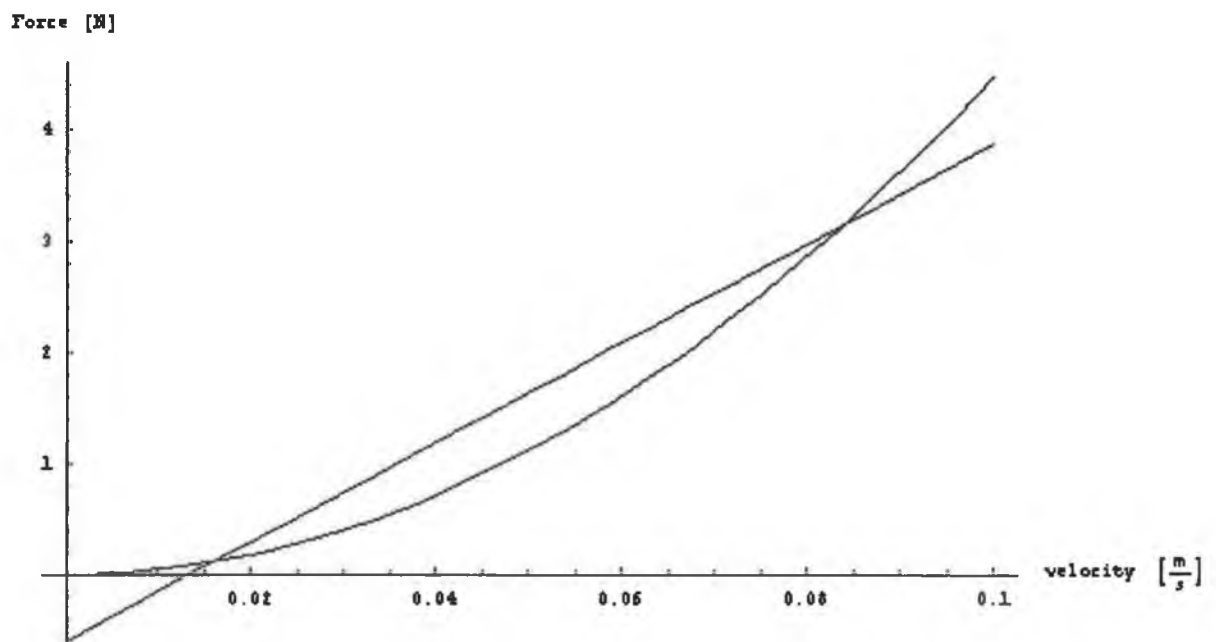
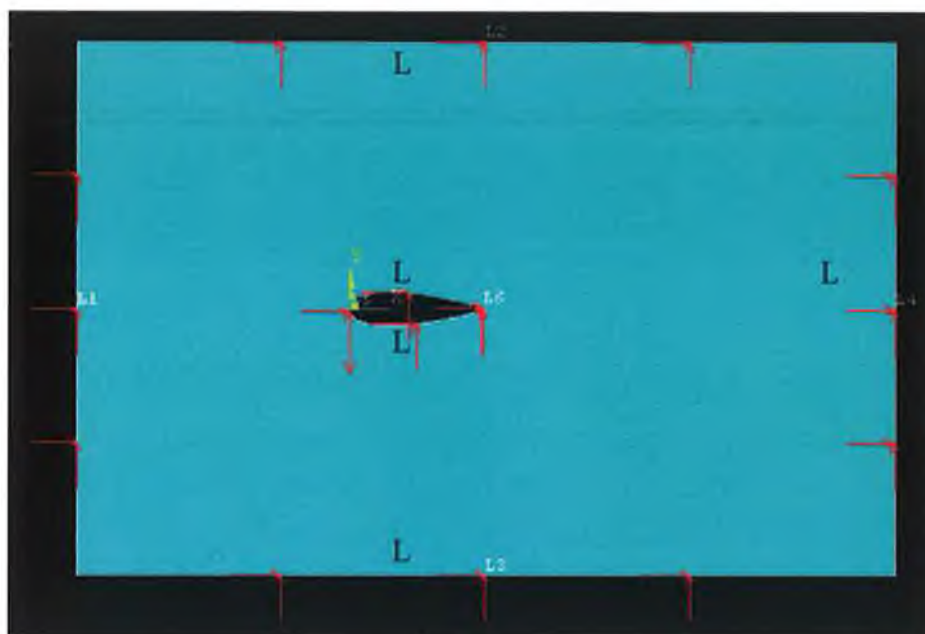


Figure A-1: Graphic of the drag and the line for V= 0.10 m/s

SIMULATION BOUNDARY CONDITIONS



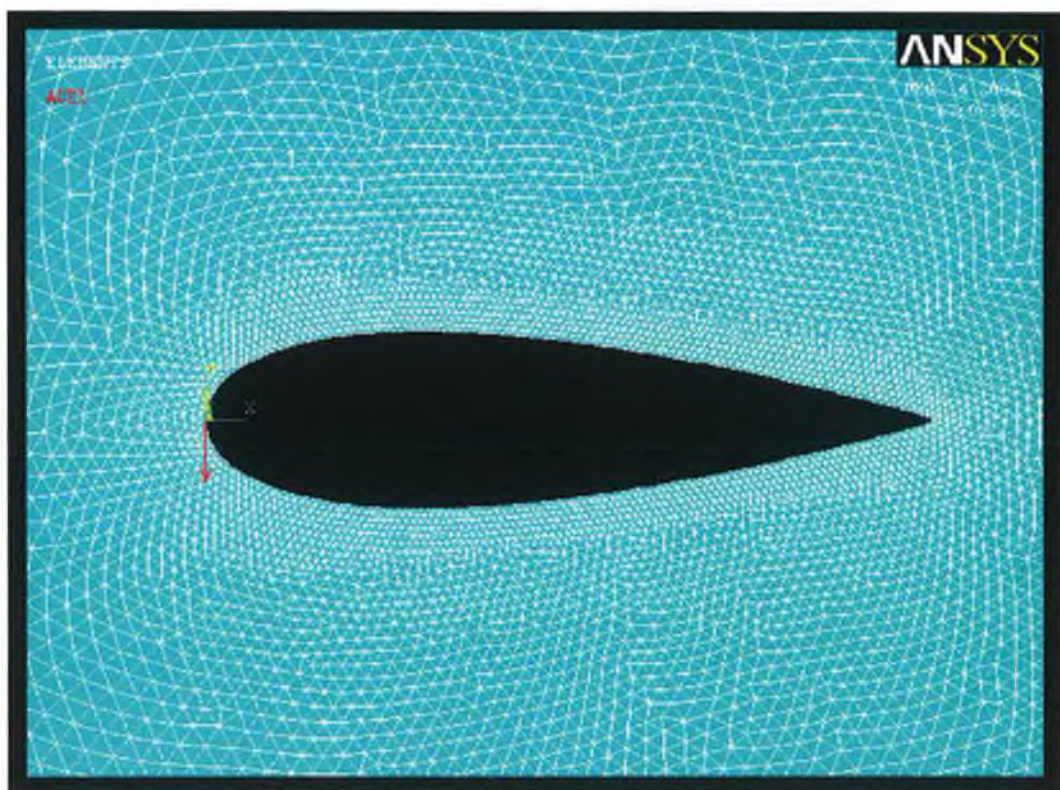
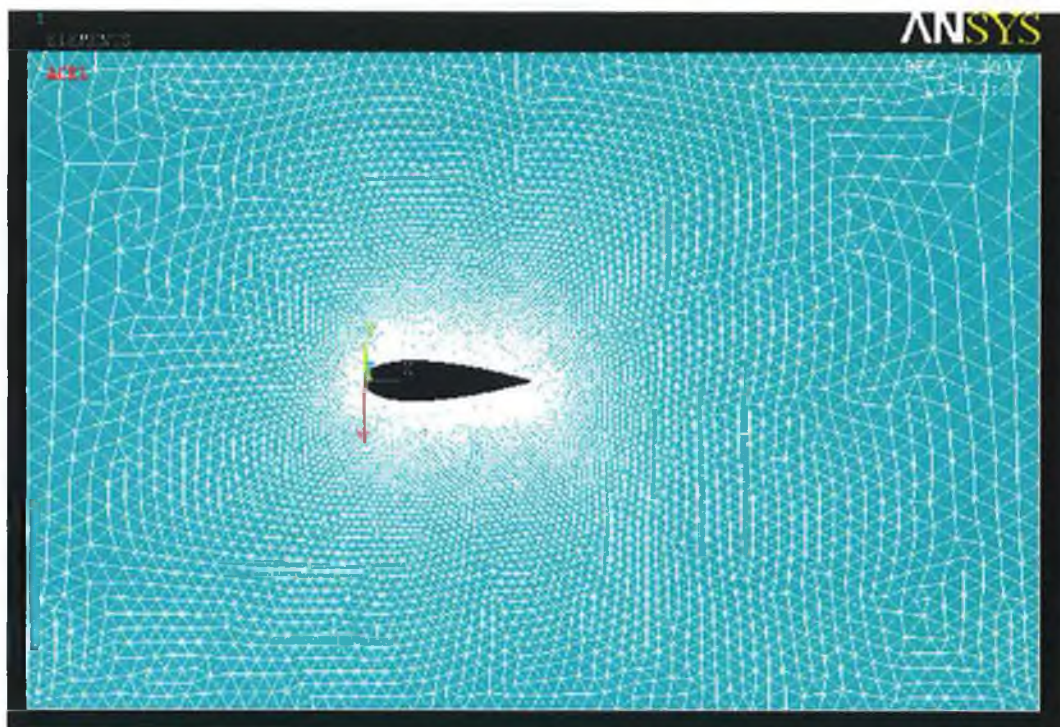
Inertia load options

Acceleration vector	GLOBAL CARTESIAN COMPONENTS ARE:
	0.0000 -9.0200 0.0000
Angular velocity vector	GLOBAL CARTESIAN COMPONENTS ARE:
	0.0000 0.0000 0.0000
Angular acceleration vector	SPIN SOFTENING NOT ACTIVATED
	GLOBAL CARTESIAN COMPONENTS ARE:
	0.0000 0.0000 0.0000
Reference coord. system origin	ORIGIN = 0.0000 0.0000 0.0000
Angular velocity vector	REFERENCE COORDINATE COMPONENTS ARE:
	0.0000 0.0000 0.0000
Angular acceleration vector	REFERENCE COORDINATE COMPONENTS ARE:
	0.0000 0.0000 0.0000
Inertia relief	NO INERTIA RELIEF

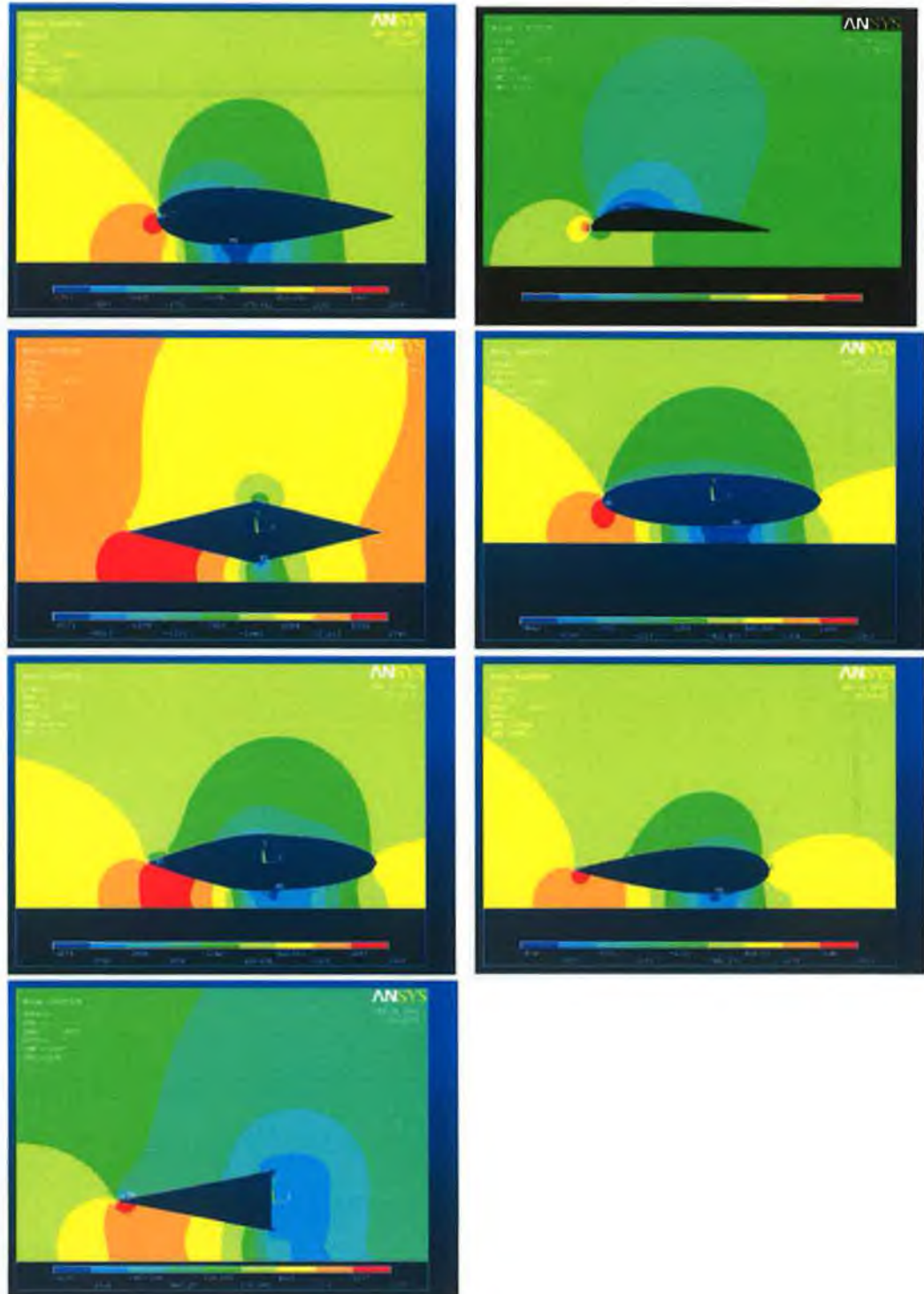
LIST CONSTRAINTS ON ALL SELECTED LINES

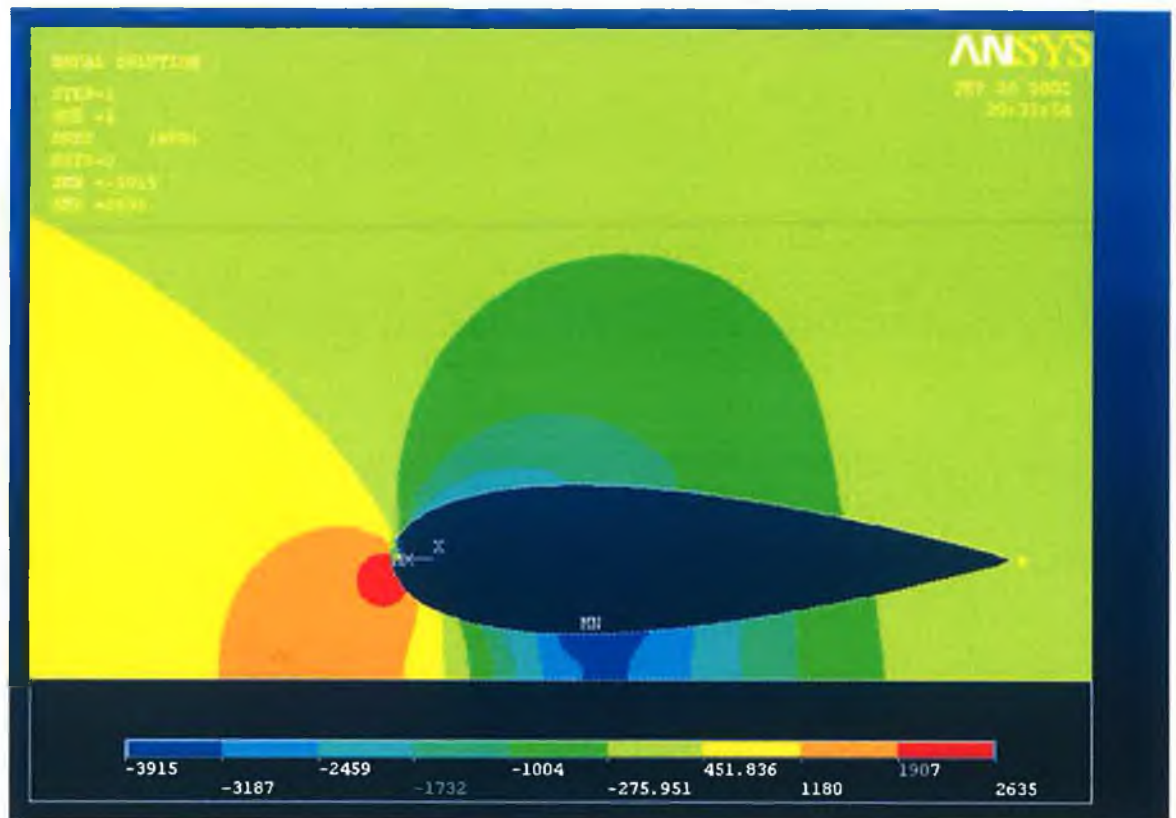
LINE	LOAD LABEL	VALUE(S)		MAREA
1	UX	2.0000	1.0000	0
1	UY	0.0000	1.0000	0
2	UX	2.0000	1.0000	0
2	UY	0.0000	1.0000	0
3	UX	2.0000	1.0000	0
3	UY	0.0000	1.0000	0
4	UX	2.0000	1.0000	0
4	UY	0.0000	1.0000	0
5	UX	0.0000	1.0000	0
5	UY	0.0000	1.0000	0
6	UX	0.0000	1.0000	0
6	UY	0.0000	1.0000	0

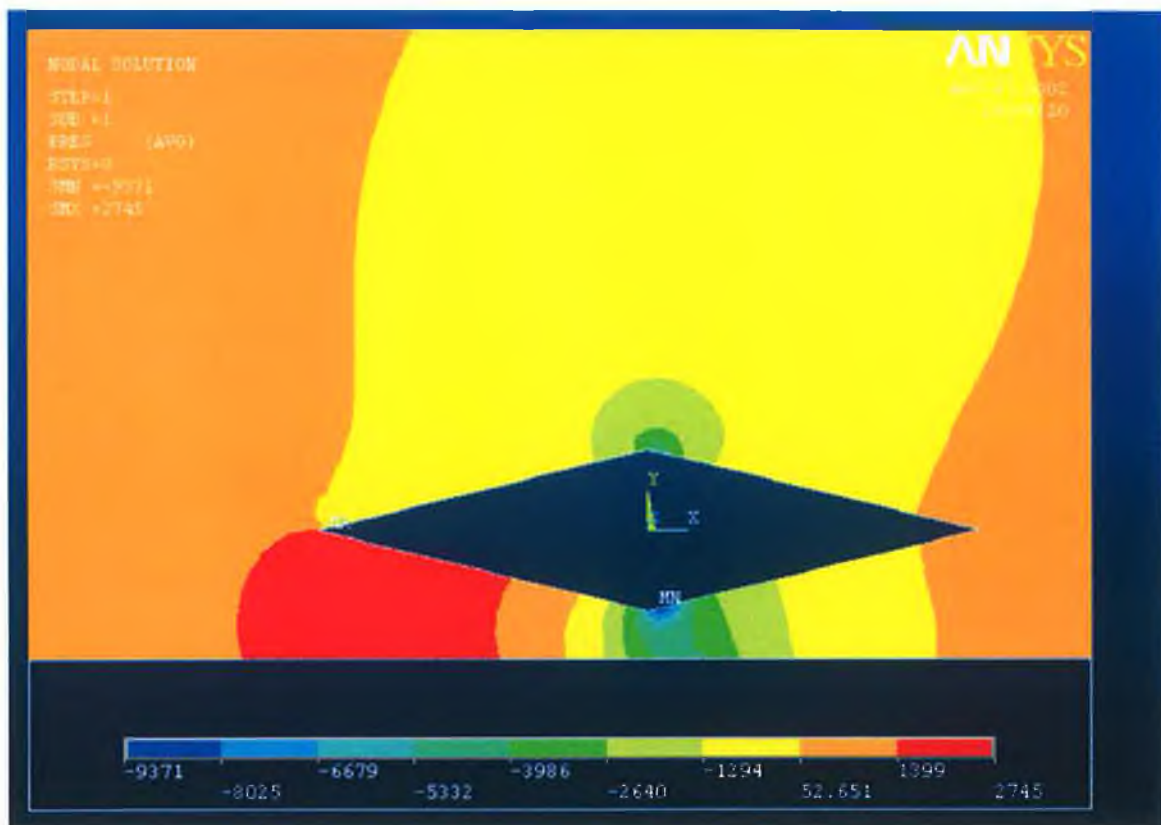
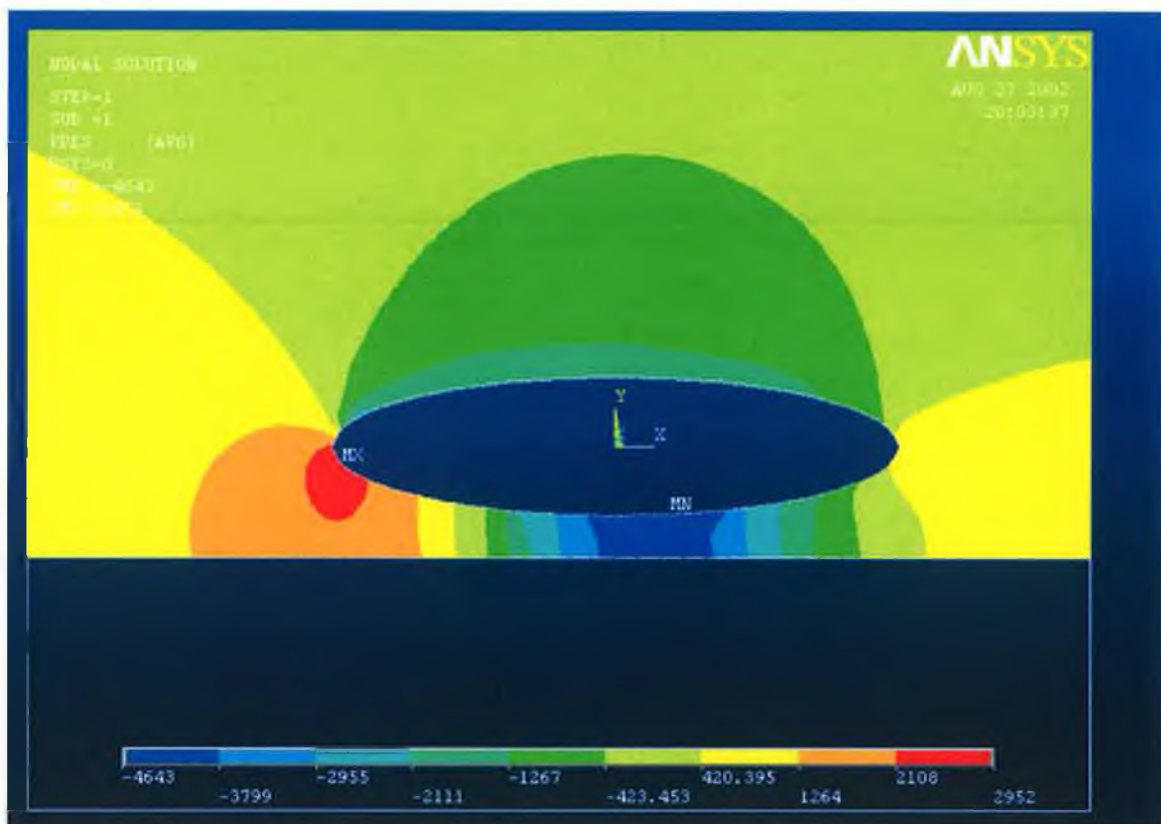
SIMULATION MESHING DISPLAY

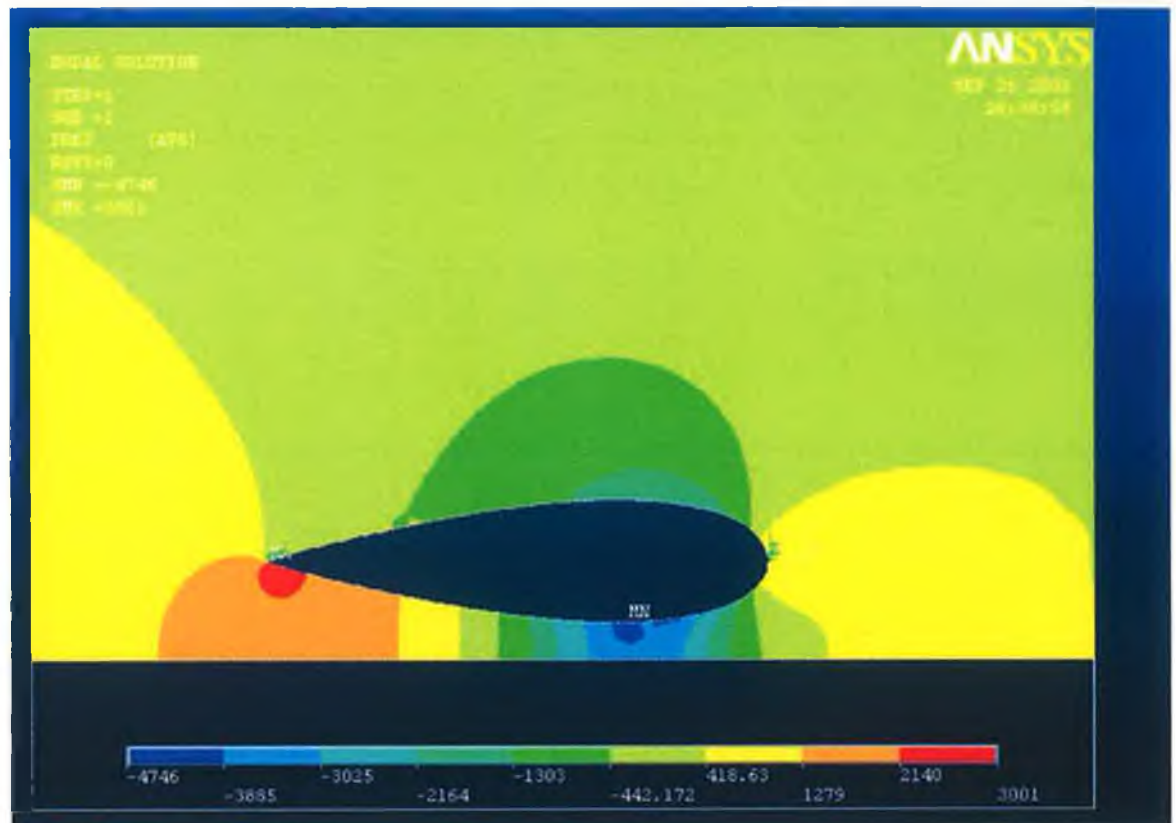
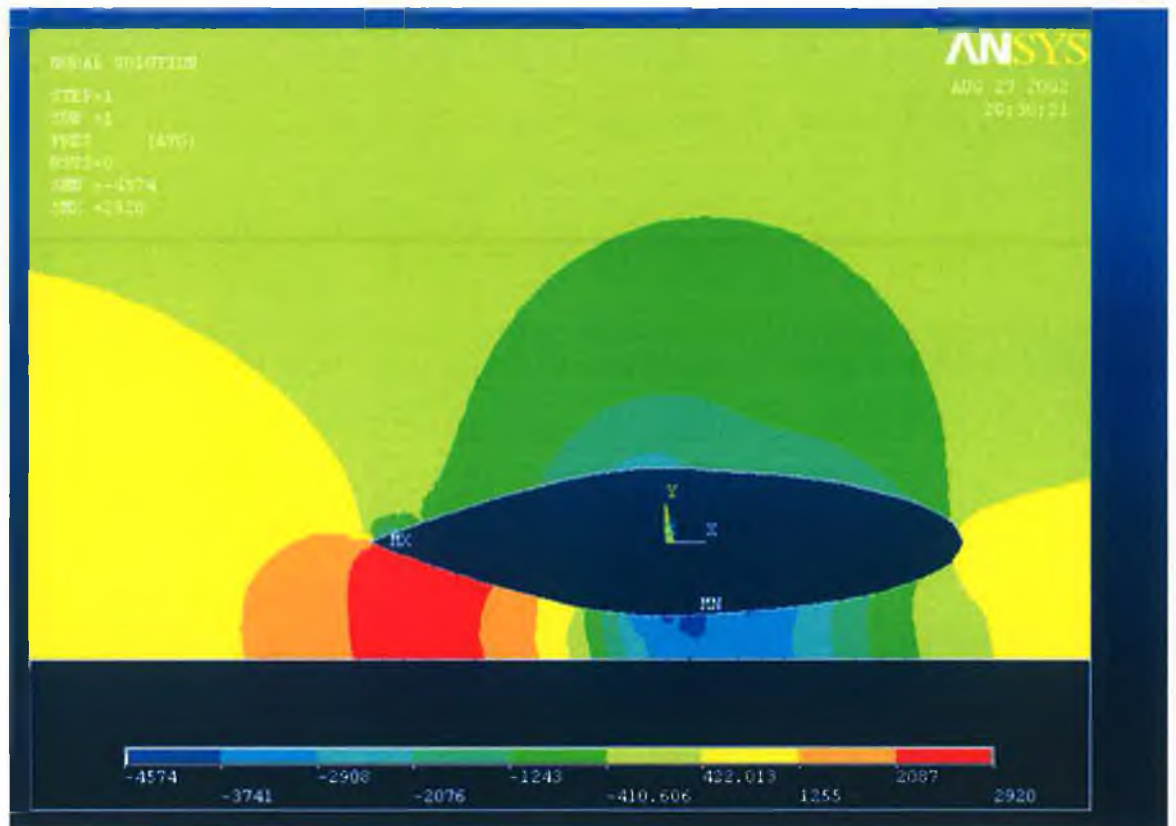


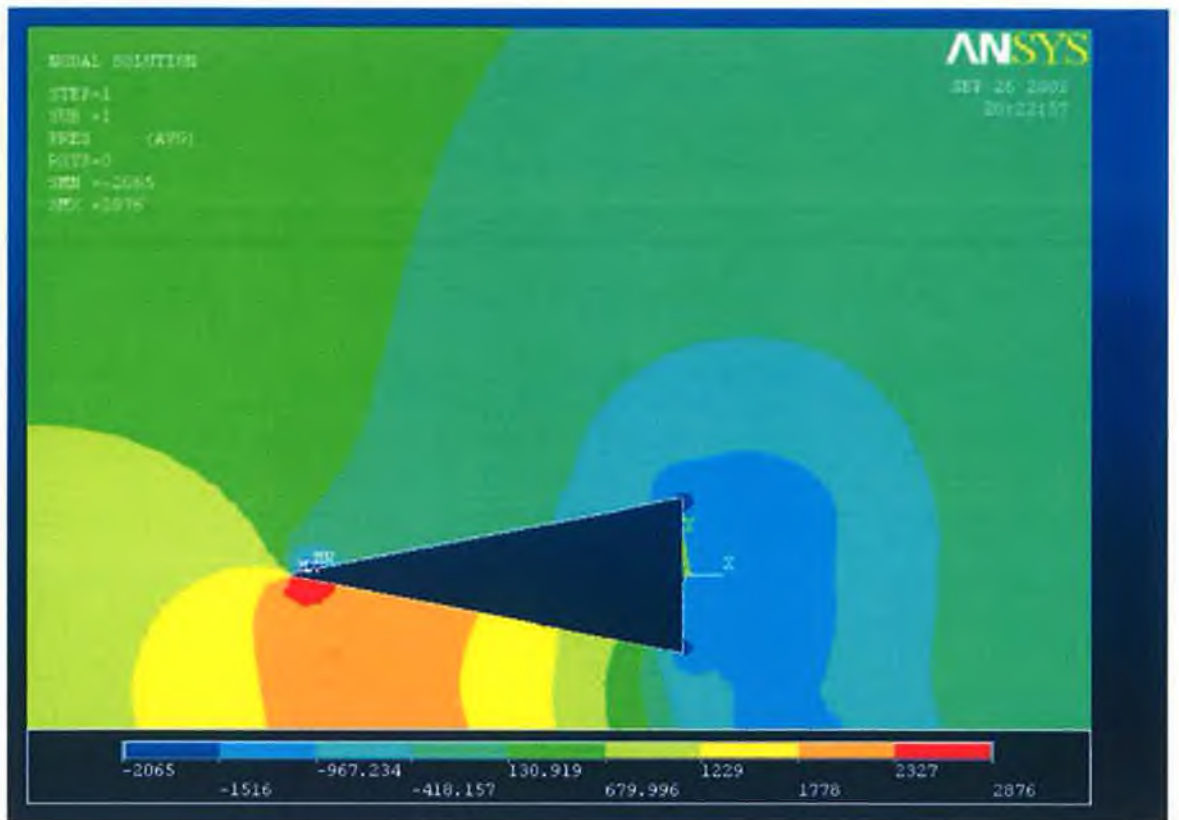
RESULTS SYNTHESSES OF FOILS CLOSE TO THE GROUND





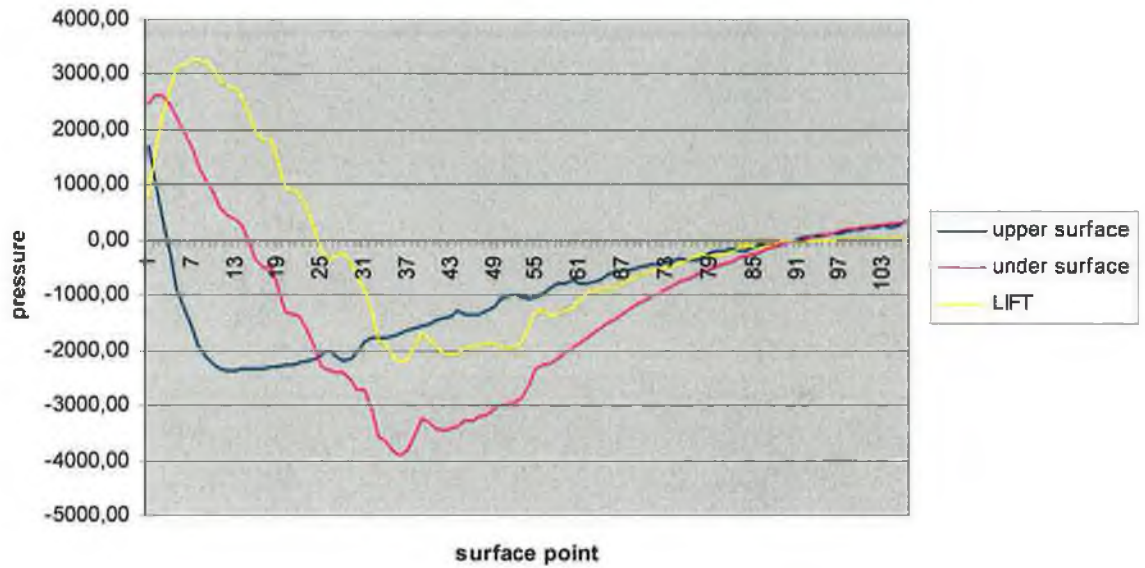




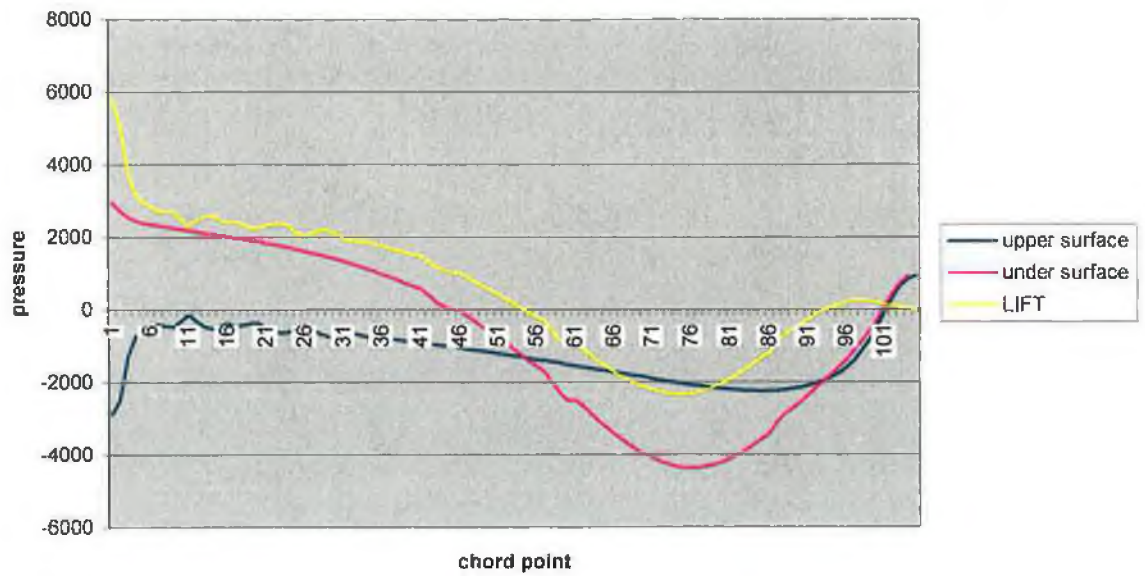


LIFT DIAGRAMS

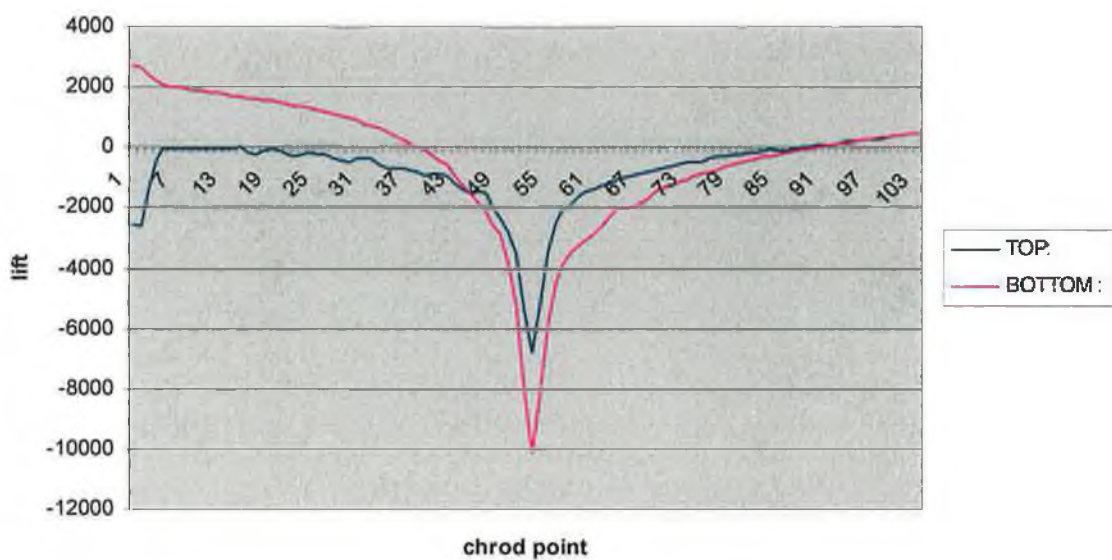
Naca 0025 on ground effect



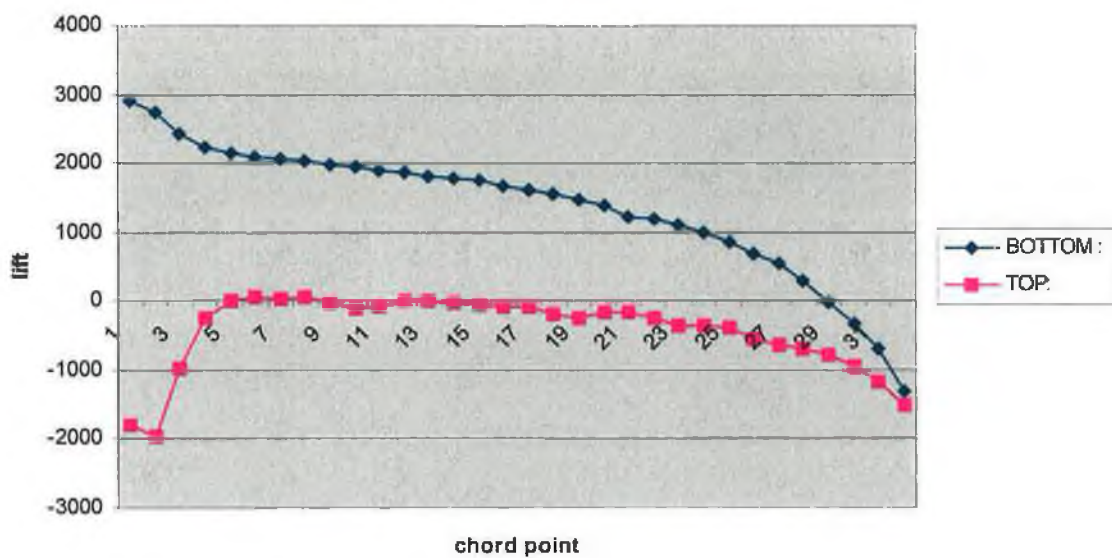
rev naca0025 lift ground effect



Lozenge 500x100 lift

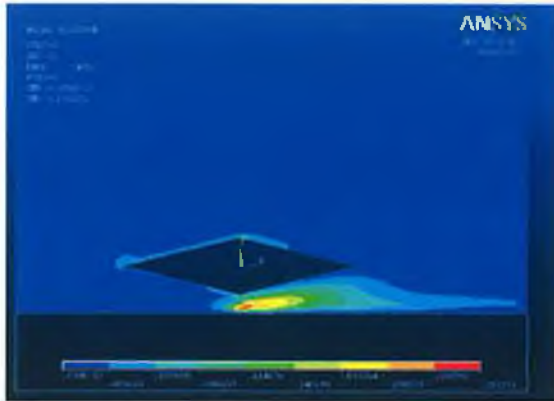


Half-Lozenge lift

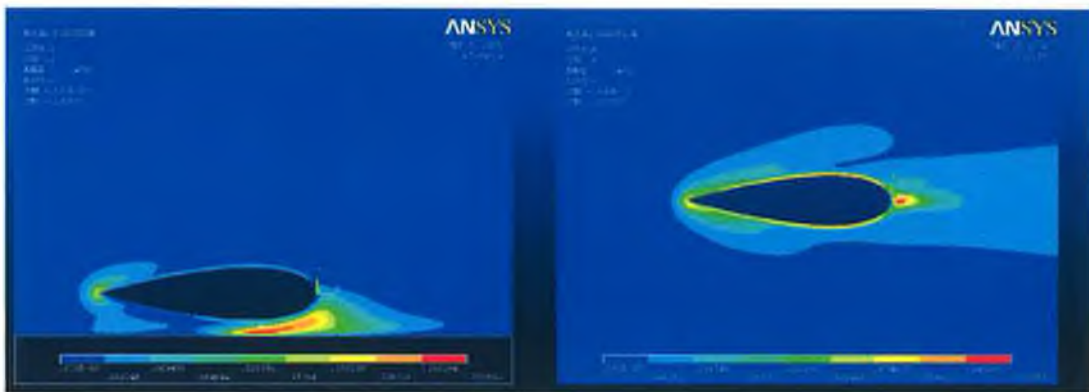


TURBULENCE STUDY

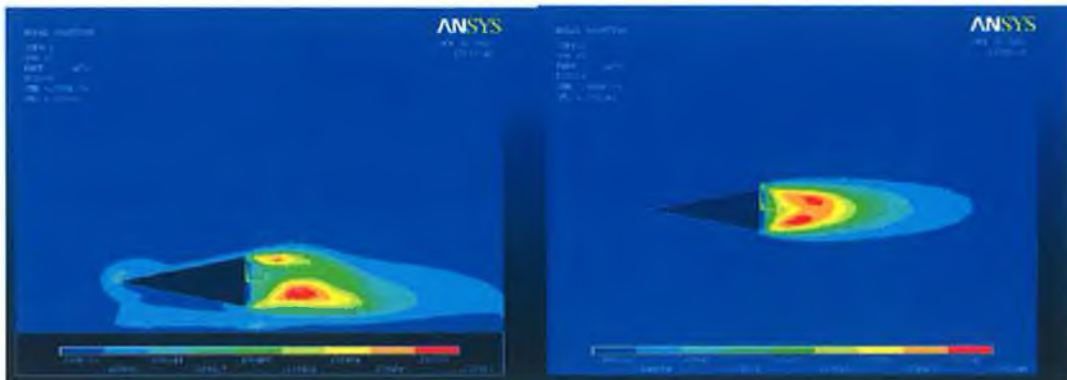
Foil 05: half diamond half ellipse section:



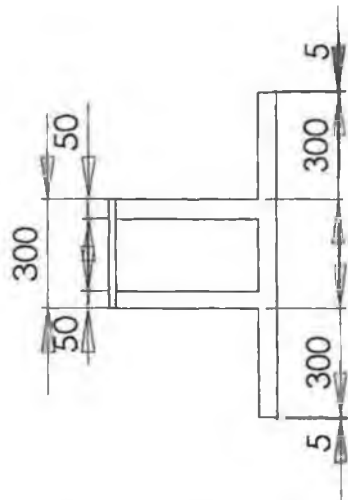
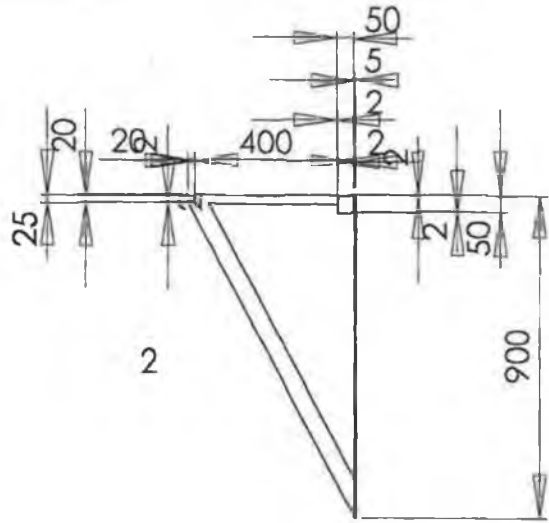
Foil 06: reverse NACA 0025:

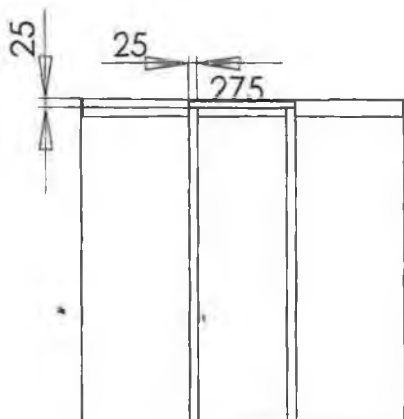


Foil 08: HALF diamond section:



TOWING TANK 2D DRAWING





NAME :

base_support

QUANTITY : 2

MATERIAL :
steel

SCALE : 1:20
A4

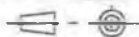
ALL DIMENSIONS
IN MILLIMETRES

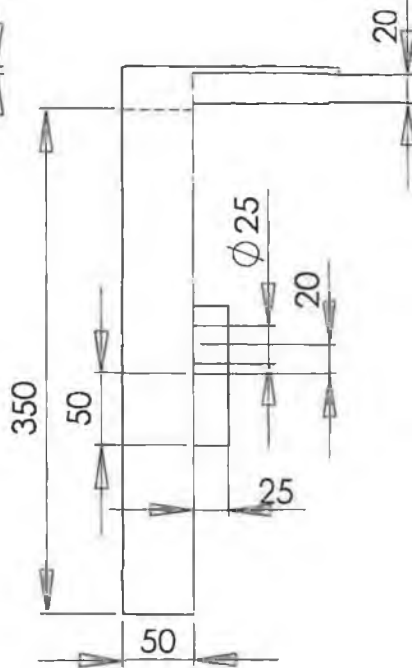
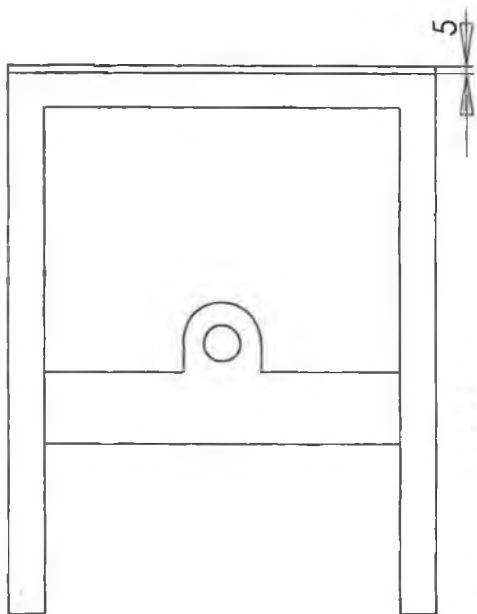
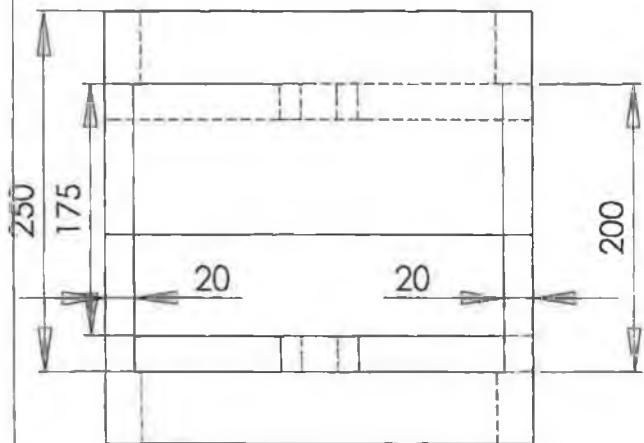
ALL TOLERANCES ± 0.2
UNLESS SPECIFIED OTHERWISE

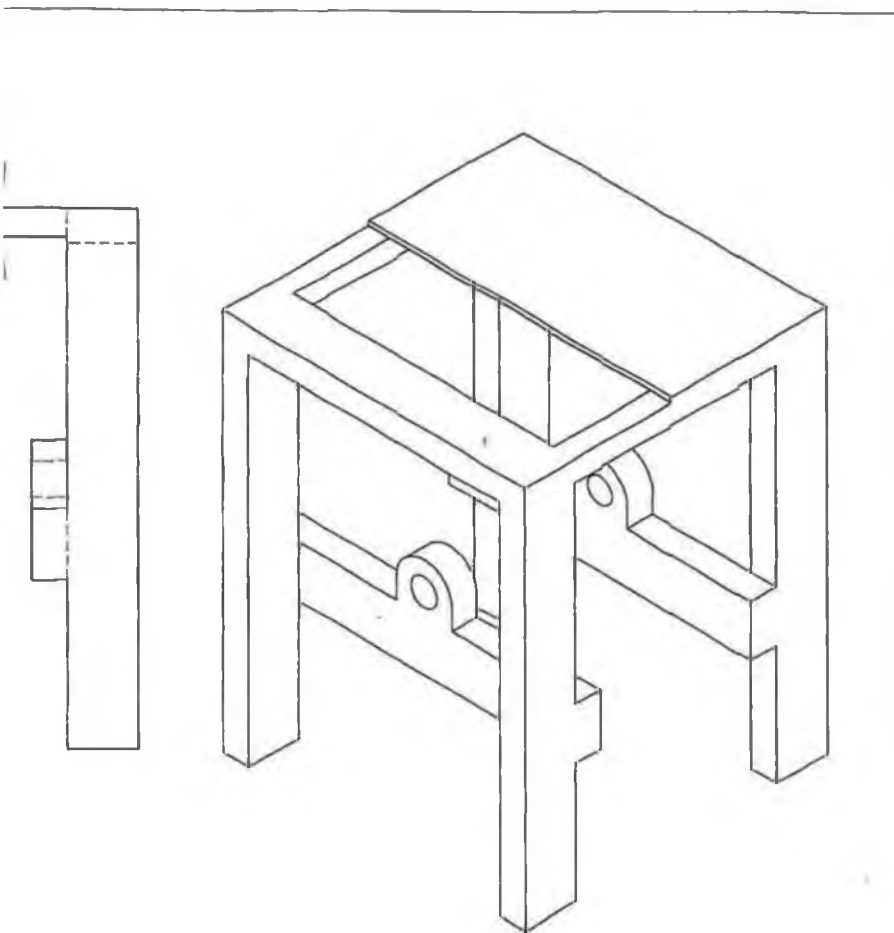
DESIGNER : 02/ 2002
Jean-Philippe ROZE

GMIT

GALWAY-MAYO INSTITUTE OF TECHNOLOGY
INSTITIÚD TEICNEOLAÍOCHTA NA GAILLIMHE-MÁIGN EO







NAME:

frame_motor

QUANTITY : 1

MATERIAL :
steel

SCALE : 1:5
A4

ALL DIMENSIONS
IN MILLIMETRES

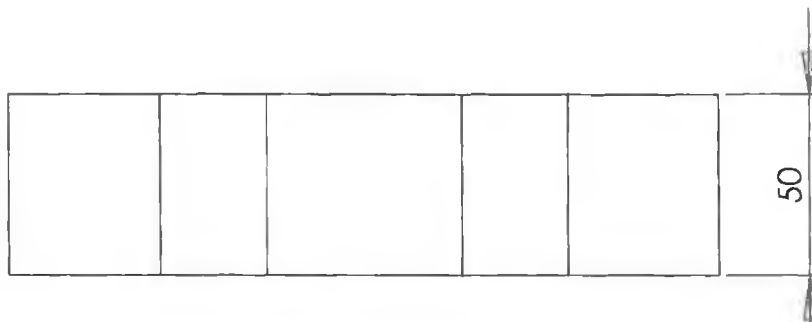
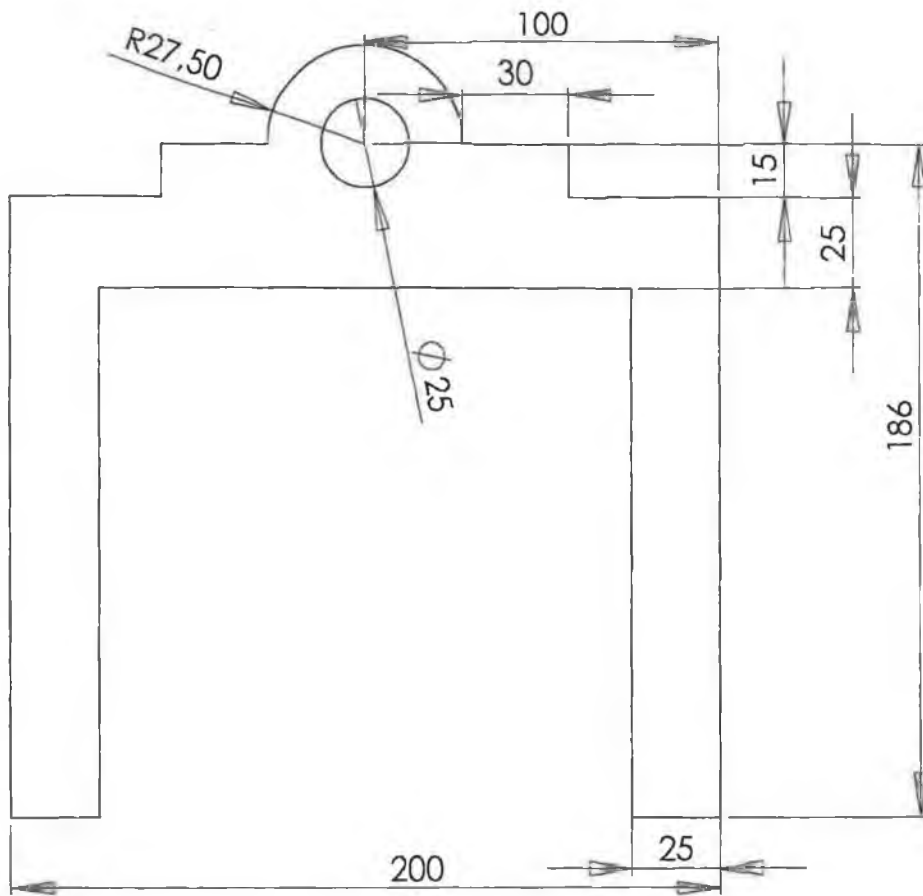
ALL TOLERANCES ± 0.2
UNLESS SPECIFIED OTHERWISE

DESIGNER : 02/ 2002
Jean-Philippe ROZE

GMIT

GALWAY - MAYO INSTITUTE OF TECHNOLOGY
INSTITIÚD TEICNEOLAÍOCHTA NA GAILLIHNE - MAIGH EÓ





NAME :

frame pulley

QUANTITY : 2

MATERIAL :
steel

SCALE : 1:2
A4

ALL DIMENSIONS
IN MILLIMETRES

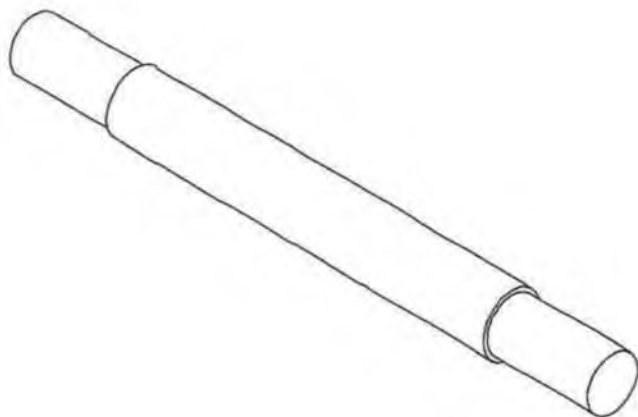
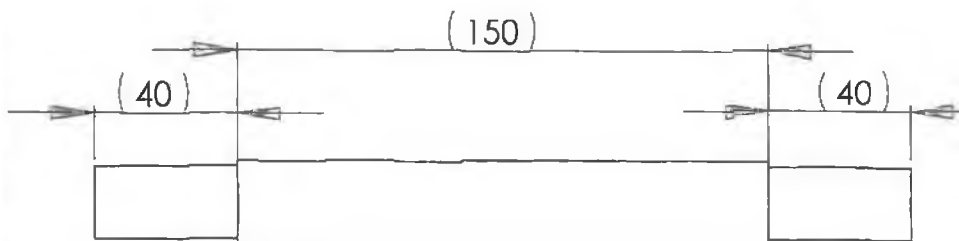
ALL TOLERANCES ± 0.2
UNLESS SPECIFIED OTHERWISE

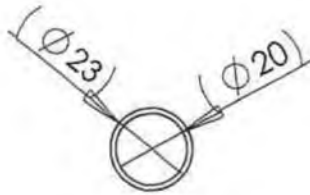
DESIGNER : 02/2002
Jean-Philippe ROZE

GMIT

GALWAY-MAYO INSTITUTE OF TECHNOLOGY
INSTITIÚD TEICNEOLAÍOCHTA NA GAILEIRHE-MÁIGN ÉG



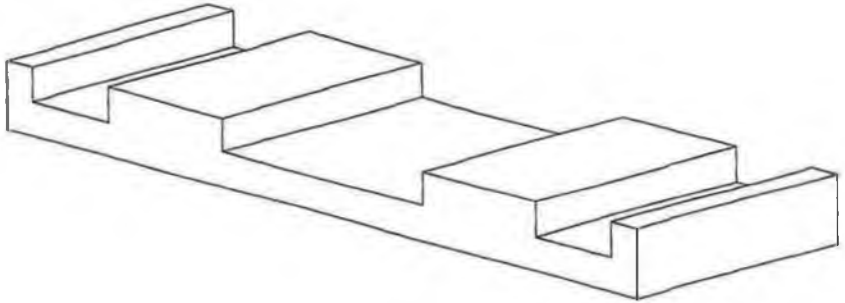
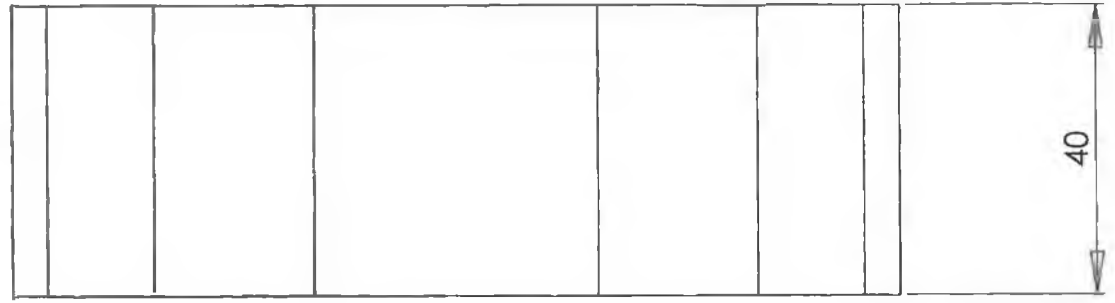
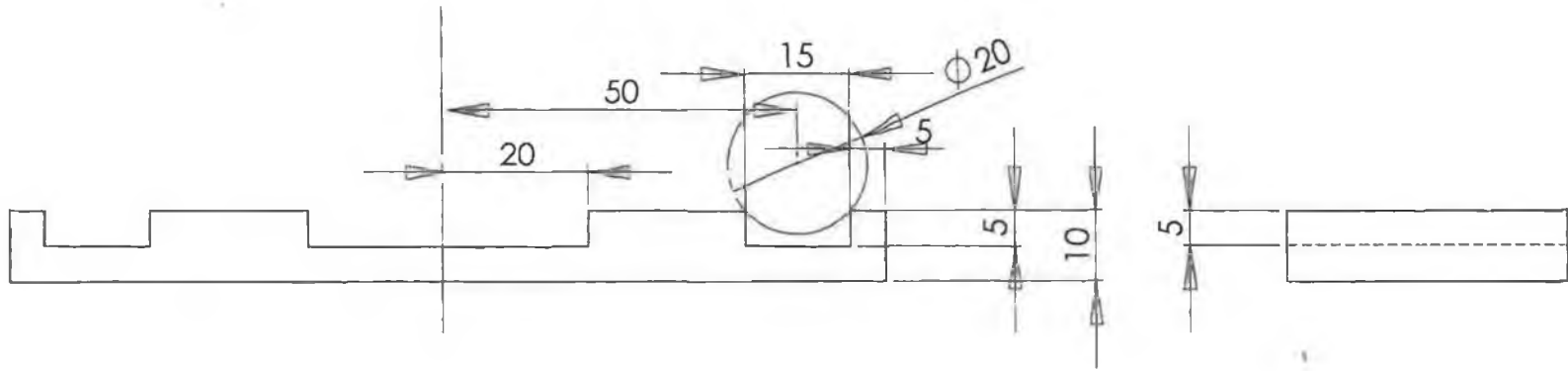




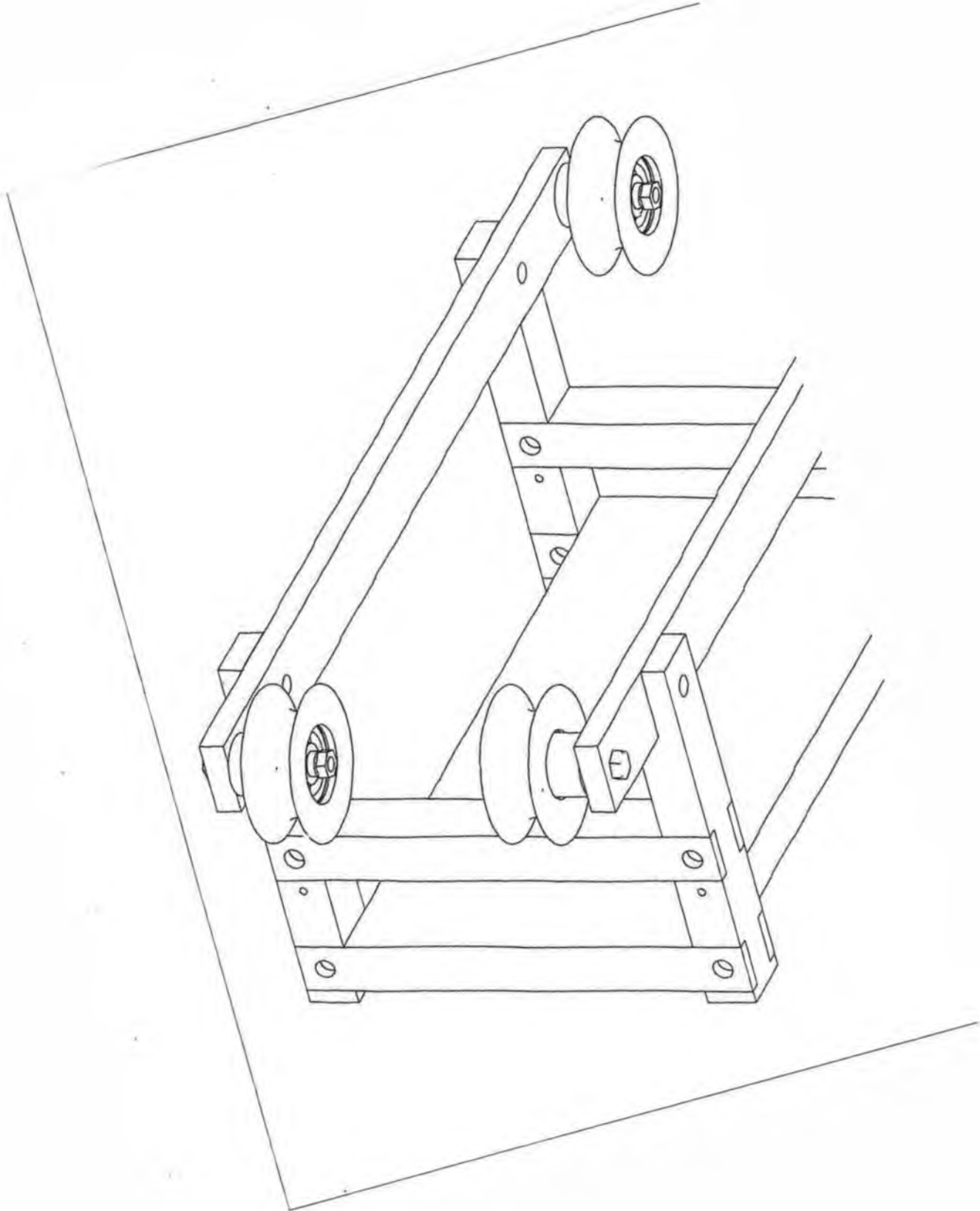
NAME :

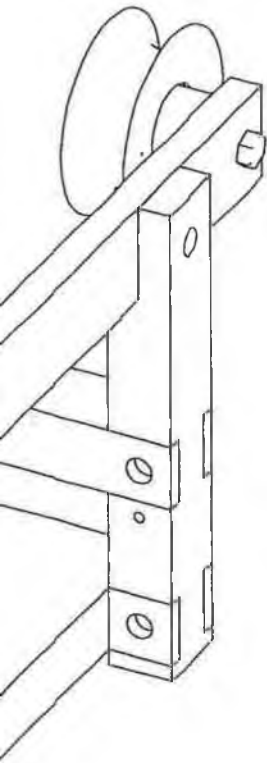
axel_pulley_b

QUANTITY : 1	MATERIAL : steel	SCALE : 1:2 A4
ALL DIMENSIONS IN MILLIMETRES	ALL TOLERANCES ± 0.2 UNLESS SPECIFIED OTHERWISE	
DESIGNER : 02/ 2002 Jean-Philippe ROZE	GMT GALWAY-MAYO INSTITUTE OF TECHNOLOGY INSTITIÚD TEICNEOLAÍOCHTA NA GAILLIMNE-MÁIGN ÉR	

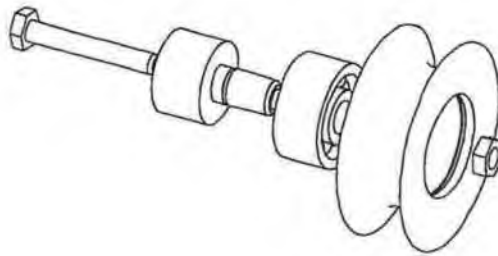


NAME : centrer_rail		
QUANTITY : ?????	MATERIAL : steel	SCALE : 1:1 A4
ALL DIMENSIONS IN MILLIMETRES	ALL TOLERANCES ± 0.2 UNLESS SPECIFIED OTHERWISE	
DESIGNER : 02/ 2002 Jean-Philippe ROZE	GMIT GALWAY-MAYO INSTITUTE OF TECHNOLOGY INSTITIÚD TEICNEOLAÍOCHTA NA GAILLIHNE-MAIGH EÁ	





No.	QUANTITY	ITEMS
1	2	hor01
2	4	vert01
3	2	long02
4	4	subass rail-wheel
	1	weel_axel
	1	bearing wheel
	1	wheel
	1	circlips_axel
	1	circlips wheel
	1	screw_m6_L30
	1	nut_m6
5	1	plateform01



NAME :

Trolley assembly

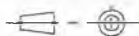
QUANTITY : 1

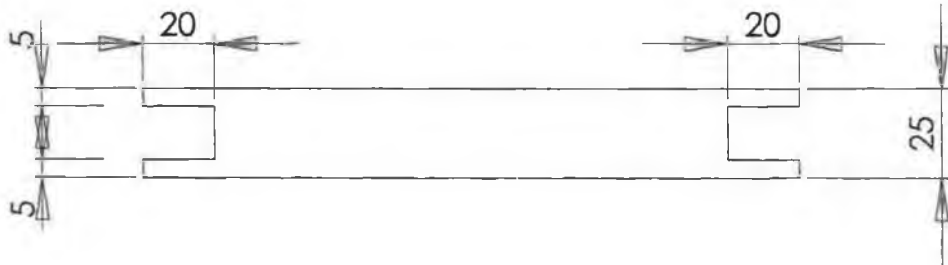
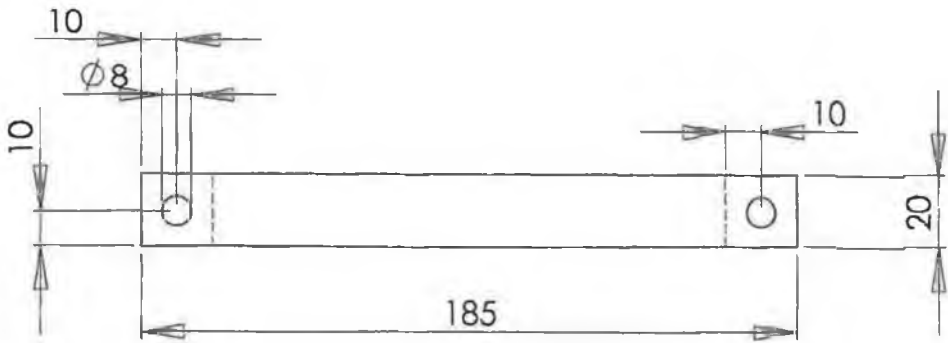
SCALE : 1:5
A4

DESIGNER : 02/ 2002
Jean-Philippe ROZE

GMIT

GALWAY-MAYO INSTITUTE OF TECHNOLOGY
EINSTITIÚID TEICNEOLAÍOCHTA NA GAILLIMHE-MAIGN ÉG







NAME :

trolley's horizontal bar

QUANTITY : 2

MATERIAL :
AU4G

SCALE : 1:2
A4

ALL DIMENSIONS
IN MILLIMETRES

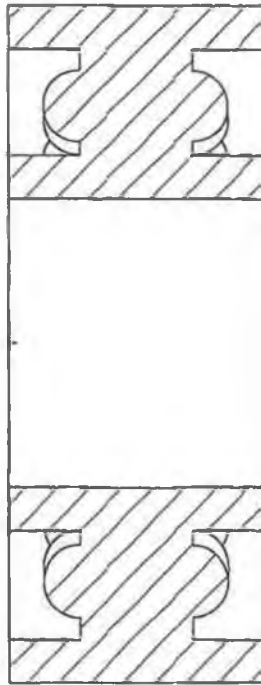
ALL TOLERANCES ± 0.2
UNLESS SPECIFIED OTHERWISE

DESIGNER : 02/ 2002
Jean-Philippe ROZE

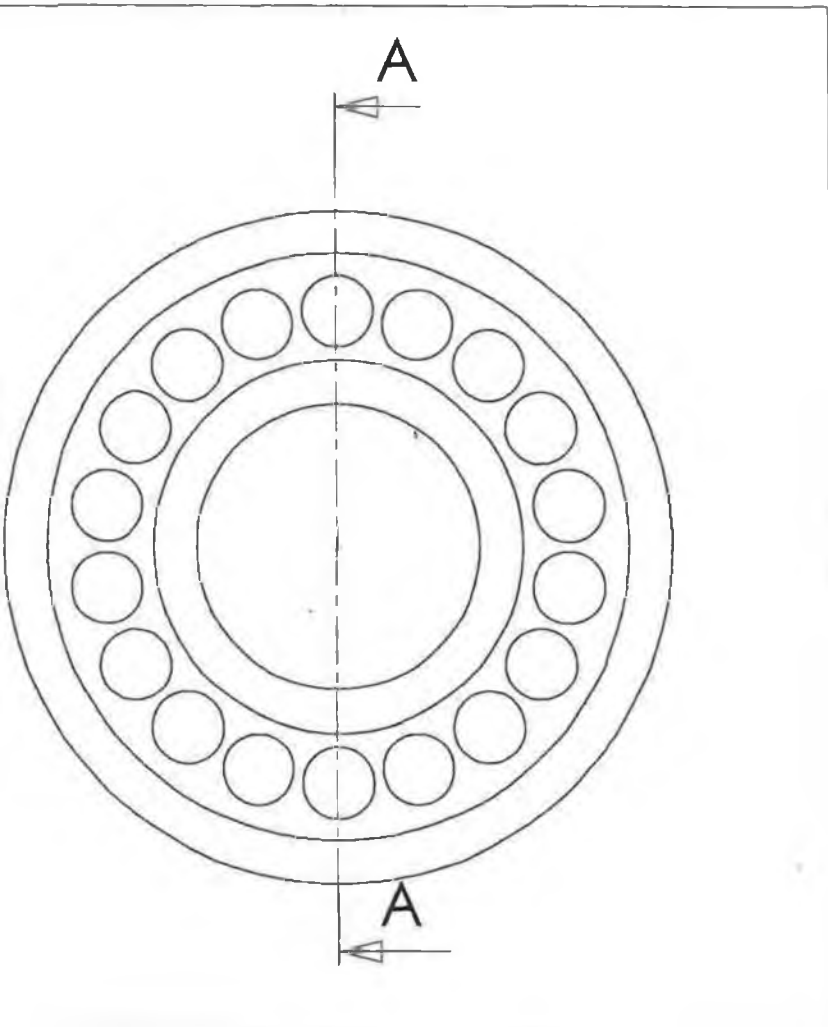
GMIT

GALWAY-MAYO INSTITUTE OF TECHNOLOGY
INSTITIÚD TEICNEOLAÍOCHTA NA GAILELHME-MAIGN ÉG





A-A



NAME :

Bearing-2204-2rs-tv

QUANTITY : 4

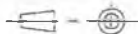
SCALE : 2:1
A4

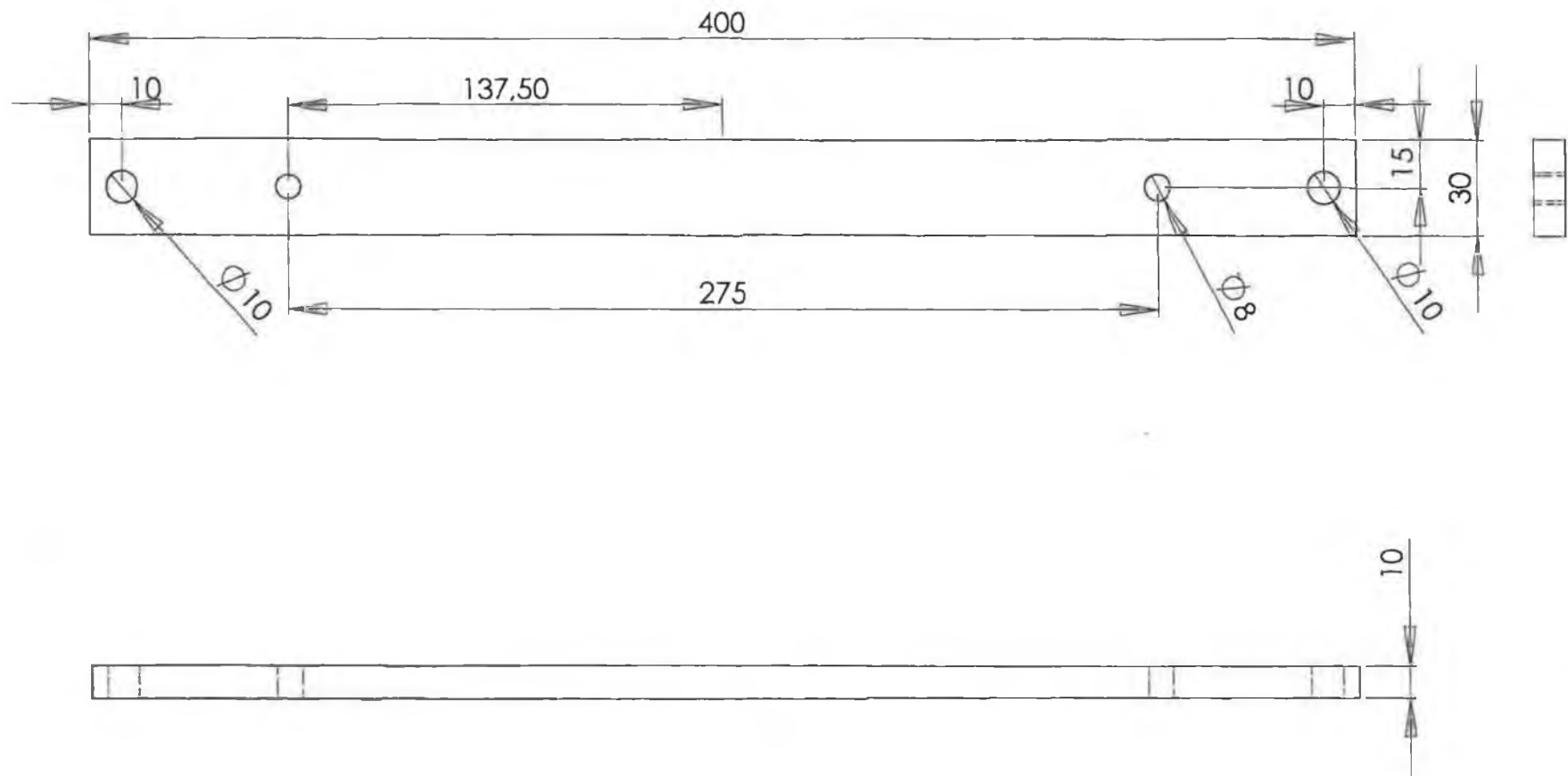
ALL DIMENSIONS
IN MILLIMETRES

DESIGNER : 02/ 2002
Jean-Philippe ROZE

GMIT

GALWAY-MAYO INSTITUTE OF TECHNOLOGY
INSTITIÚD TEICNEOLAÍOCHTA NA GAILLIMHÉ-MAIGH ÉO





NAME :

Trolley's longitudinal bar

QUANTITY : 2

MATERIAL :
AU4G

SCALE : 1:2
A4

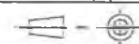
ALL DIMENSIONS
IN MILLIMETRES

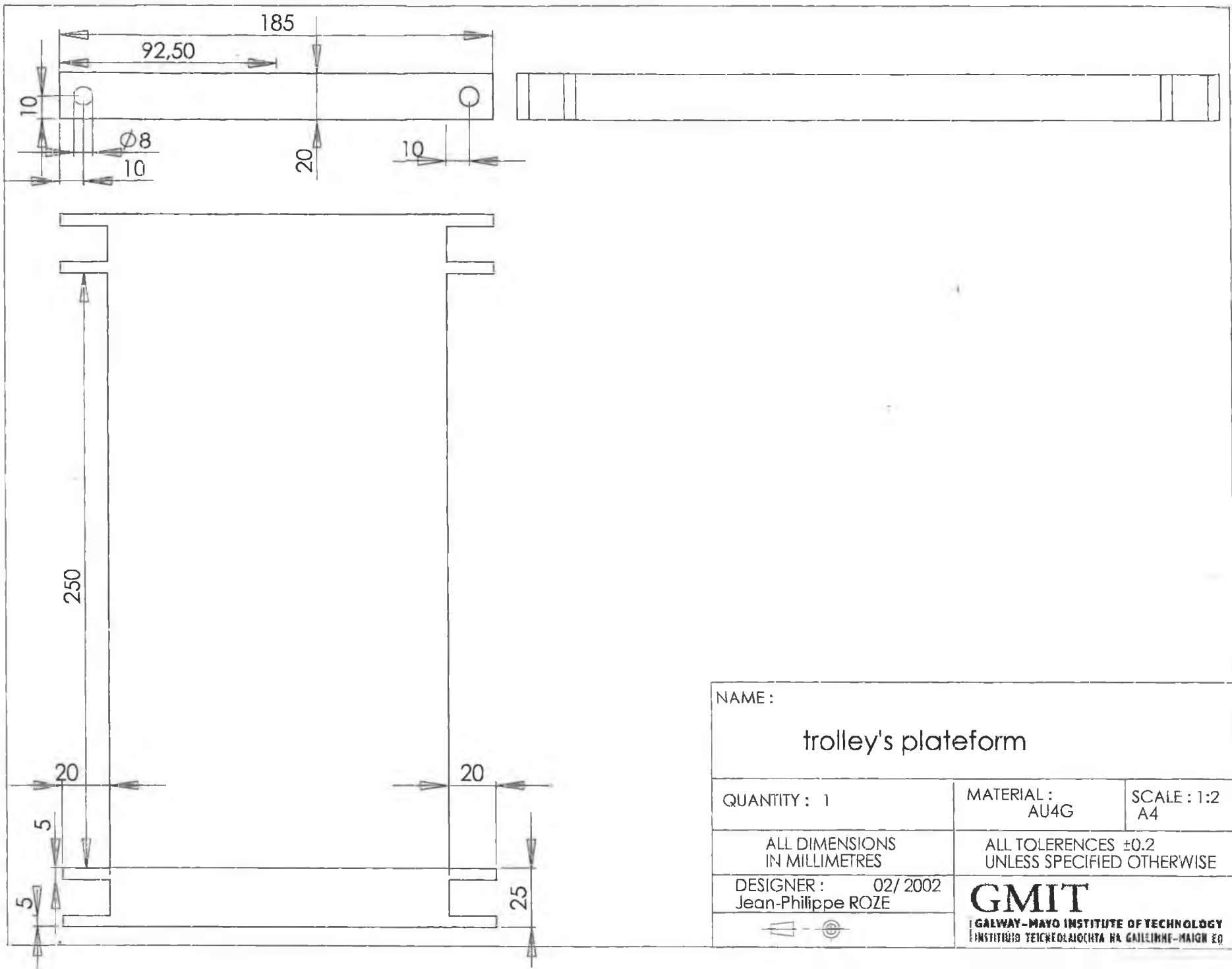
ALL TOLERANCES ± 0.2
UNLESS SPECIFIED OTHERWISE

DESIGNER : 02/ 2002
Jean-Philippe ROZE

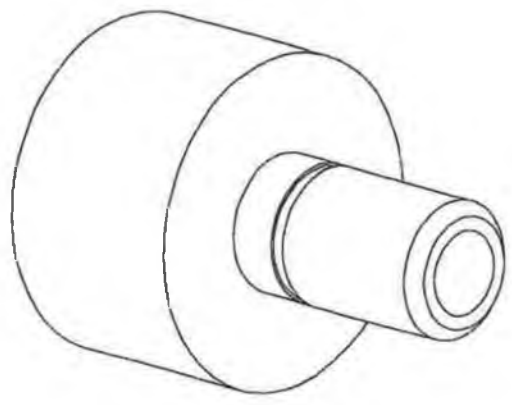
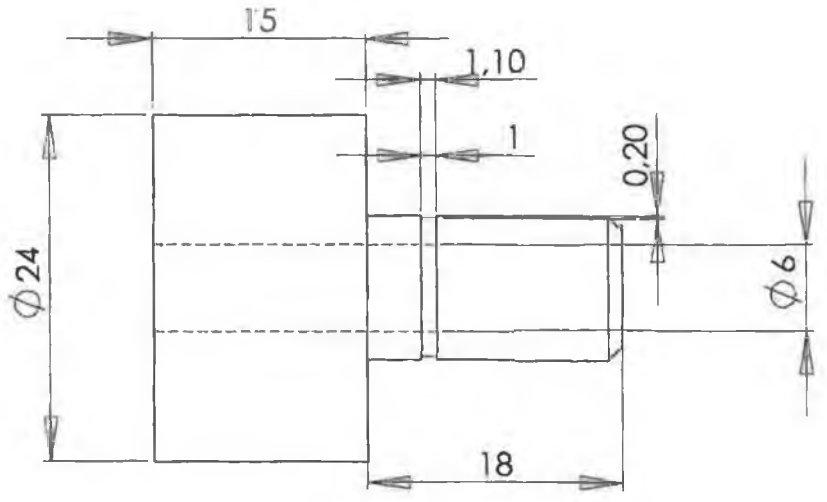
GMIT

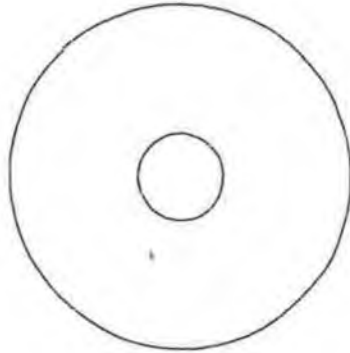
GALWAY-MAYO INSTITUTE OF TECHNOLOGY
INSTITIÚD TEICNEOLAÍOCHTA NA GAILEMHE-MAIGN EQ





NAME :		
trolley's platform		
QUANTITY : 1	MATERIAL : AU4G	SCALE : 1:2 A4
ALL DIMENSIONS IN MILLIMETRES	ALL TOLERANCES ± 0.2 UNLESS SPECIFIED OTHERWISE	
DESIGNER : 02/ 2002 Jean-Philippe ROZE	GMIT GALWAY-MAYO INSTITUTE OF TECHNOLOGY EINSTITIÚID TEICNEOLAÍOCHTA NA GAILLIMHE-MAIGH EÓ	





NAME :

Weel axel

QUANTITY : 4

MATERIAL :
AU4G

SCALE : 2:1
A4

ALL DIMENSIONS
IN MILLIMETRES

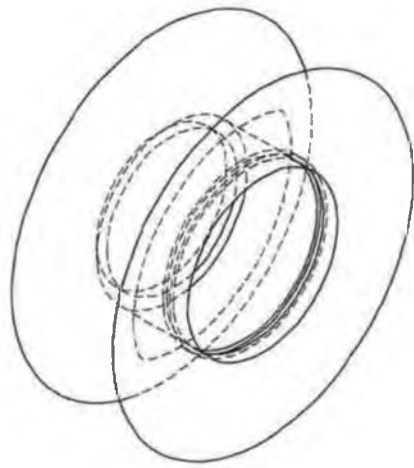
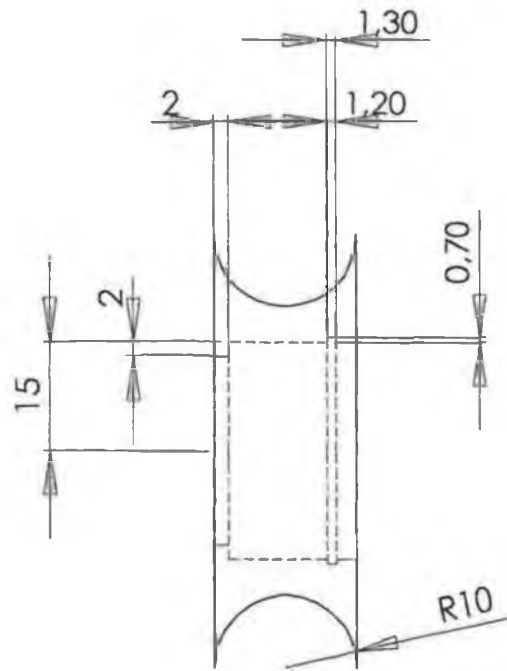
ALL TOLERANCES ± 0.2
UNLESS SPECIFIED OTHERWISE

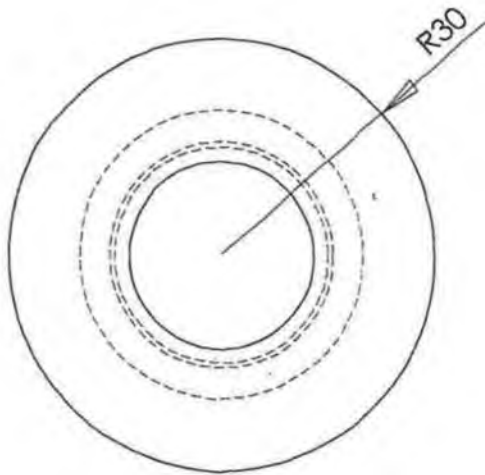
DESIGNER : 02/ 2002
Jean-Philippe ROZE

GMIT

GALWAY-MAYO INSTITUTE OF TECHNOLOGY
INSTITIÚD TEICNEOLAÍOICHEA NA GAILLIHNE-MAIGH EÓ







NAME :

Trolley's wheel

QUANTITY : 4

MATERIAL :
Teflon

SCALE : 1:1
A4

ALL DIMENSIONS
IN MILLIMETRES

ALL TOLERANCES ± 0.2
UNLESS SPECIFIED OTHERWISE

DESIGNER : 02/ 2002
Jean-Philippe ROZE

GMIT

GALWAY - MAYO INSTITUTE OF TECHNOLOGY
INSTITIÚD TEICNEOLAÍOCHTA NA GRILLINNE - MAIGN EÓ



CHARACTERISTICS OF THE INVERTER

ALTIVAR 28 Quick Reference Guide

Keypad Operation & Reference

Using the Keypad Display



Menu 1 – Adjustment Menu (SEt)

Parameter	Code	Factory Setting
Speed Reference via the Display Module	LFr	
PI Reference	rP1	0.0
Direction of Operation	rDt	For
Acceleration time	rCc	3 sec
Deceleration Time	dEc	3 sec
Acceleration Ramp #2	rC#2	4 sec
Deceleration Ramp #2	dE#2	5 sec
Low Speed	LSP	0 Hz
High Speed	HSP	(bFr)
Motor Full Load Current (protection)	IeH	(In)
Optimize Low Speed Torque (voltage boost)	UF	20
Slip Compensation	SLP	0.0–5.0 Hz
Frequency Loop Gain	FLG	33
DC Injection Braking Current	IdL	0.7In
DC Injection Braking Time at Standstill	t dL	0.5 sec
Skip Frequency	JPF	0 Hz
Jog Frequency	JOG	10 Hz
PI Regulator Proportional Gain	rPG	1
PI Regulator Integral Gain	rIG	1/s
PI Feedback Multiplication Coefficient	r bS	1
PI Regulator Reverse Coefficient	PIC	no
Preset Speed 2nd	SP2	10 Hz
Preset Speed 3rd	SP3	16 Hz
Preset Speed 4th	SP4	20 Hz
Preset Speed 5th	SP5	26 Hz
Preset Speed 6th	SP6	30 Hz
Preset Speed 7th	SP7	35 Hz
Frequency Threshold where R2 Closes	Ft d	(bFr)
Current Threshold where R2 Closes	Ct d	1.5In
Motor Thermal where R2 Closes	t t d	100%
Low Speed Operation Time	t L S	0

Menu 2 – Drive Menu (DrC)

Parameter	Code	Factory Setting
Nominal Motor Voltage	UnS	230/460V
Nominal Motor Frequency	FrS	50/60 Hz
Auto-tuning	t Un	no
Maximum Output Frequency	t Fr	60/72 Hz
Type of Volts/Hz Ratio	Fk	n
Automatic Ramp Modification for Decel	b r R	YES
Alternate Acc/Decel Ramp Frequency	r r t	0 Hz
Carrier Switching Frequency	SFr	4.0
Random Carrier Frequency Modulation	r r d	YES
Automatic Restart	Rt r	no
Enable Output Phase Failure Fault	DPL	YES
Enable Line Supply Phase Failure Fault	IPL	YES
Controlled Stop on Loss of Line Supply	SEp	no
Enable Smooth Restart after Fault	FLr	no
Lower Tripping Threshold of Undervoltage	d r n	no
Scale Factor of Output Frequency for Speed	SdS	30
Return to Factory Settings	FCS	no

Menu 3 – I/O Menu (I-O)

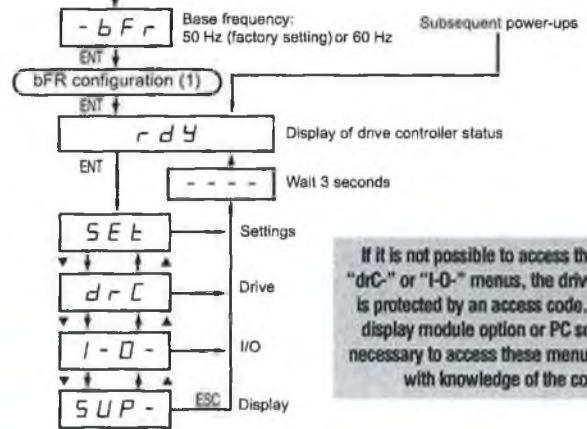
Parameter	Code	Factory Setting
Control Strategy Configuration (2-wire/3-wire)	t C E	2C
2-Wire Control	2C	
3-Wire Control	3C	
Presence of Local Control Option	DPt	
Enable for Start/Stop using Remote Display	L L L	no
Logic Input 2 Assignment	L I 2	rS
Logic Input 3 Assignment	L I 3	PS2
Logic Input 4 Assignment	L I 4	PS4
Not Assigned	no	
Reverse Rotation	r r S	
Ramp Switching	r r t	

The parameters in colored boxes appear if the corresponding functions have been configured in the dcr or I/O menus.

Electrical equipment should be serviced only by qualified personnel. No responsibility is assumed by Schneider Electric for any consequences arising out of the use of this material. This document is not intended as an instruction manual for untrained persons.

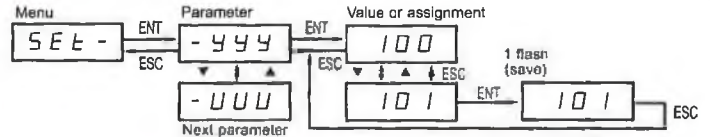
Access to Menus

1st power-up after factory configuration



If it is not possible to access the "SEt", "DrC" or "I-O" menus, the drive controller is protected by an access code. A remote display module option or PC software is necessary to access these menus, together with knowledge of the code.

Access to Parameters



Menu 3 – I/O Menu (I-O) continued

Parameter	Code	Factory Setting
Jog Operation	JOG	
2 Preset Speeds	PS2	
4 Preset Speeds	PS4	
8 Preset Speeds	PS8	
Freewheel Stop	r S t	
DC Injection Braking	d C I	
Fast Stop	F S t	
Forced Local Mode	F L D	
Fault Reset	r S t	
Analog Speed Reference Switching	r F C	
Analog Input Assignment of 2nd Input	R I C	SAI
Not Assigned	no	
Summing with All	S R I	
PI Regulator Feedback, setpoint = parameter rP1	P I I	
PI Regulator Feedback, setpoint = All	P I R	
Minimum Value on Analog Current Input	C r L	4 mA
Maximum Value on Analog Current Input	C r H	20 mA
Assignment of Analog Output	R O	rFr
Not Assigned	no	
Motor Current	D c r	
Motor Frequency	r F r	
Motor Torque	D L D	
Drive Power Supplied	D P r	
Assignment of Offset for Analog Output	R O t	0
Assignment of R2 Relay	r 2	SrA
Not Assigned	no	
Frequency Threshold Reached	F t R	
Current Threshold Reached	C t R	
Speed Reference Reached	S r R	
Motor Thermal Threshold Reached	t t R	
Drive Address via Serial Link	R d d	1
Serial Link transmission Speed	b d r	19.2

Menu 4 – Display Menu (SUP)

Parameter	Code	Factory Setting
Control Strategy Configuration (2-wire/3-wire)	r r H	Hz
Enable for Start/Stop using Remote Display	r F r	Hz
Display Calculated Value of Speed or Production Rate (rFr X SoS)	S P d	A
Display Motor Current	L C r	%
Display Motor Power	D P r	V
Display Line Voltage	U L n	%
Display Motor Thermal State	t H r	%
Display Drive Controller Thermal State	t H d	
Display Last Fault	L F t	
Display Drive Controller Software Version	C P U	
Access Code Protection	C O d	
Display of Controller Status		



SQUARE D
Schneider Electric